CALIFORNIA INSTITUTE OF TECHNOLOGY

EARTHQUAKE ENGINEERING RESEARCH LABORATORY

SEISMIC RESPONSE OF STEEL FRAME BUILDINGS TO NEAR-SOURCE GROUND MOTIONS

BY

JOHN F. HALL

REPORT NO. EERL 97-05

PASADENA, CALIFORNIA

1997

A REPORT ON RESEARCH PARTIALLY SUPPORTED BY
KAJIMA-CUREE JOINT RESEARCH PROGRAM, PHASE II:
MITIGATION OF THE EFFECTS OF EARTHQUAKES AND
OTHER NATURAL HAZARDS FOR SAFETY OF URBAN AREAS

SEISMIC RESPONSE OF STEEL FRAME BUILDINGS TO NEAR-SOURCE GROUND MOTIONS

John F. Hall, Caltech

June 1997

TABLE OF CONTENTS

1. INTRODUCTION

Strong near-source ground motions contain large, rapid displacement pulses that can have severe effects on structures. In the U.S. it is generally agreed that our design codes do not adequately address this kind of ground motion, and changes are being made to increase the design force levels, which will result in stronger buildings. In Japan, the design force levels for buildings have for some time been considerably greater than in the U.S. Even so, Japanese engineers are also concerned about the adequacy of their design provisions for strong near-source ground motions.

The issue of building strength appropriate for near-source ground motions is investigated in this report. Two different heights of buildings are selected, 6 stories and 20 stories, and for each height, designs of two different strengths are produced. The first design is according to the 1994 Uniform Building Code (1), and the second design follows current Japanese provisions (2). All four buildings are steel moment frames.

One important part of assessing near-source ground motions is to quantify the size of the region that is affected. An aspect of this is that near-source effects are directional and so are confined to only a portion of the near-fault zone. In this study, ground motions at a grid of sites sufficient to cover the region of near-source effects are employed. This is accomplished by using simulated ground motions. Three earthquake simulations are run: one based on the 1994 Northridge earthquake (M_W 6.7), another for the 1995 Kobe earthquake (M_W 6.9), and the third of a hypothetical M_W 7.0 earthquake on the Elysian Park fault in Los Angeles. In addition, various recorded motions from actual earthquakes, including Northridge and Kobe, are employed.

Previous studies of strong near-source ground motions have shown the potential for large story drifts in buildings and even collapse (3-7). Future design measures for near-source ground motions will likely have to consider all contributions to the strength of a building in order to be feasible. It follows from this that since future design methods will be based on assessment studies like the present one, the assessments should also be done as realistically as possible and include all important contributions to the strength of a structure. Such an approach is followed here. In addition, since strong near-source ground motions will likely produce severely nonlinear responses, it becomes necessary to include structural degradation effects. In this study, due to the common occurrence of welded-connection failure in the Northridge and Kobe earthquakes and because this behavior would seem to be an important degradation mode, treatment of connection fracture is

included. As there is now wide-spread interest in fracture of welded connections, this is an important part of the present investigation.

The Appendix contains a description of the computer program used for the analyses. Some of the notation used in this report is defined in this Appendix.

2. DESCRIPTIONS OF BUILDINGS

2.1 Design

A total of four buildings are studied. They are referred to by the following notation:

U6, a 6-story-plus-basement building designed according to the 1994 Uniform Building Code (1)

J6, a 6-story-plus-basement building designed according to current Japanese provisions (2)

U20, a 20-story-plus-basement building designed according to the 1994 Uniform Building Code (1)

J20, a 20-story-plus-basement building designed according to current Japanese provisions (2).

Geometries and structural details of the buildings are shown in Figures 2.1 to 2.4 and in Tables 2.1 to 2.4. Floor plans, story heights, and overall building dimensions are the same for U6 and J6, as are those for U20 and J20. Since the earthquake response in the plane of the narrow dimension of the buildings is of most interest, detailed designs are carried out in this direction only. However, the elements of the perpendicular frames that appear in Figures 2.1 to 2.4 are probably reasonable.

A36 steel is used for both beams and columns. Design dead loads are 0.391 tons/m^2 (80 psf) for the roof, 0.464 tons/m^2 (95 psf) for the floors, and 0.171 tons/m^2 (35 psf) for the cladding. The floor design live load is 0.244 tons/m^2 (50 psf).

Designs are carried out for gravity plus wind and gravity plus seismic loads. The design for the lateral loads does not include Frames B in U6, J6, U20 and J20 which contain only simply-supported beams. Half-building models are used: a single Frame A for U6 and U20 and a single Frame A plus a half Frame C for J6 and J20. Panel zones of the columns are thickened, if necessary, to make the panel zone yield moment equal to 0.8 times the sum of the plastic moment capacities of the connecting beams.

Gravity loads are applied directly to the columns of the included frames based on tributary areas to these columns. Girders are not loaded within their spans. Gravity loads are computed using full dead load and 0.073 tons/m^2 (15 psf) of floor live load.

Horizontal seismic loads for U6 and U20 are based on the dead weight above ground level. The weight used to compute the horizontal seismic loads for J6 and J20 also includes 0.049 tons/m^2 (10 psf) of floor live load. The total above-ground building weight used in the seismic design is denoted as W; values are listed below.

	U6	J6	U20	J20
W (tons)	1310.	1400.	3190.	3450
W (kips)	2880.	3090.	7040.	7610.

UBC design parameters for U6 and U20, including the resulting base shear coefficient V/W, are as follows:

	Z	I	R_w	S	T	C	V/W	drift limit
U6	.4	1	12	1.2	1.22 sec	1.312	0.0437	0.25 %
U20	.4	1	12	1.2	2.91 sec	0.736	0.0300	0.25 %.

Design parameters from the Japanese provisions (2) for J6 and J20, including the resulting base shear coefficient Q/W, are as follows:

	Z	Soil	T	R_t	C_o	Q/W	drift limit
J6	1.	Type 2	0.73 sec	0.990	0.2	0.1980	---
J20	1.	Type 2	2.34 sec	0.410	0.2	0.0820	0.50 %.

The above base shear coefficients are for allowable stress design, and the nominal allowable stress for combined gravity and seismic is 90% of the yield stress for the Japanese provisions and is computed using the 33% increase for the UBC. The Japanese code also requires a check on ultimate strength. For J6 and J20, which are regular and symmetric buildings, the required ultimate strength corresponds to 1.25 of the base shear coefficient given above that is used for the allowable stress check.

Wind loading controls some features of the design of building U20 only. For this building, the UBC wind design parameters are taken as follows: $I_w = 1$, wind speed = 113 kph, exposure B, $C_q = 0.8$ for the windward side and 0.5 for the leeward side.

Analyses carried out in the design process use a planar-frame fiber model developed by the author. Capabilities of this computer program are summarized in the Appendix, where notation is also defined. For the design of buildings U6, J6, U20 and J20, the foundation is taken as rigid; composite slab action is neglected; and P-delta effects are considered only for gravity loads tributary to the included frames (Frames A and C). The basement walls are taken to be concrete with a modulus of 211 tons/cm^2 (3000 ksi). The simple beam-to column connections in Frame C ('o' marks in Figures 2.2 and 2.4) are accomplished by the method discussed in the Appendix. Thus, for the two segments at the simply-supported end of a girder, flange fiber areas are zeroed and web fiber areas are reduced to a value of 0.3 of the full areas.

Details of the seismic design of buildings U6, J6, U20 and J20 are given in Tables 2.5 to 2.8. Column stresses are the maxima occurring for any column in the indicated story and frame; beam stresses are the maxima occurring for any beam in the indicated level and frame. All stresses are listed as fractions of the nominal yield stress. The M_p ratio equals

the sum of plastic moments for all columns at a joint divided by the sum of plastic moments for all beams at a joint, and the values given are minima occurring for any joint in the indicated level and frame. Reductions in column plastic moment capacity due to the presence of axial force are considered. The ultimate strength requirements for J6 and J20 are shown to be satisfied through push-over analyses that give ultimate strengths corresponding to base shear values of 0.31W and 0.13W, respectively, which are adequate. Table 2.9 shows details of the wind design for building U20. All weight and force values in Tables 2.5 to 2.9 are for half-building models (one side of the plane of symmetry).

2.2 Models for earthquake analysis

The computer models used in the earthquake analysis of the six buildings are made as realistic as possible so as to make the computed earthquake responses as realistic as possible. Composite slab action is included, and the slab geometric parameters are defined in Figures 2.1 to 2.4 and in Tables 2.1 to 2.4. For the slab concrete, E_C = 211 tons/cm^2 (3000 ksi), σ_{CY} = 0.28 tons/cm^2 (4 ksi), and $\sigma_{CF} = \sigma_{CY}/10$. The same modulus is used for the basement walls. Stress-strain parameters of steel are taken to be

E	2040 tons/cm^2	(29000 ksi)
E_{SH}	40.8 tons/cm^2	(580 ksi)
σ_Y	2.96 tons/cm^2	(42.0 ksi)
σ_U	3.52 tons/cm^2	(50.0 ksi)
ε_{SH}	0.012	
ε_U	0.160	
σ_{RES}	0.42 tons/cm^2	(6.0 ksi)
τ_Y	1.69 tons/cm^2	(24.0 ksi)
G	816 tons/cm^2	(11600 ksi).

For all buildings, panel zones are thickened, if necessary, to make the panel zone yield moment equal to 0.8 times the sum of the plastic moment capacities of the connecting beams. The values above for σ_Y and τ_Y are used.

As in the static analysis, gravity loads are applied directly to the columns, and girders are not loaded within their spans. The same gravity loads are used in the dynamic analysis. For all buildings, masses for the horizontal and vertical frame degrees of freedom are based on these gravity loads (which include both dead and live parts) except that the floor live load for the horizontal-degree-of-freedom masses is reduced to 0.049 tons/m^2 (10 psf). Recall that no live load mass was used in the seismic design of U6 and U20.

Half-models (one side of the plane of symmetry) are employed, and all frames are included. This fully accounts for P-delta effects. Identical frames are lumped into a single

frame by increasing the width of all beams, columns, panel zones, slabs, walls and foundations. Shown below are the width multiplication factors that are used for each included frame.

	Frame A	Frame B	Frame C
U6	1.0	1.5	---
J6	1.0	1.0	0.5
U20	1.0	1.5	---
J20	1.0	1.0	0.5

Note that the width factor for Frame C on the plane of symmetry is one half. The simple connections in Frames B and C ('o' marks in Figures 2.1 to 2.4) are accomplished as described in the previous section. Moment connections in Frames A and C also use the 0.3 reduction factor for web fiber areas in order to account for reduced capacity of bolted web plates.

Foundation interaction is included and the parameters are defined in Figures 2.1 to 2.4 and in Tables 2.1 to 2.4. In addition, $\alpha = 0.15$. Yield strengths of the foundation springs are computed as the maxima of two values. The first value is twice the gravity load carried by the corresponding basement-level columns. In computing these loads, the full design live load is used. The second value is computed by multiplying the areas of the corresponding basement-level columns by 1.27 tons/cm^2 (18 ksi) for U6 and J6, and by 1.69 tons/cm^2 (24 ksi) for U20 and J20. The strengths thus obtained are used for the horizontal springs (F_{YH}) and for the vertical springs in the downward direction (F_{YD}). Half these values are used for the vertical springs in the upward direction (F_{YU}). Initial stiffnesses of the foundation springs (K_H and K_V) are computed from assumed yield displacements of 2.54 cm for the horizontal springs (D_{YH}) and for the vertical springs in the downward direction (D_{YD}), and 1.27 cm for the vertical springs in the upward direction (D_{YU}).

Viscous damping consists of a small amount (0.5%) of stiffness-proportional damping at the fundamental mode plus a larger amount of inter-story damping. The strength of the inter-story dampers is taken to be equal to the story shears produced by the seismic design forces scaled to a fraction of the seismic-design weight W: 0.02 for U6 and J6 and 0.01 for U20 and J20. The story shear velocity at yield is set to 10 cm/sec.

Analyses are run that assume perfect connections, and others are run with fracture-prone connections present. Buildings with perfect (non-fracturing) connections are denoted by a suffix P, ie, J6P. Buildings with fracture-prone connections are denoted by suffix B or T ,ie, U20B or U20T, depending on the quality of the connections, the quality for Case-T buildings being lower than that for Case-B buildings. Four sets of fracture

strains for the welds are defined:

Set B1, $\varepsilon_F/\varepsilon_Y$ = 1, 10 and 100 at 40%, 30% and 30%, respectively;

Set B2, $\varepsilon_F/\varepsilon_Y$ = 0.7, 1, 10, 50, and 100 at 20%, 40%, 20%, 10% and 10%, respectively;

Set T1, $\varepsilon_F/\varepsilon_Y$ = 1 at 100%; Set T2, $\varepsilon_F/\varepsilon_Y$ = 0.7 at 100%.

For the Case-B buildings, Set B2 is used for the bottom girder flange at the girder-to-column connections, and Set B1 is used for all other flange welds including girder-to-column, column splice ('+' marks in Figures 2.1 to 2.4) and column base plate. Sets T1 and T2 are used similarly for the Case-T buildings. The above percentages and fracture strains are chosen arbitrarily, but the Case-B assumption seems reasonable in light of recent earthquake experience, and the T assumption may represent a worst case. The Case-T buildings are considered only for the UBC designs, ie, U6T and U20T. The complete list of buildings analyzed is as follows:

U6P, U6B, U6T, J6P and J6B for the 6-story buildings and

U20P, U20B, U20T, J20P and J20B for the 20-story buildings.

Elastic first-mode periods of the Case-P buildings without damping are

U6P, 1.54 sec

J6P, 1.16 sec

U20P, 3.47 sec

J20P, 3.04 sec.

Geometric stiffness effects from gravity loads are included in the period calculation.

2.3 Push-over analyses

To quantify the actual strength of each building, push-over analyses are run. In these analyses, the buildings are subjected to a slow, ramped, horizontal ground acceleration that increases by 0.3g per minute, and the building response is computed dynamically. The structural models are identical to those used in the earthquake analyses except that masses for the horizontal degrees of freedom are recalculated to total the seismic-design mass W/g with a distribution proportional to the seismic design loads. Thus, in this analysis technique, the lateral loads are essentially the horizontal seismic-design forces proportionally increasing with time at a slow rate. As stated earlier, W is dead weight only for U6 and U20, and it includes 0.049 tons/m^2 (10 psf) live load for J6 and J20.

Results appear in Figures 2.5 to 2.8. The vertical scale is the building base shear divided by the seismic-design weight W. The base shear is computed by summing the horizontal components of the shear and axial forces in the first-story columns, considering the updated geometries of these columns. The drop-offs in the curves in Figures 2.5 to 2.8 are due to P-Δ effects, which eventually cause the base shear to become negative, and, for

the Case-B and Case-T buildings, the loss of strength due to connection fracture is an additional important factor. Since the push-overs are run as dynamic analyses, stiffness changes that accompany yielding and, especially, connection fracture cause vibrations. The resulting vibrational oscillations are apparent in Figures 2.5 to 2.8.

The push-over results show that the buildings are quite strong compared to the design base shears. This is is a result of drift controlling in some cases and contributions from factors not considered in the design (composite slab action, inclusion of frames with simply-connected beams, higher steel yield stress than the nominal value, and further increase in steel strength from strain-hardening). Inclusion of fracture-prone connections significantly reduces a building's lateral strength; however, the residual strength is still at or above the code-design base shear coefficients. For the Case-B buildings, three different random assignments of the fracture strains are used in the push-over analyses, and each of these results is shown in Figures 2.5 to 2.8. Approximate ultimate lateral strengths of each building as a fraction of its W value are

U6,	0.23 for U6P	0.15 for U6B	0.10 for U6T
J6,	0.40 for J6P	0.25 for J6B	
U20,	0.11 for U20P	0.06 for U20B	0.05 for U20T
J20,	0.15 for J20P	0.08 for J20B.	

2.4 Connection fracture study

In order to demonstrate the effects of connection fracture, a W30X116 beam with composite slab that is connected to freely rotating W30X191 column stubs (Figure 2.9) is subjected to the end rotation history shown in Figure 2.10. This substructure is taken from the 2nd-floor interior bay of Frame A of building U20 (see Figure 2.3). All dimensions and material properties are the same except that the panel zones are set to be rigid. Beam-to-column connections are either perfect (Case P) or fracture prone at $\varepsilon_F/\varepsilon_Y = 1$ for the top flange welds and $\varepsilon_F/\varepsilon_Y = 0.7$ for the bottom flange welds (Case 1/.7). Two situations are considered regarding axial restraint for the beam: complete restraint and no restraint. The specified end rotations force the beam into double curvature as occurs under lateral loading from an earthquake.

Results are presented in Figures 2.11 (Case P) and 2.12 (Case 1/.7) for moments M_1 and M_2 generated at the left and right ends of the composite beam and for the force F generated in the spring that provides the axial restraint. These quantities are plotted over the cyclic rotation history and are normalized with the plastic rotation capacity M_P of the W beam section, in the case of M_1 and M_2, and with the axial yield force F_Y of the W beam section, in the case of F. With perfect connections (Figure 2.11), strain hardening and

composite slab action enable M_1 and M_2 to exceed M_P. This effect is greater when axial restraint is present because the generated axial compression prevents some of the loss in moment capacity due to slab cracking. With fracture-prone connections (Figure 2.12), the moment capacity of the beam deteriorates to zero after a few cycles as the welds fracture, unless axial restraint is present. For complete axial restraint, a considerable amount of the moment capacity is retained. The amount of axial restraint for beams in an actual building will be between the extremes considered in this example. The building models used in this report contain some axial restraint, which should be an accurate amount, that owes to frame action in the members around a beam.

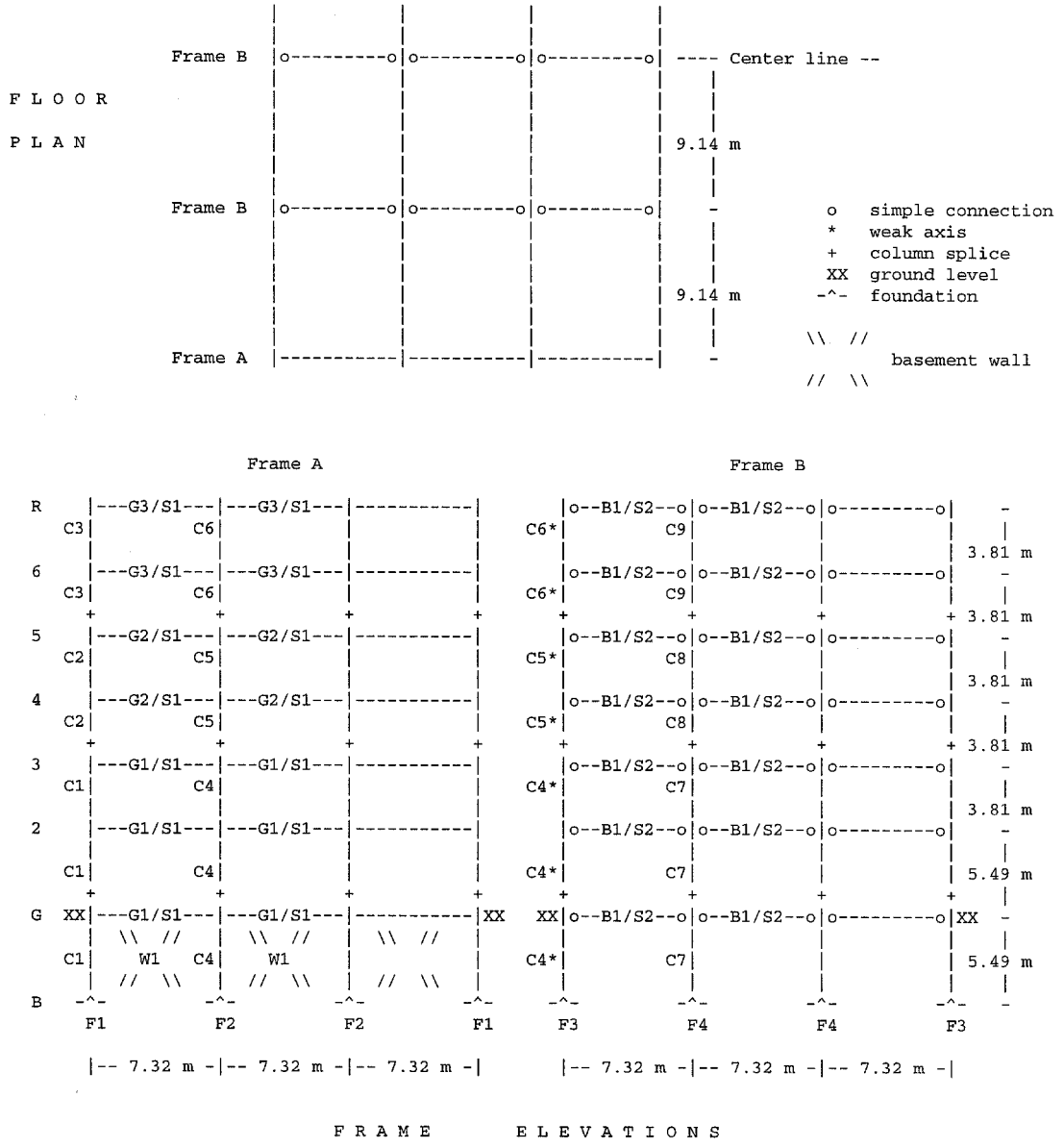

Figure 2.1 Building U6 floor plan and frame elevations.

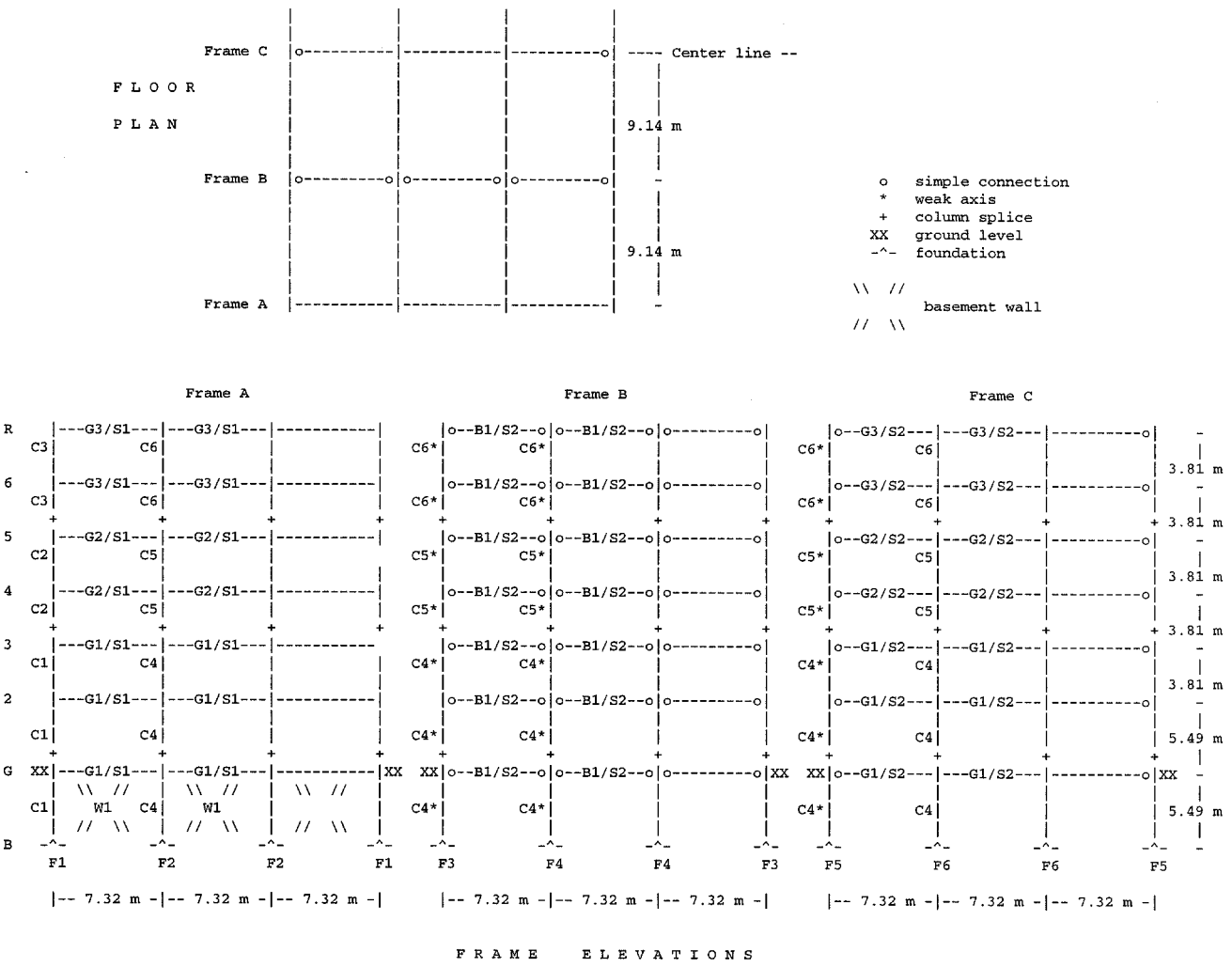

Figure 2.2 Building J6 floor plan and frame elevations.

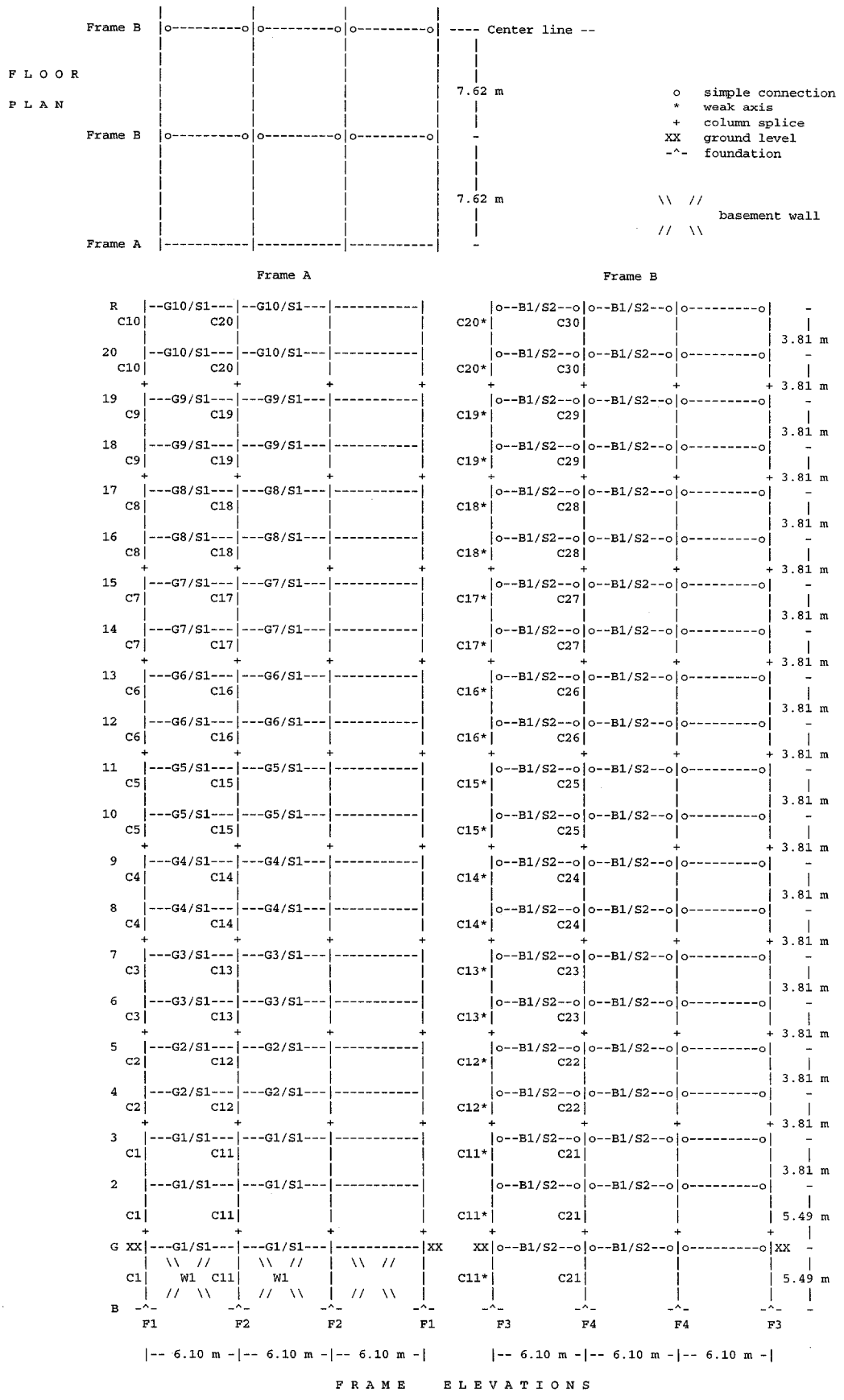

Figure 2.3 Building U20 floor plan and frame elevations.

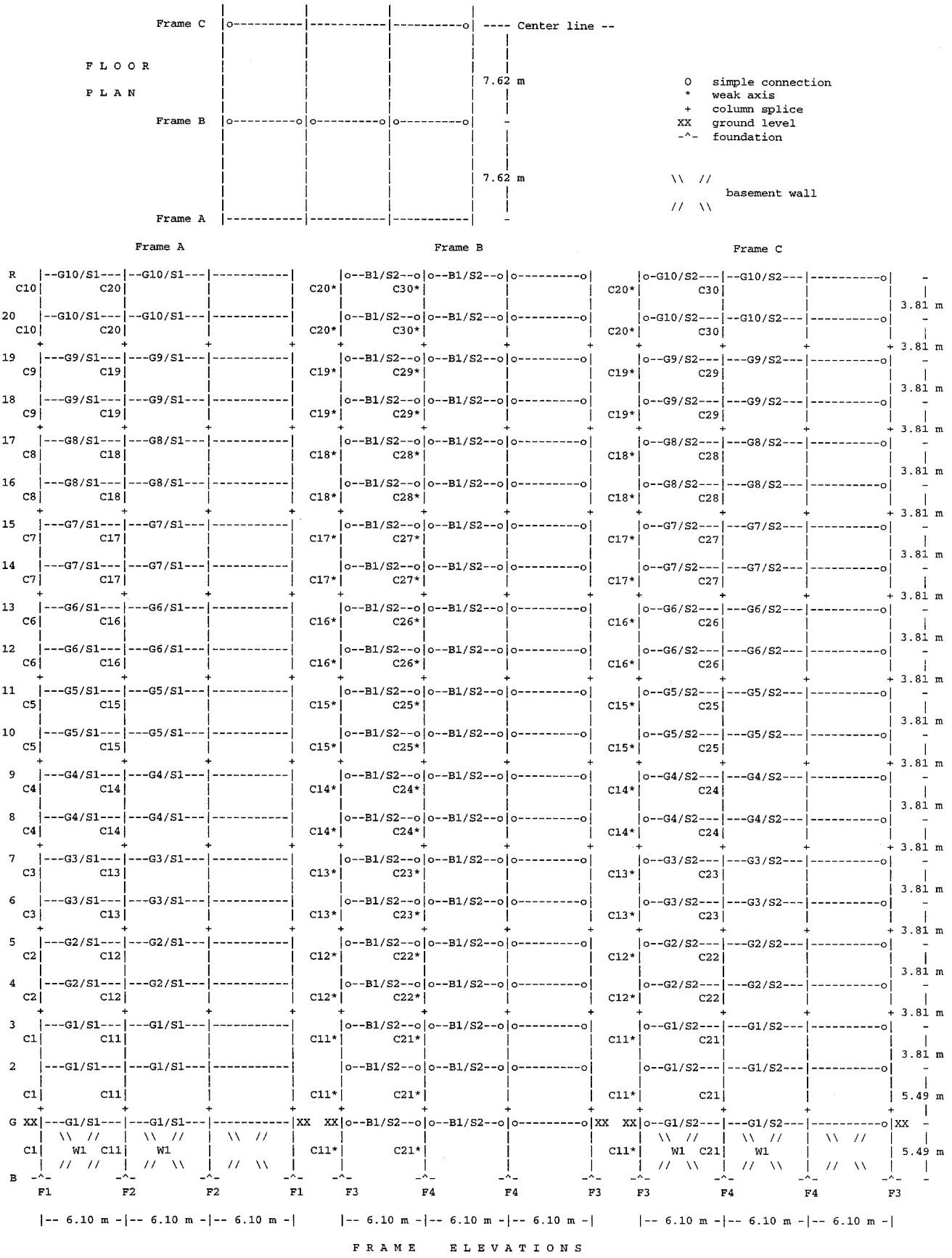

Figure 2.4 Building J20 floor plan and frame elevations.

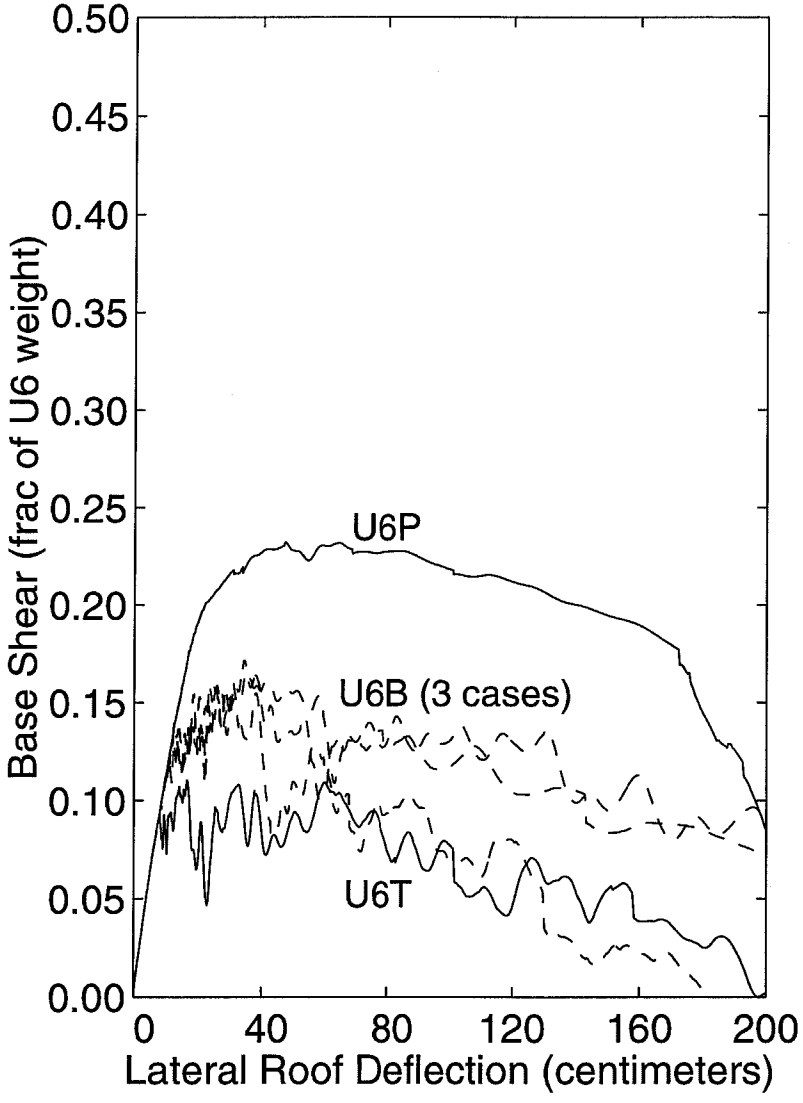

Figure 2.5 Push–over results for U6.

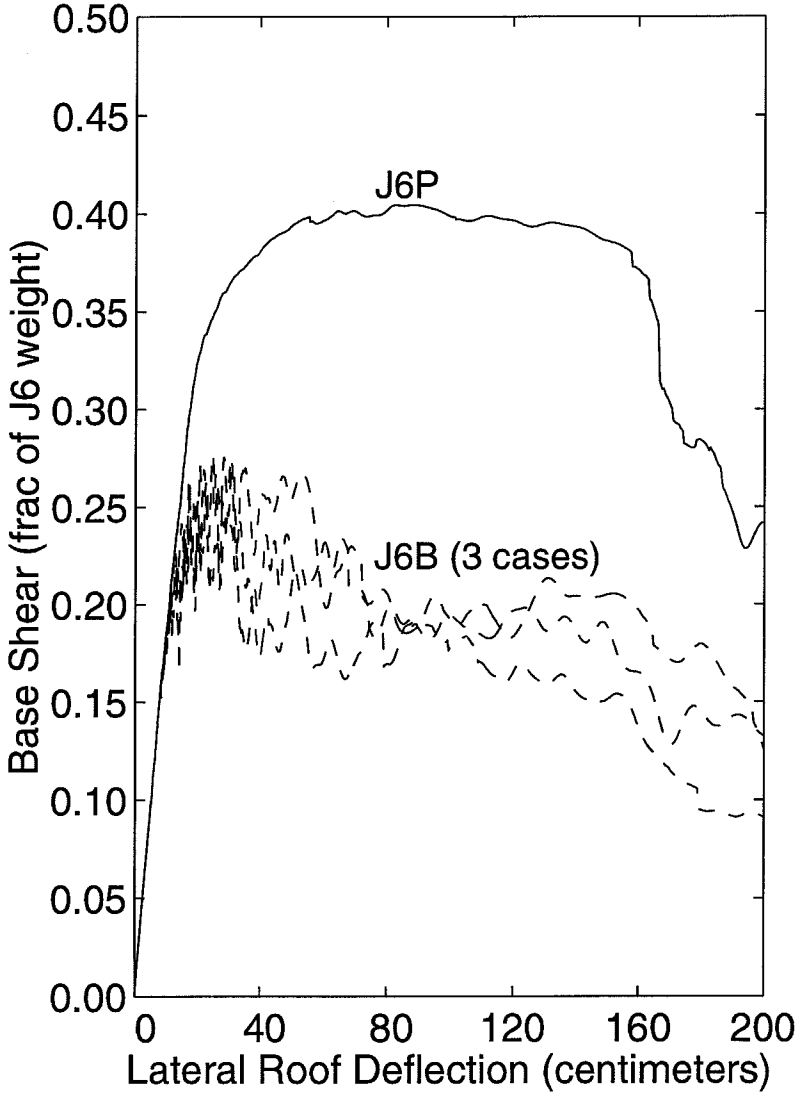

Figure 2.6 Push–over results for J6.

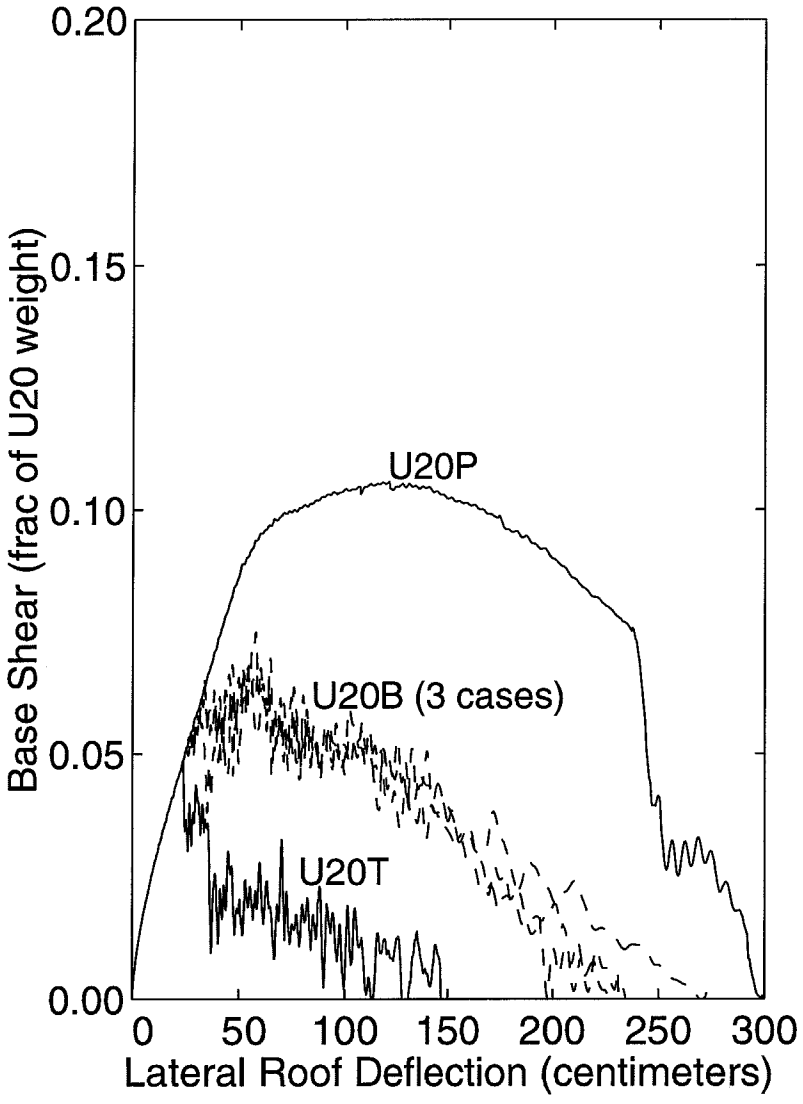

Figure 2.7 Push–over results for U20.

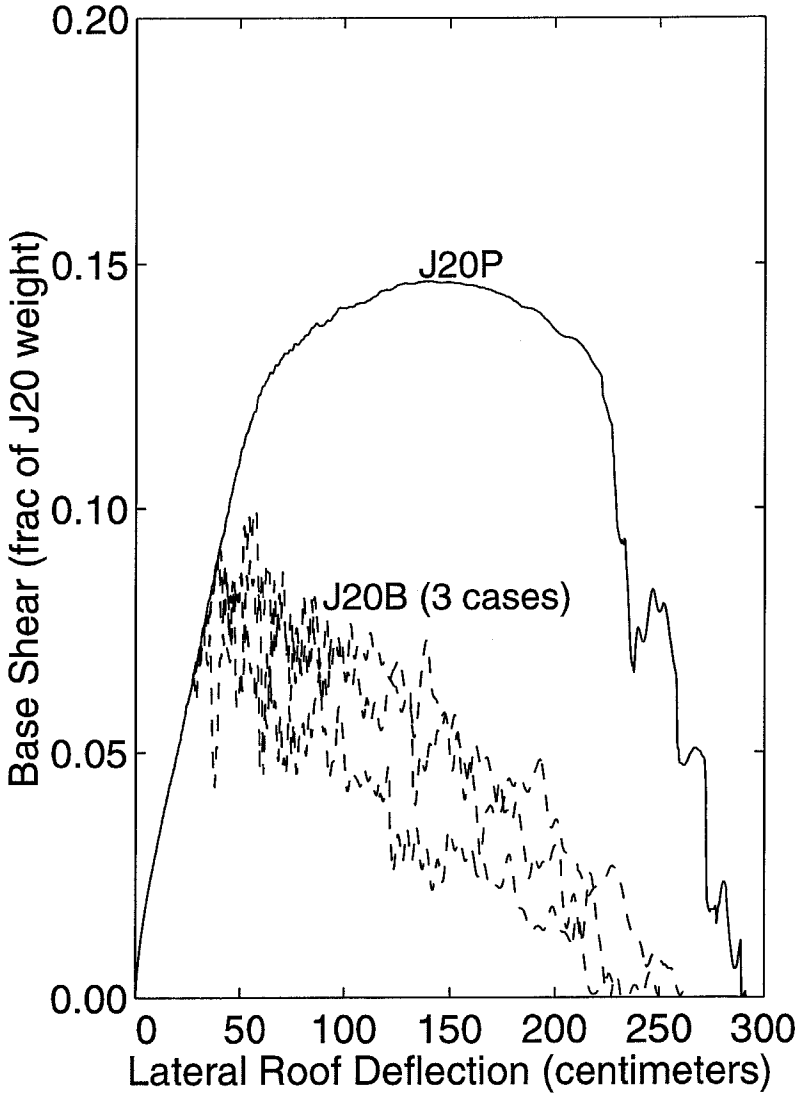

Figure 2.8 Push–over results for J20.

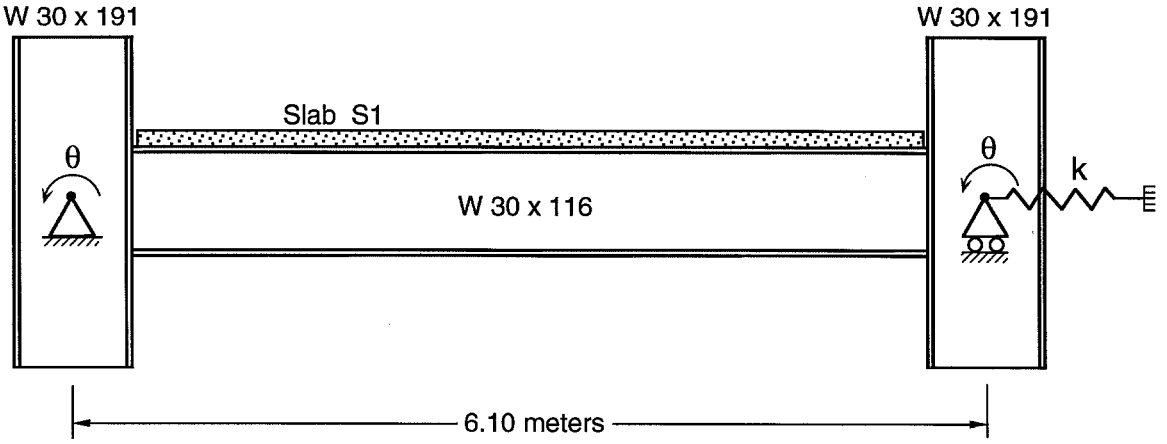

Figure 2.9 Set–up for connection fracture study. The spring stiffness k equals zero for no axial restraint, and k equals infinity for complete axial restraint.

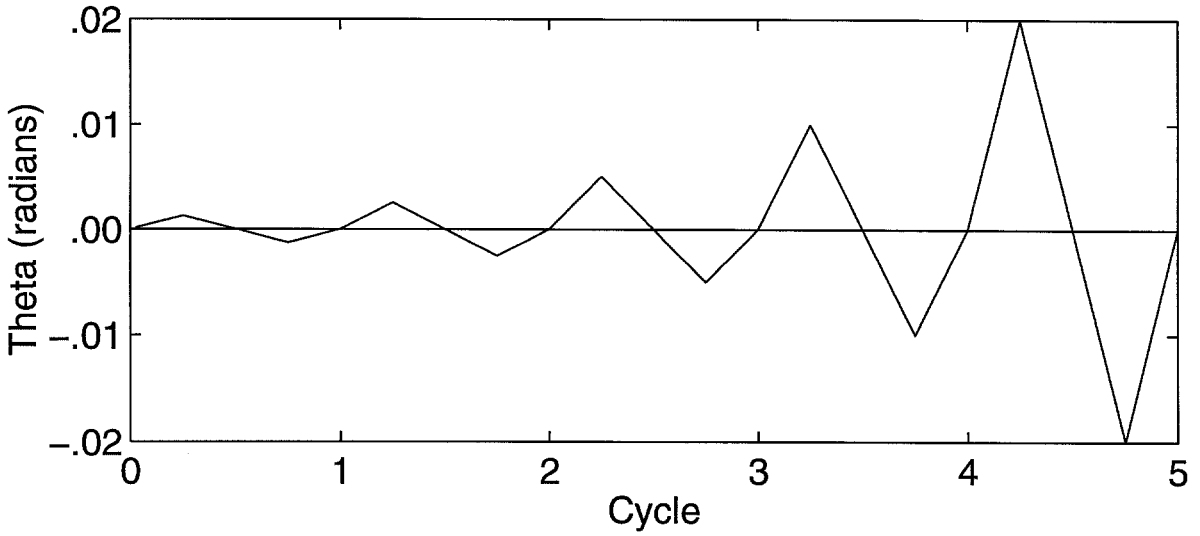

Figure 2.10 End rotation history of beam.

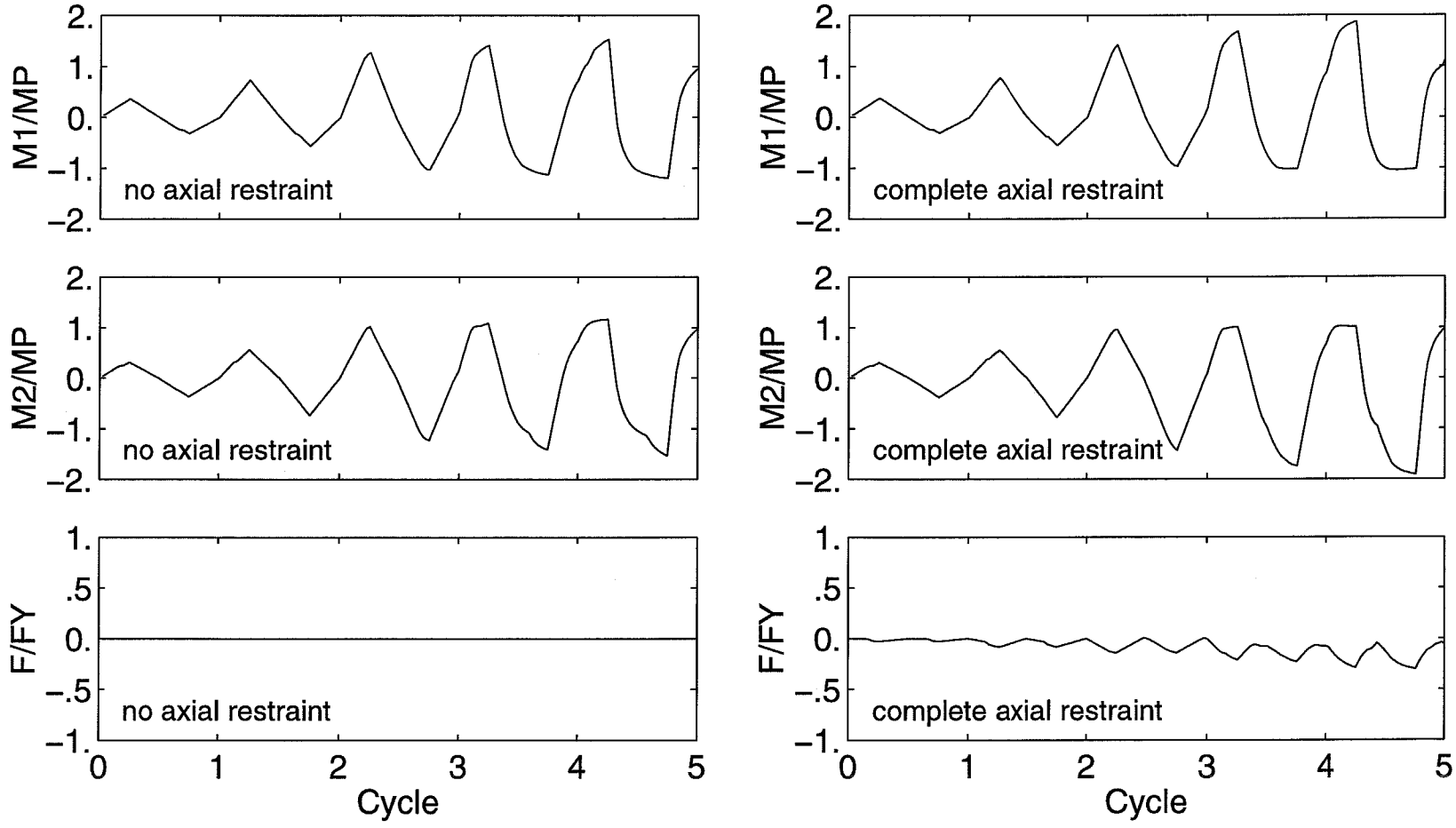

Figure 2.11 Results of bending beam example with perfect connections (Case P).

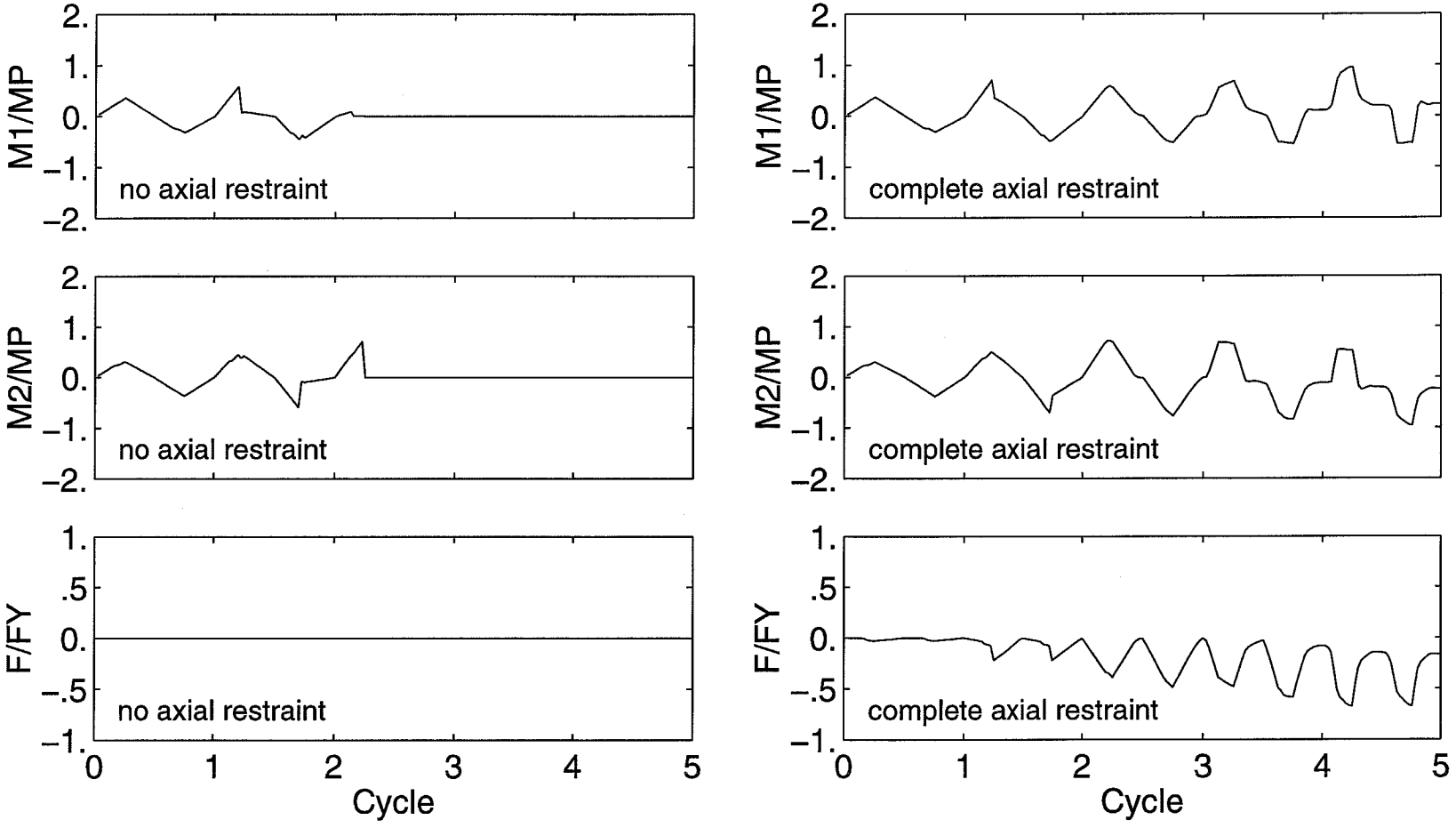

Figure 2.12 Results of bending beam example with fracture-prone connections (Case 1/.7).

Columns

C3	W14X99	C6	W24X84	C9	W14X74
C2	W14X132	C5	W27X114	C8	W14X74
C1	W14X159	C4	W27X161	C7	W14X132

Girders		Beams		Foundations		Slabs	
G3	W24X55	B1	W24X55	F1	150-2.5	S1	1160-7.6
G2	W24X76			F2	153-2.5	S2	2090-7.6
G1	W24X94			F3	161-2.5		
		Walls		F4	247-2.5		
		W1	61 cm thk				

foundations:	K_H-D_{YH} where K_H = horizontal stiffness (tons/cm) and D_{YH} = yield displacement for horizontal (cm). For vertical: $K_V = K_H$, $D_{YD} = D_{YH}$ (down) and $D_{YU} = D_{YH}/2$ (up).
slabs:	A_{10}-h_{10} where A_{10} = effective area (cm^2) and h_{10} = distance from top of girder/beam to centroid of slab (cm).

Table 2.1 Schedules for building U6.

Columns

C3	W14X120	C6	W24X104
C2	W14X176	C5	W27X178
C1	W14X211	C4	W30X211

Girders		Beams		Foundations		Slabs	
G3	W24X84	B1	W24X55	F1	199-2.5	S1	1160-7.6
G2	W27X102			F2	199-2.5	S2	2090-7.6
G1	W30X124			F3	199-2.5		
		Walls		F4	247-2.5		
				F5	199-2.5		
		W1	61 cm thk	F6	247-2.5		

foundations: K_H-D_{YH} where K_H = horizontal stiffness (tons/cm) and D_{YH} = yield displacement for horizontal (cm). For vertical: $K_V = K_H$, $D_{YD} = D_{YH}$ (down) and $D_{YU} = D_{YH}/2$ (up).

slabs: A_{10}-h_{10} where A_{10} = effective area (cm^2) and h_{10} = distance from top of girder/beam to centroid of slab (cm).

Table 2.2 Schedules for building J6.

Columns

C10	W14X109	C20	W21X122	C30	W14X74
C9	W14X132	C19	W24X146	C29	W14X74
C8	W14X159	C18	W24X146	C28	W14X82
C7	W14X176	C17	W24X162	C27	W14X109
C6	W14X211	C16	W24X176	C26	W14X132
C5	W14X257	C15	W24X176	C25	W14X159
C4	W14X283	C14	W27X178	C24	W14X193
C3	W14X311	C13	W27X178	C23	W14X211
C2	W14X342	C12	W27X178	C22	W14X233
C1	W14X370	C11	W30X191	C21	W14X283

Girders		Beams		Foundations		Slabs	
G10	W27X84	B1	W21X50	F1	468-2.5	S1	1160-7.6
G9	W27X94			F2	336-2.5	S2	2090-7.6
G8	W30X99			F3	353-2.5		
G7	W30X108		Walls	F4	534-2.5		
G6	W30X116						
G5	W30X116	W1	61 cm thk				
G4	W30X116						
G3	W30X116						
G2	W30X116						
G1	W30X116						

foundations: K_H-D_{YH} where K_H = horizontal stiffness (tons/cm) and D_{YH} = yield displacement for horizontal (cm). For vertical: $K_V = K_H$, $D_{YD} = D_{YH}$ (down) and $D_{YU} = D_{YH}/2$ (up).

slabs: A_{10}-h_{10} where A_{10} = effective area (cm^2) and h_{10} = distance from top of girder/beam to centroid of slab (cm).

Table 2.3 Schedules for building U20.

Columns

C10	W14X109	C20	W21X122	C30	W21X122
C9	W14X132	C19	W24X146	C29	W24X146
C8	W14X159	C18	W24X162	C28	W24X162
C7	W14X176	C17	W24X176	C27	W27X178
C6	W14X211	C16	W27X178	C26	W30X191
C5	W14X257	C15	W27X178	C25	W30X211
C4	W14X283	C14	W30X191	C24	W30X235
C3	W14X311	C13	W30X191	C23	W30X261
C2	W14X342	C12	W30X211	C22	W30X292
C1	W14X370	C11	W30X235	C21	W30X292

Girders		Beams	Foundations		Slabs	
G10	W27X84	B1 W21X50	F1	468-2.5	S1	1160-7.6
G9	W27X102		F2	336-2.5	S2	2090-7.6
G8	W30X108		F3	353-2.5		
G7	W30X116	Walls	F4	534-2.5		
G6	W30X124					
G5	W30X132	W1 61 cm thk				
G4	W30X132					
G3	W30X132					
G2	W30X132					
G1	W30X132					

foundations: K_H-D_{YH} where K_H = horizontal stiffness (tons/cm) and D_{YH} = yield displacement for horizontal (cm). For vertical: $K_V = K_H$, $D_{YD} = D_{YH}$ (down) and $D_{YU} = D_{YH}/2$ (up).

slabs: A_{10}-h_{10} where A_{10} = effective area (cm^2) and h_{10} = distance from top of girder/beam to centroid of slab (cm).

Table 2.4 Schedules for building J20.

Lev	Sty	W_i	F_{xi}	Drift	Maximum Stress A ECol	A ICol	A Grdr	Min M_p rat A ECol	A ICol
R		176.	16.7				.17	1.3	.8
	6			.15	.13	.22			
6		224.	12.7				.29	2.5	1.6
	5			.22	.20	.32			
5		224.	10.4				.32	1.9	1.3
	4			.23	.22	.33			
4		224.	8.1				.37	2.1	1.5
	3			.25	.27	.38			
3		224.	5.7				.37	1.8	1.4
	2			.25	.27	.32			
2		233.	3.5				.40	1.9	1.7
	1			.25	.39	.52			
G		(241.)	0.0				.17	2.0	1.8
	B			.00	.14	.22			

Lev = floor or roof level
Sty = story
W_i = roof or floor weight
F_{xi} = lateral seismic design force at roof or floor
Weights and forces are in tons for half building only.
Drift = story drift in per cent
ECol = exterior column
ICol = interior column
Grdr = girder
A = Frame A
Stresses are given as fractions of nominal yield.
M_p = plastic moment
M_p rat = ratio of column M_p to girder M_p at a joint

Table 2.5 Seismic design information for building U6.

					Maximum Stress					Minimum M_p rat		
					A	A	A	C	C	A	A	C
Lev	Sty	W_i	F_{xi}	Drift	ECol	ICol	Grdr	ICol	Grdr	ECol	ICol	ICol
R		176.	78.0				.33		.28	.9	.6	.6
	6			.35	.31	.48		.44				
6		244.	63.5				.60		.57	1.8	1.2	1.2
	5			.51	.46	.67		.66				
5		244.	49.2				.77		.75	1.6	1.3	1.2
	4			.51	.43	.52		.51				
4		244.	38.4				.87		.85	1.9	1.7	1.5
	3			.53	.53	.60		.63				
3		244.	28.8				.87		.87	1.5	1.4	1.3
	2			.50	.53	.54		.59				
2		252.	20.3				.95		.95	1.6	1.6	1.4
	1			.51	.77	.98		1.05				
G		(261.)	0.0				.41		.41	1.6	1.7	1.2
	B			.00	.29	.47		.76				

Lev = floor or roof level
Sty = story
W_i = roof or floor weight
F_{xi} = lateral seismic design force at roof or floor
Weights and forces are in tons for half building only.
Drift = story drift in per cent
ECol = exterior column
ICol = interior column
Grdr = girder
A = Frame A, C = Frame C
Stresses are given as fractions of nominal yield.
M_p = plastic moment
M_p rat = ratio of column M_p to girder M_p at a joint

Table 2.6 Seismic design information for building J6.

					Maximum Stress			Min M_p rat	
					A	A	A	A	A
Lev	Sty	W_i	F_{xi}	Drift	ECol	ICol	Grdr	ECol	ICol
R		125.	25.1				.16	.8	.6
	20			.18	.18	.21			
20		161.	6.9				.26	1.5	1.2
	19			.21	.21	.24			
19		161.	6.6				.29	1.4	1.2
	18			.22	.23	.24			
18		161.	6.2				.32	1.5	1.4
	17			.23	.28	.28			
17		161.	5.8				.35	1.5	1.2
	16			.23	.29	.32			
16		161.	5.5				.37	1.6	1.2
	15			.24	.33	.36			
15		161.	5.1				.37	1.5	1.1
	14			.24	.35	.36			
14		161.	4.8				.39	1.5	1.2
	13			.25	.39	.40			
13		161.	4.4				.39	1.5	1.1
	12			.24	.37	.39			
12		161.	4.1				.41	1.6	1.1
	11			.25	.40	.42			
11		161.	3.7				.43	1.8	1.1
	10			.25	.37	.44			
10		161.	3.4				.45	2.0	1.1
	9			.25	.40	.47			
9		161.	3.0				.46	2.1	1.1
	8			.25	.38	.46			
8		161.	2.7				.47	2.2	1.2
	7			.25	.41	.49			
7		161.	2.3				.48	2.2	1.1
	6			.24	.40	.50			
6		161.	1.9				.48	2.3	1.1
	5			.24	.42	.52			
5		161.	1.6				.49	2.4	1.1
	4			.24	.41	.54			
4		161.	1.2				.49	2.5	1.1
	3			.24	.43	.55			
3		161.	0.9				.48	2.6	1.2
	2			.23	.40	.52			
2		168.	0.5				.49	2.7	1.2
	1			.22	.54	.69			
G		(175.)	0.0				.20	3.1	1.5
	B			.00	.22	.21			

Lev = floor or roof level, Sty = story
W_i = roof or floor weight
F_{xi} = lateral seismic design force at roof or floor
Weights and forces are in tons for half building only.
Drift = story drift in per cent
ECol = exterior column, ICol = interior column
Grdr = girder
A = Frame A
Stresses are given as fractions of nominal yield.
M_p = plastic moment
M_p rat = ratio of column M_p to girder M_p at a joint

Table 2.7 Seismic design information for building U20.

					Maximum Stress					Minimum M_p rat		
					A	A	A	C	C	A	A	C
Lev	Sty	W_i	F_{xi}	Drift	ECol	ICol	Grdr	ICol	Grdr	ECol	ICol	ICol
R		125.	41.4				.20		.27	.8	.6	.6
	20			.30	.20	.26		.21				
20		175.	30.6				.34		.37	1.5	1.2	1.2
	19			.38	.30	.36		.32				
19		175.	25.0				.43		.41	1.3	1.1	1.1
	18			.41	.34	.39		.35				
18		175.	22.0				.51		.45	1.4	1.3	1.2
	17			.44	.42	.45		.42				
17		175.	19.8				.57		.50	1.3	1.2	1.1
	16			.45	.45	.48		.45				
16		175.	18.1				.62		.53	1.4	1.2	1.1
	15			.48	.51	.54		.52				
15		175.	16.5				.64		.54	1.3	1.1	1.1
	14			.48	.55	.56		.54				
14		175.	15.1				.68		.56	1.3	1.2	1.2
	13			.50	.61	.61		.59				
13		175.	13.9				.69		.56	1.3	1.1	1.1
	12			.49	.59	.62		.58				
12		175.	12.7				.72		.57	1.4	1.1	1.2
	11			.49	.63	.67		.64				
11		175.	11.5				.71		.58	1.4	1.0	1.1
	10			.49	.60	.69		.63				
10		175.	10.4				.73		.61	1.5	1.0	1.1
	9			.49	.64	.73		.68				
9		175.	9.3				.76		.64	1.5	1.1	1.2
	8			.48	.62	.69		.65				
8		175.	8.3				.79		.67	1.6	1.1	1.2
	7			.48	.67	.72		.70				
7		175.	7.2				.80		.71	1.6	1.1	1.2
	6			.48	.66	.74		.68				
6		175.	6.2				.82		.75	1.6	1.1	1.2
	5			.47	.70	.77		.74				
5		175.	5.2				.83		.78	1.7	1.1	1.3
	4			.46	.67	.72		.70				
4		175.	4.2				.84		.81	1.7	1.2	1.3
	3			.45	.71	.74		.75				
3		175.	3.3				.86		.85	1.8	1.3	1.2
	2			.44	.69	.68		.77				
2		182.	2.4				.88		.93	1.8	1.3	1.1
	1			.41	.92	1.01		1.14				
G		(189.)	0.0				.37		.40	2.3	1.6	1.7
	B			.00	.37	.39		.39				

Lev = floor or roof level, Sty = story
W_i = roof or floor weight
F_{xi} = lateral seismic design force at roof or floor
Weights and forces are in tons for half building only.
Drift = story drift in per cent
ECol = exterior column, ICol = interior column
Grdr = girder
A = Frame A, C = Frame C
Stresses are given as fractions of nominal yield.
M_p = plastic moment
M_p rat = ratio of column M_p to girder M_p at a joint

Table 2.8 Seismic design information for building J20.

				Maximum Stress		
				A	A	A
Lev	Sty	F_{xi}	Drift	ECol	ICol	Grdr
R		3.6				.08
	20		.08	.09	.09	
20		7.1				.15
	19		.11	.13	.14	
19		7.0				.18
	18		.12	.16	.16	
18		6.9				.22
	17		.14	.21	.20	
17		6.9				.25
	16		.16	.23	.25	
16		6.8				.29
	15		.17	.26	.29	
15		6.6				.30
	14		.18	.29	.31	
14		6.5				.33
	13		.19	.32	.34	
13		6.4				.34
	12		.20	.32	.35	
12		6.4				.37
	11		.21	.35	.39	
11		6.3				.40
	10		.22	.33	.42	
10		6.2				.43
	9		.23	.36	.45	
9		6.0				.46
	8		.23	.36	.46	
8		5.9				.47
	7		.24	.39	.48	
7		5.7				.50
	6		.25	.39	.51	
6		5.6				.52
	5		.26	.41	.54	
5		5.4				.54
	4		.26	.40	.56	
4		5.2				.56
	3		.27	.43	.59	
3		4.9				.58
	2		.27	.42	.68	
2		5.6				.60
	1		.27	.58	.77	
G		0.0				.25
	B		.00	.25	.25	

Lev = floor or roof level, Sty = story
F_{xi} = lateral wind design force at roof or floor
Forces are in tons for half building only.
Drift = story drift in per cent
ECol = exterior column
ICol = interior column
Grdr = girder
A = Frame A
Stresses are given as fractions of nominal yield.

Table 2.9 Wind design information for building U20.

3. GROUND MOTIONS

Four sets of ground motions are employed in the earthquake analyses: motions from a simulation of the 1994 Northridge earthquake (M_W 6.7) produced by Dr. David Wald of the USGS, motions from a simulated Kobe earthquake (M_W 6.9) produced by Kajima corporation with assistance from Dr. Wald, motions from a simulated M_W 7.0 Elysian Park earthquake produced by Dr. Wald and Prof. Thomas Heaton of Caltech, and various actual recordings from Northridge, Kobe and other earthquakes. The simulated Northridge motions and most of the actual recordings consist of both horizontal components and the vertical component. The simulated Kobe motions are single horizontal components in the direction perpendicular to the fault. The simulated Elysian Park motions contain both horizontal components, but no vertical component. For use in the planar building analyses, the two horizontal components, when available, are resolved into the single horizontal component that maximizes the peak-to-peak ground velocity.

3.1 Northridge simulation

The first step in the simulation was to determine a source rupture model for the Northridge earthquake that is consistent with the available geodetic, leveling, strong motion, and teleseismic data. This work is described in reference 8. Next, a square grid of target sites was chosen in the near-fault area, in this case 144 sites over an area of approximately 3600 km^2 at a station spacing of about 5 km. Using the source model, long-period ground motions (> 1 second period) were computed for each grid station. The grid of stations used is shown in Figure 3.1 as small circles; open circles depict rock sites and solid circles represent soil sites. Green's functions at rock and soil sites were computed with different velocity structures (8) to better approximate the shallow impedance contrasts.

For each grid station, high frequency (< 1 second period) ground motions were taken from an actual earthquake recording made nearby so as to best approximate the correct directivity, site conditions, and epicentral distance. Locations of the actual recordings are shown as triangles in Figure 3.1, and each of these locations together with its associated group of grid stations are enclosed by a dashed line. A matched pair of filters was used to remove the short periods from the computed records and to remove the long periods from the actual records, and then the pairs of filtered records were summed to produce the final ground motions.

A subset of the 144 grid sites consisting of the inner 10 by 10 grid is used in this

study. Peak ground acceleration, velocity and displacement for the horizontal components (oriented for maximum peak-to-peak velocity) and vertical components are shown in Tables 3.1 and 3.2. For the horizontal component, the largest acceleration is 854 cm/sec^2 at site H06; the largest velocity is 176 cm/sec at site H04; and the largest displacement is 61 cm at site H06. Time histories and pseudo-acceleration response spectra (5% damping) for sites E06, F08 and H06 are presented in Figures 3.2 to 3.4. For reference, in the pseudo-acceleration plots, the first-mode periods of the Case-P buildings are marked.

The highest ground motions produced in the simulation are due to near-source effects, but they also occur at soil sites where some amplification of the motion takes place. Rupture on the fault starts at the epicenter, located between grid sites C07 and D07, and propagates to the north within the sector between northeast and northwest. The region in this direction where the extended fault plane intersects the ground surface is where the strong near-source effects are found.

3.2 Kobe simulation

The procedure again involved an inversion to determine the source rupture model (9) and a forward calculation to determine long-period ground motions (> 1 second period) for a linear grid along the fault consisting of 50 stations at a half-kilometer spacing. Ground motions at stations away from the fault line were generated by Kajima using a two-step procedure. At stations 1, 3, ... 45, cross-sections were constructed that modelled a step, or structural boundary, in the subsurface topography consisting of rock on the inland side of the boundary and sediment on the seaward side. Ground motions at the surface of these 23 cross-sections were computed by a hyper-element method using the originally generated rock motions as input. Each cross-section extended 1.1 km inland from the boundary and 3.1 km seaward, and the grid spacing was 0.1 km. Then all of these motions were fed into a one-dimensional nonlinear soil column at each site to account for soft soils at the surface. Details of the Kobe ground motion simulation can be found in reference 10.

A subset of these sites, consisting of a grid of 7 sites perpendicular to the fault (0.5 km spacing) by 12 sites parallel to the fault (2 km spacing) is shown in Figure 3.5. Peak ground accelerations, velocities and displacements for the fault-perpendicular components of the ground motions at the 84 sites of Figure 3.5 are listed in Table 3.3. The largest acceleration is 543 cm/sec^2 at site 5/F1; the largest velocity is 141 cm/sec at site 6/F1; and the largest displacement is 58 cm at site 6/F1. Time histories and pseudo-acceleration response spectra (5% damping) for sites 6/B3, 6/D2 and 6/F1 are presented in Figures 3.6 to 3.8.

The source model determination (9) showed that the fault rupture was bi-lateral

with at least half of the energy directed away from Kobe. This reduced the near-source effects experienced in Kobe below what could be expected from a M_W 6.9 earthquake with a uni-lateral rupture.

3.3 Elysian Park simulation

This hypothetical event is consistent with a possible M_W 7.0 earthquake on the Elysian Park blind-thrust fault directly beneath Los Angeles. Geometry of the simulation is shown in Figure 3.9. The fault dips 23 degrees to the north in a vertically stratified crustal model that approximates the rock properties in the Los Angeles Basin. The rupture surface is 35 km long and 18 km wide and is confined to depths between 9 and 16 km.

As details of the simulation are discussed in reference 6, only a short summary is included here. The procedure is similar to that used for the Northridge earthquake in that the long periods (>1 second) are computed deterministically by a Green's function approach and the short periods are taken from actual recordings. The fault slip history is that determined previously for the Homestead Valley segment of the 1992 Landers earthquake adjusted to fit the characteristics of the subject earthquake. Resulting average and peak slips for the simulation are 2.2 m and 5.1 m, respectively, and the direction of the rupture propagation is up-fault. The actual recordings supplying the short periods are from the 1994 Northridge earthquake; the free-field record at the Olive View Hospital is used for sites in the direction of the rupture propagation, and the Stone Canyon Reservoir record is used elsewhere.

Ground motions are simulated on the rectangular grid of sites in Figure 3.9, 11 stations by 11 stations at a 5 km grid spacing covering 3025 km^2. Peak ground accelerations, velocities and displacements for the horizontal components (oriented for maximum peak-to-peak velocity) at the 121 sites of Figure 3.9 are listed in Table 3.4. The largest acceleration is 1040 cm/sec^2 at site I05; the largest velocity is 180 cm/sec at site H05; and the largest displacement is 200 cm at site D05. The area that experiences a peak displacement over 1 meter is about 600 km^2 in extent, and over most of this area the peak velocity exceeds 1 m/sec. Time histories and pseudo-acceleration response spectra (5% damping) for sites C05, G04 and H05 are presented in Figures 3.10 to 3.12.

As seen from the figures, ground motions at many of the sites located in the direction toward which the rupture propagates are dominated by a large forward-and-back displacement pulse, this being the near-source effect. This displacement reaches an amplitude of 2 meters at one site and is much greater than any ground displacement associated with the Northridge and Kobe earthquakes. The size of this displacement owes to the uni-lateral nature of the fault rupture and to the larger magnitude of the earthquake.

3.4 Various records

Twenty records, including 17 from actual earthquakes and three from simulated earthquakes, are used in this study and are listed below.

earthquake	record	designation	hor comp	ver?	figure
Northridge simulation	Grid site H06	H06	PPV	yes	3.4
Kobe simulation	Grid site 6/F1	6/F1	fault per	no	3.8
Elysian Park simulation	Grid site C05	C05	PPV	no	3.10
1940 Imperial Valley	ElCentro	ELC	N-S	no	3.13
1989 Loma Prieta	Lexington Dam	LEX	PPV	yes	3.14
1989 Loma Prieta	Los Gatos Pres Center	LGP	PPV	yes	3.15
1992 Landers	Lucerne Valley	LUC	PPV	yes	3.16
1994 Northridge	Rinaldi Receiving Sta.	RRS	PPV	yes	3.17
1994 Northridge	Olive View Hosp ff	OVH	PPV	yes	3.18
1995 Kobe	Higashi-Kobe Bridge GL	EKB	PPV	yes	3.19
1995 Kobe	Fukiai	FKI	PPV	no	3.20
1995 Kobe	Kobe JMA	JMA	PPV	yes	3.21
1995 Kobe	PHRI Office	KBH	PPV	yes	3.22
1995 Kobe	Kobe University	KBU	PPV	yes	3.23
1995 Kobe	PHRI DAI8	KH8	PPV	yes	3.24
1995 Kobe	Juto Shin-Nagata B1F	NGT	PPV	yes	3.25
1995 Kobe	NTT B3F	NTT	PPV	yes	3.26
1995 Kobe	Takenaka Shin-Kobe B3	SKB	PPV	yes	3.27
1995 Kobe	Shin-Kobe Henden	SSS	PPV	yes	3.28
1995 Kobe	Takatori	TAK	PPV	yes	3.29

The designation PPV means that the horizontal component used is the one that maximizes the peak-to-peak ground velocity. Record H06 from the Northridge simulation set discussed in Section 3.1, record 6/F1 from the Kobe simulation set discussed in Section 3.2, and record C05 from the Elysian Park simulation set discussed in Section 3.3 are the largest, or close to the largest, records from the respective simulations. The eleven actual Kobe records are a reasonable sample of the ground motions in that city, and most of these records were provided by Kajima corporation. Some of these records contain amplifications from soft soils. The locations where the Kobe records were obtained are shown on the map in Figure 3.5.

The listed figures present time histories of acceleration, velocity and displacement along with pseudo-acceleration response spectra (5% damping). Integrating the records

produces drifts in some cases, and no corrections to eliminate the drifts are made. All of the drifts are slow and do not affect the computed responses.

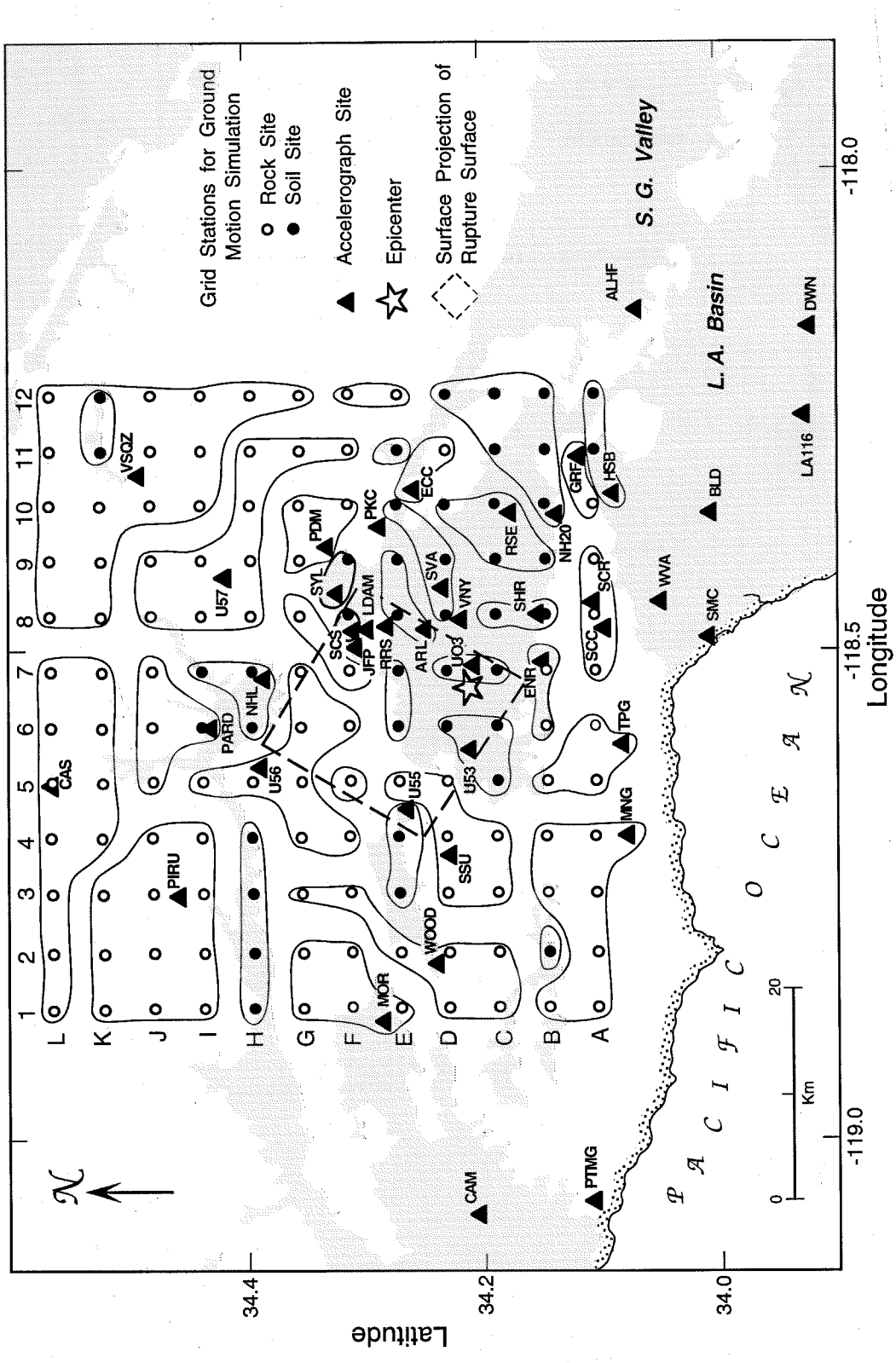

Figure 3.1 Map of San Fernando Valley and vicinity showing 144 grid stations for the ground motion simulation. The shaded zones are basin areas.

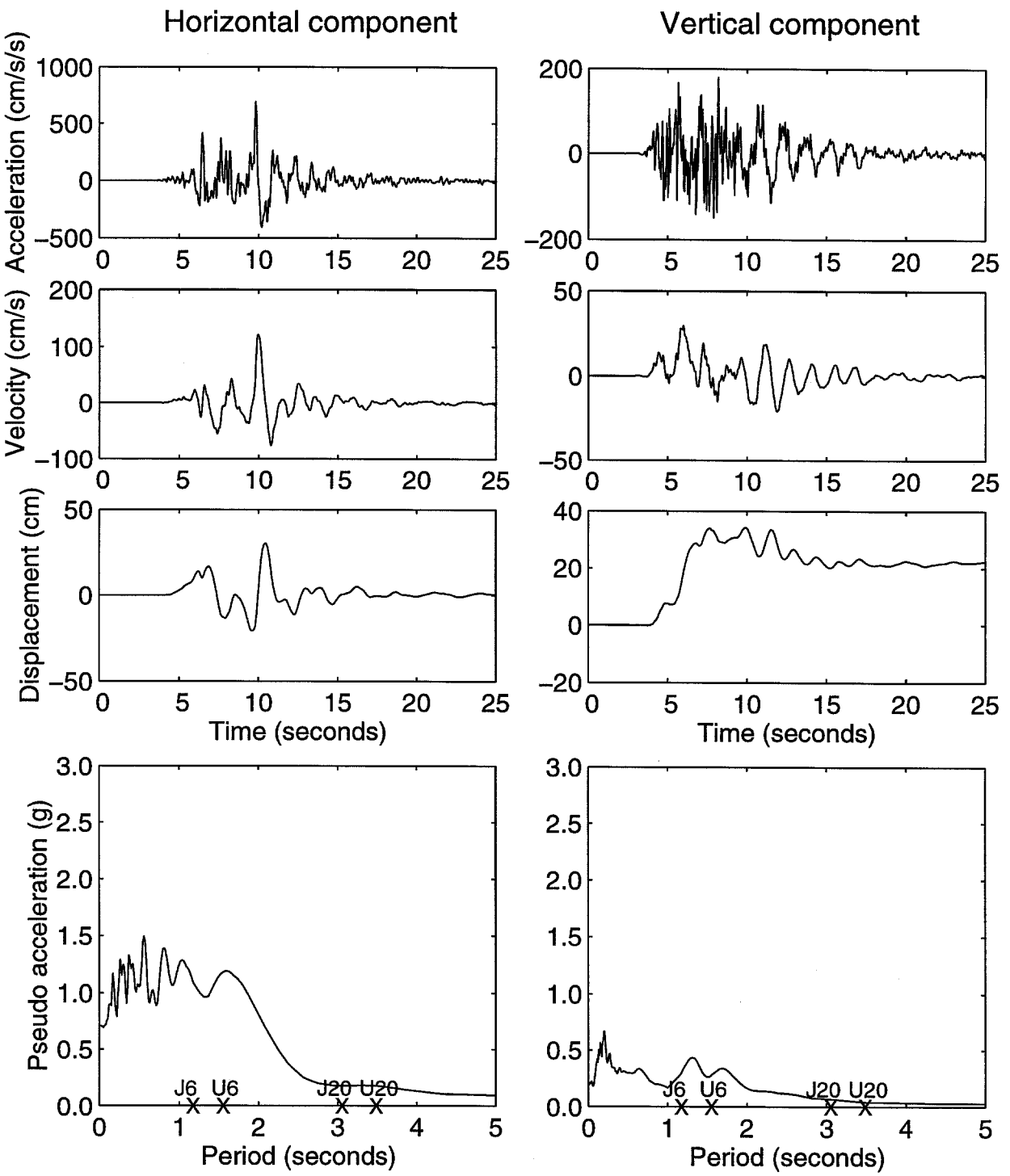

Figure 3.2 E06 ground motion time histories and pseudo acceleration from the simulated Northridge earthquake.

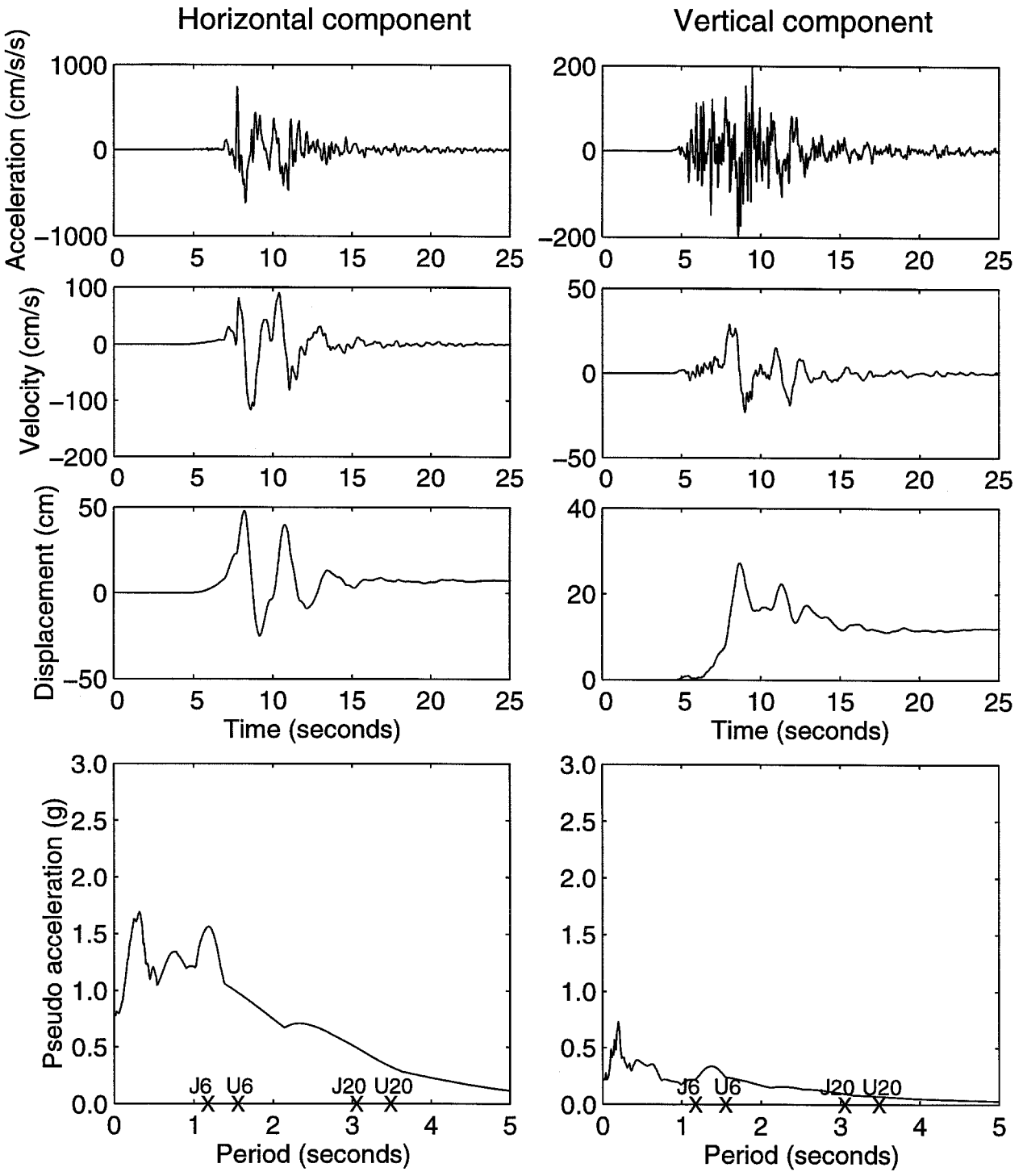

Figure 3.3 F08 ground motion time histories and pseudo acceleration from the simulated Northridge earthquake.

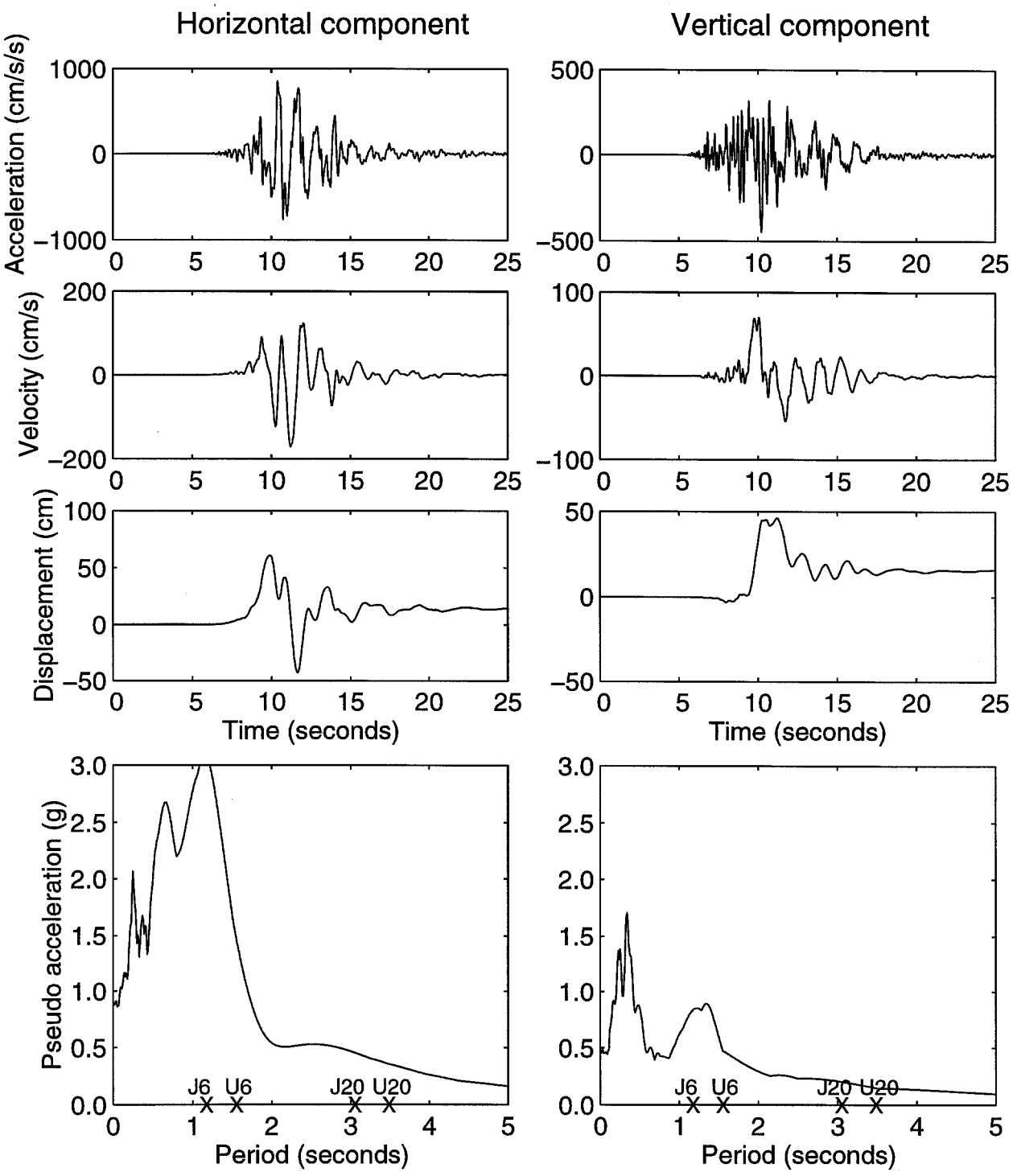

Figure 3.4 H06 ground motion time histories and pseudo acceleration from the simulated Northridge earthquake.

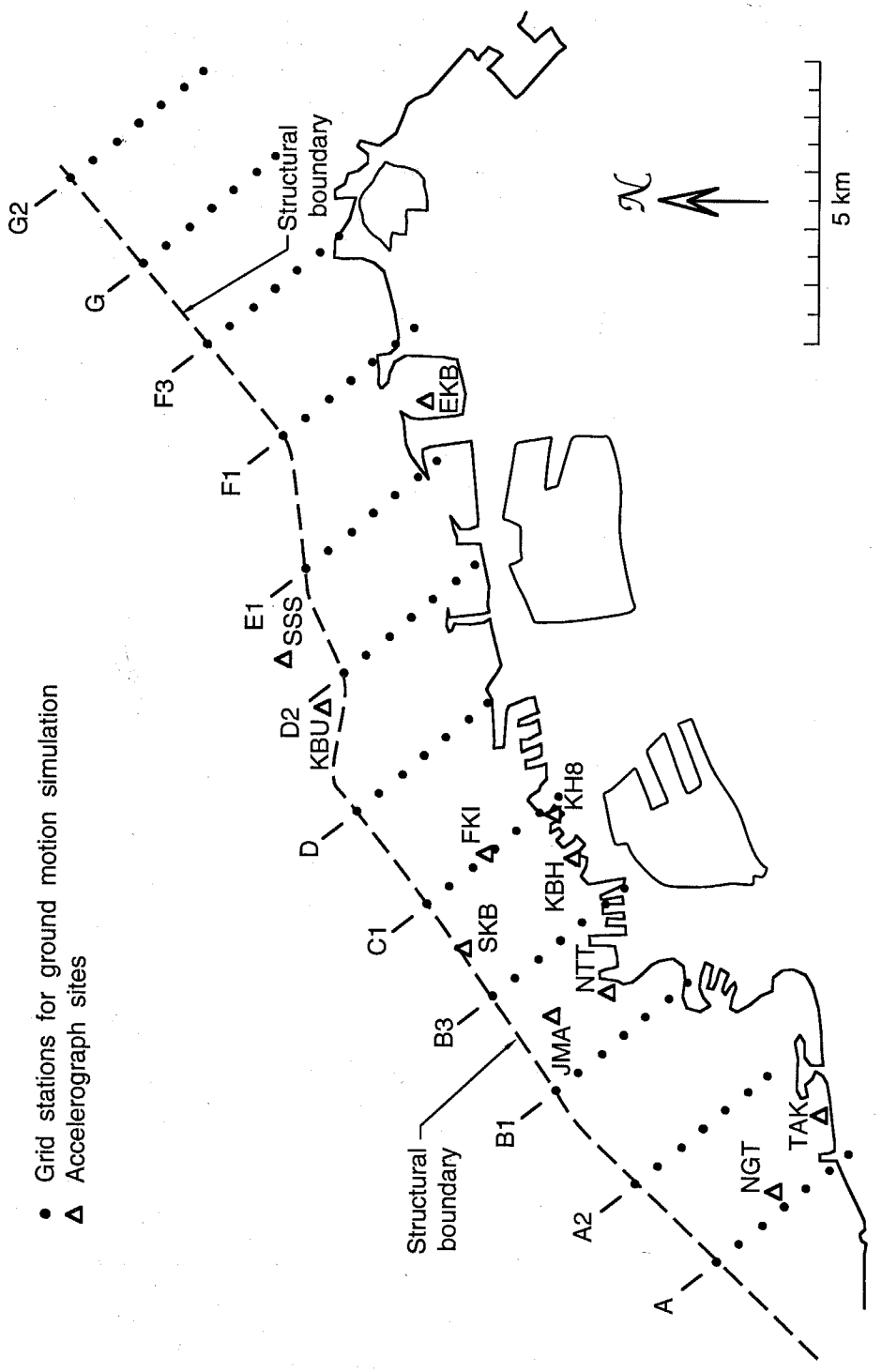

Figure 3.5 Map of Kobe showing 84 grid stations for the ground motion simulation and 11 accelerograph sites where actual ground motions were recorded.

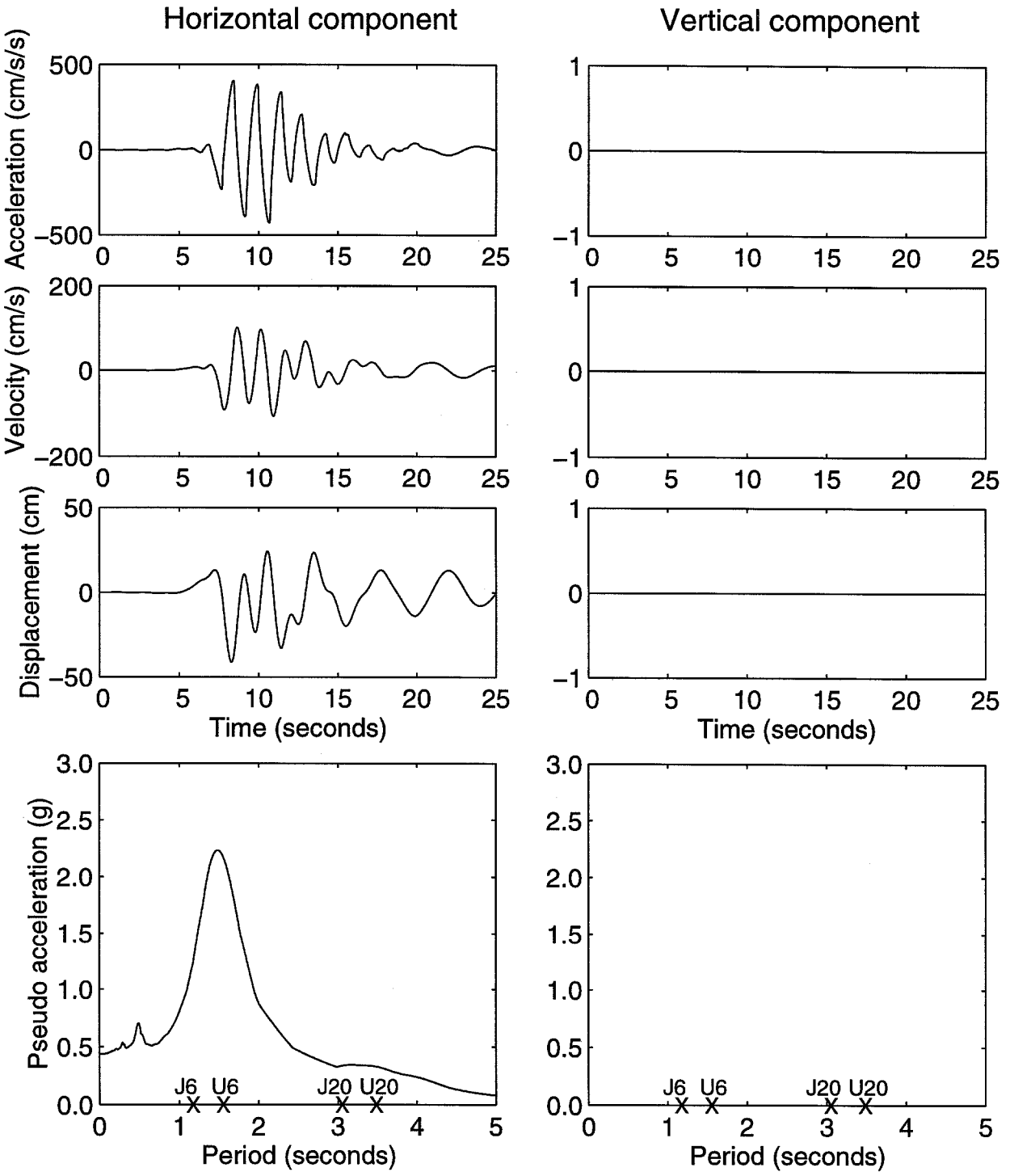

Figure 3.6 6/B3 ground motion time histories and pseudo acceleration from the simulated Kobe earthquake.

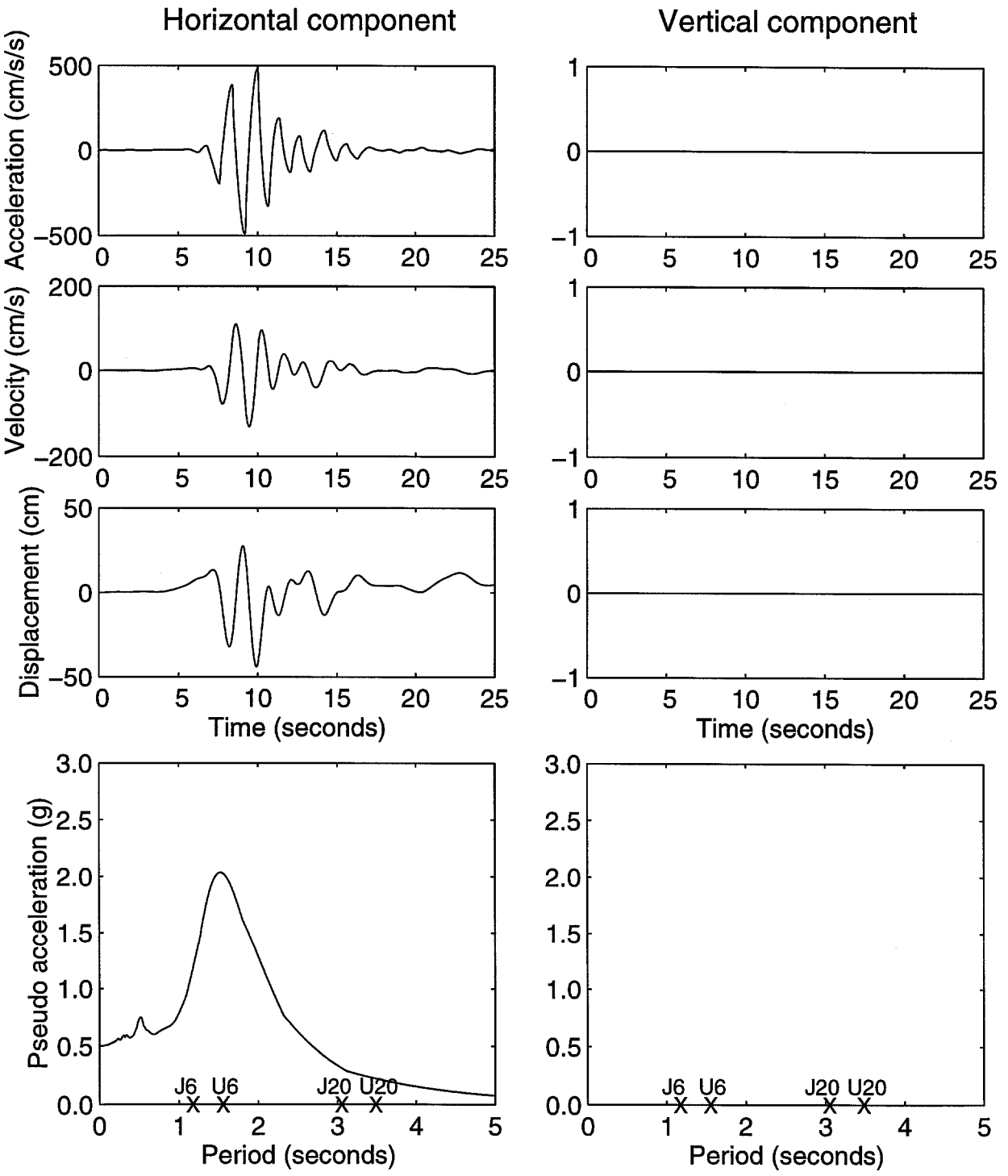

Figure 3.7 6/D2 ground motion time histories and pseudo acceleration from the simulated Kobe earthquake.

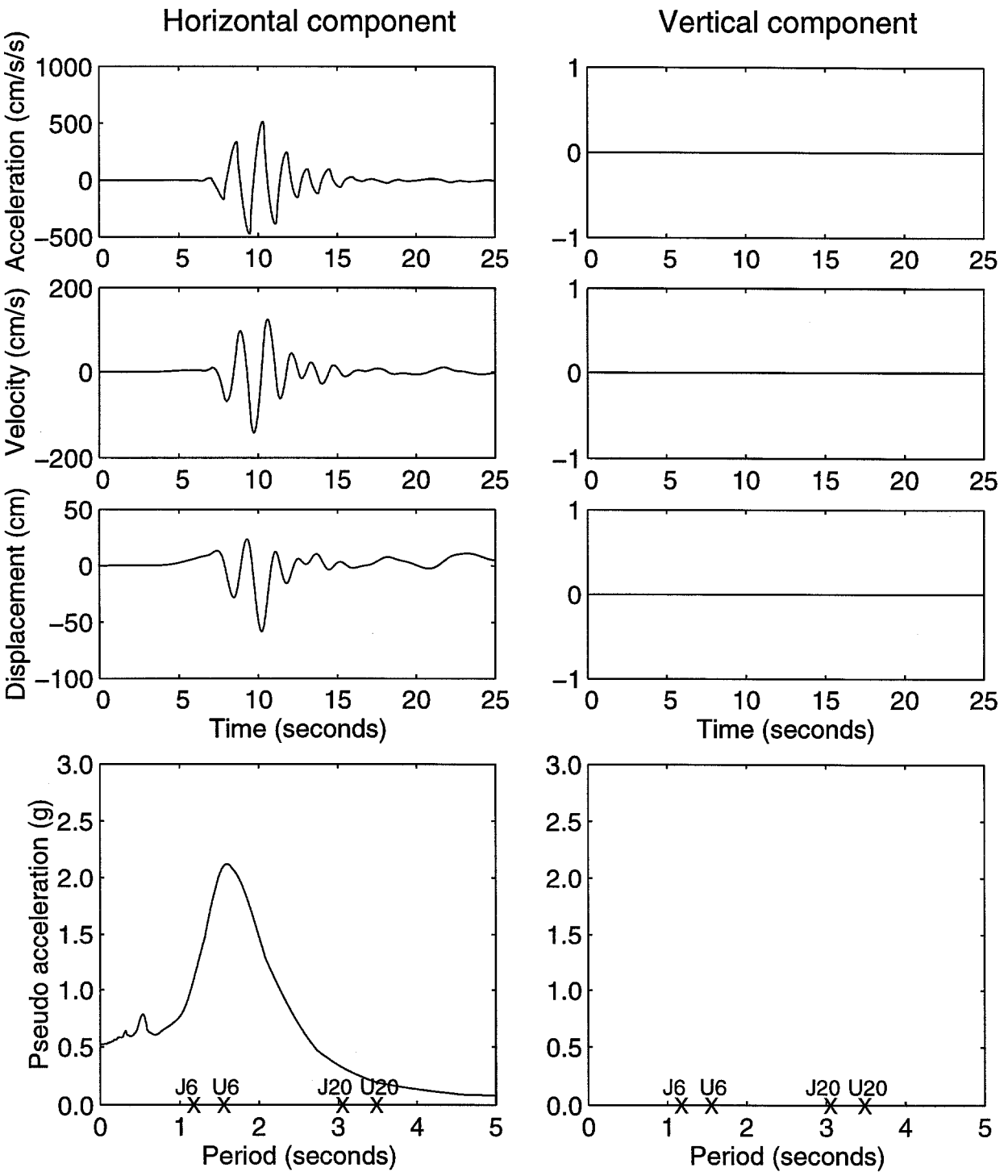

Figure 3.8 6/F1 ground motion time histories and pseudo acceleration from the simulated Kobe earthquake.

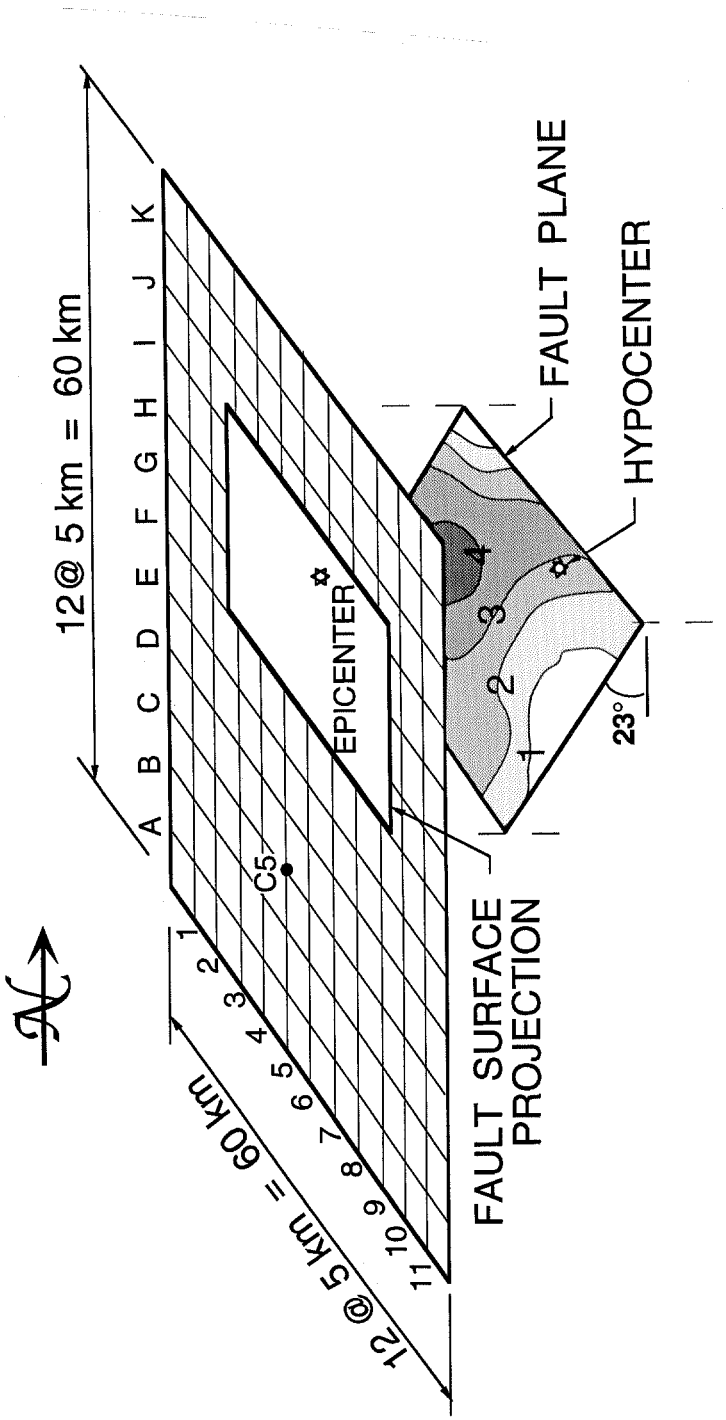

Figure 3.9 Details of the M_W 7.0 Elysian Park earthquake simulation showing the dipping fault plane, contours of fault slip in meters, and 121 grid stations where motions are computed.

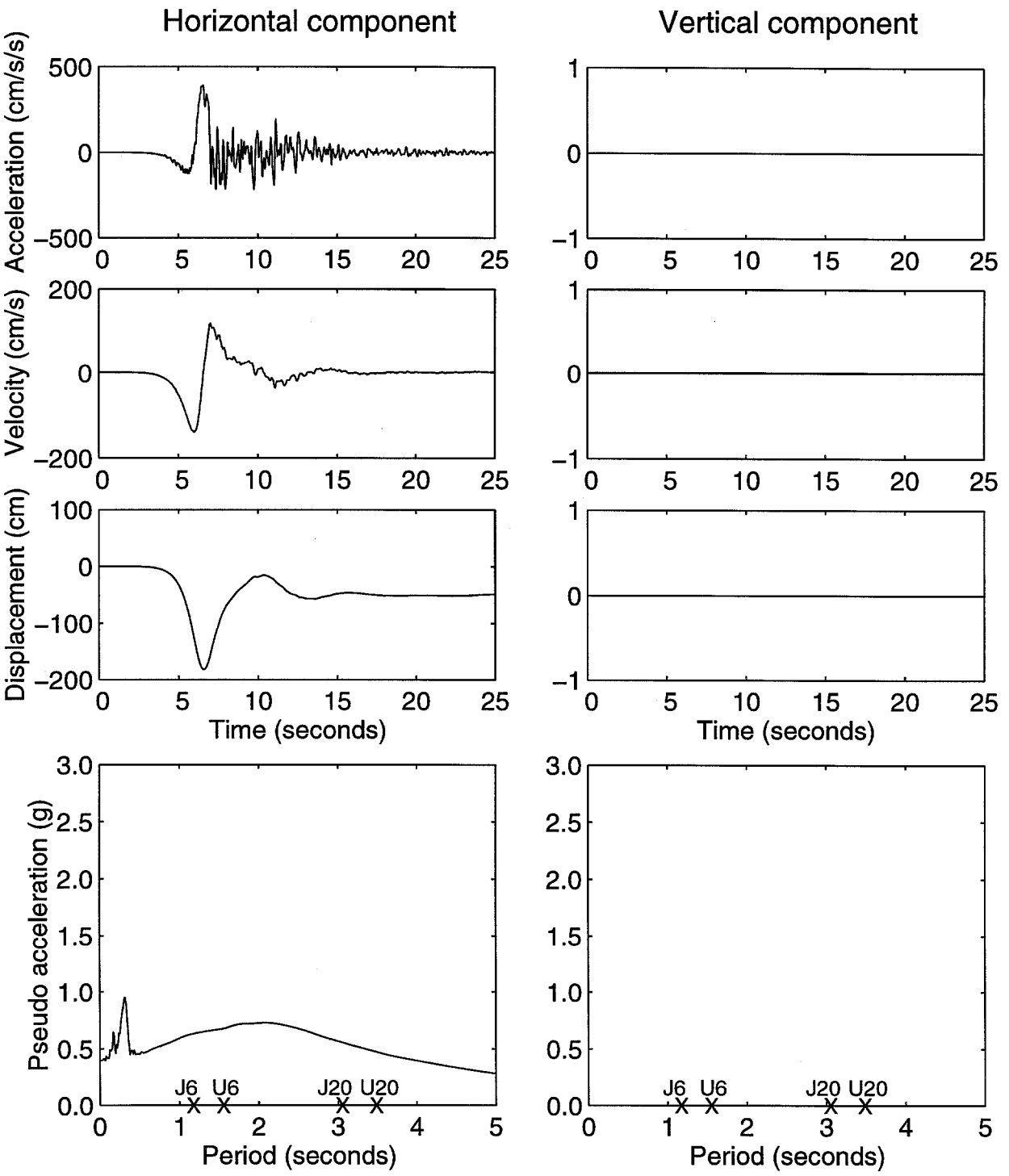

Figure 3.10 C05 ground motion time histories and pseudo acceleration from the simulated Elysian Park earthquake.

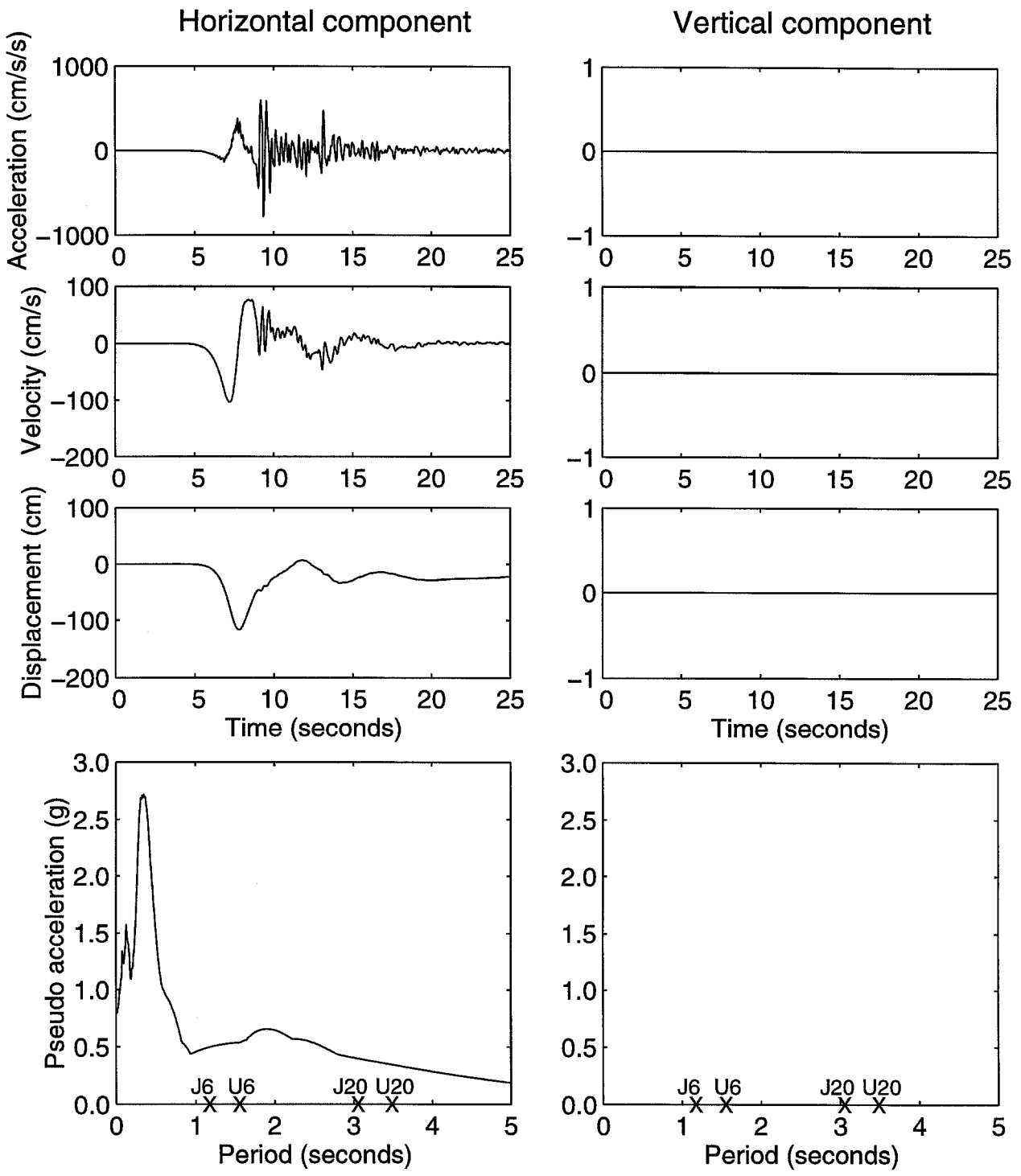

Figure 3.11 G04 ground motion time histories and pseudo acceleration from the simulated Elysian Park earthquake.

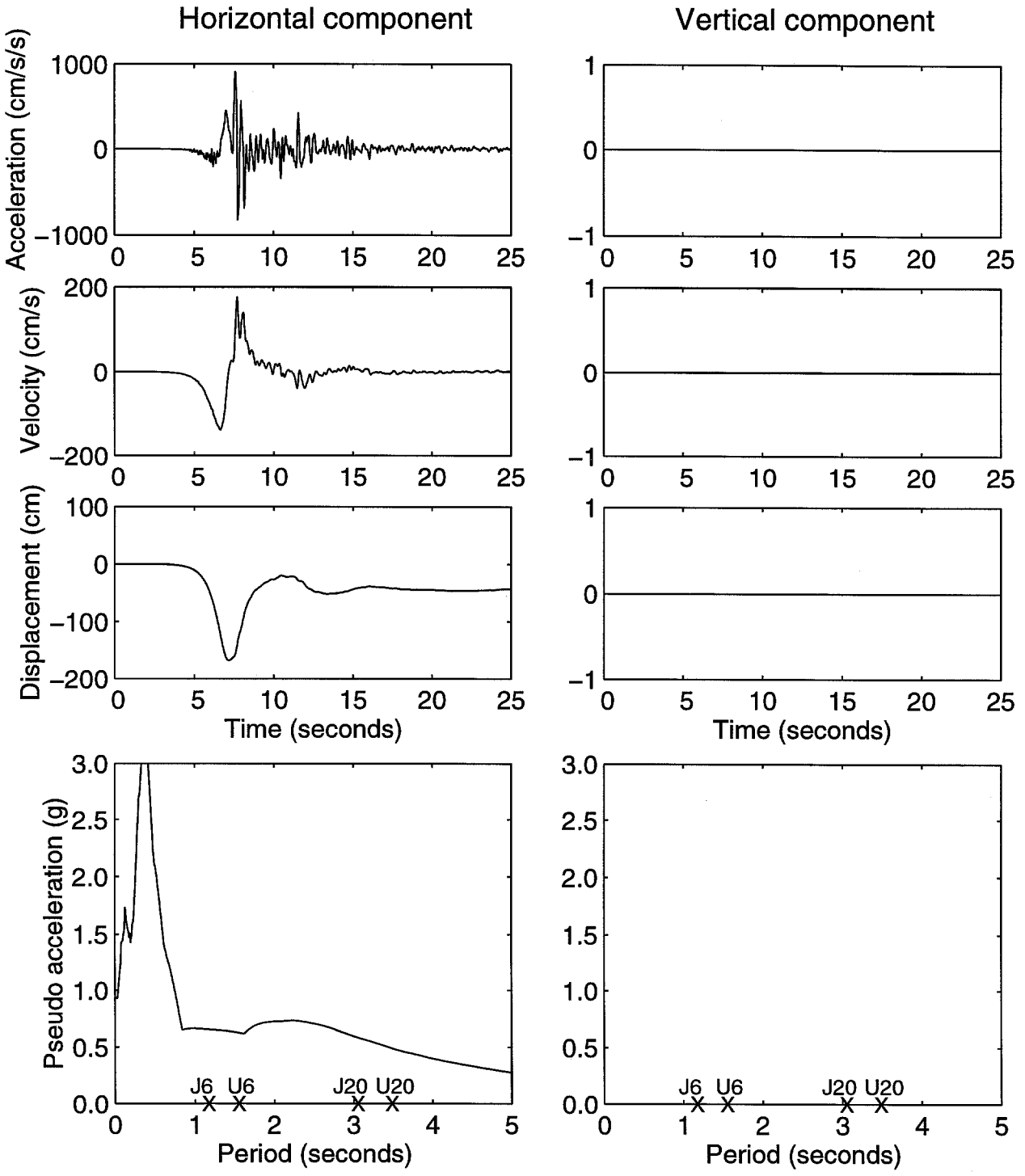

Figure 3.12 H05 ground motion time histories and pseudo acceleration from the simulated Elysian Park earthquake.

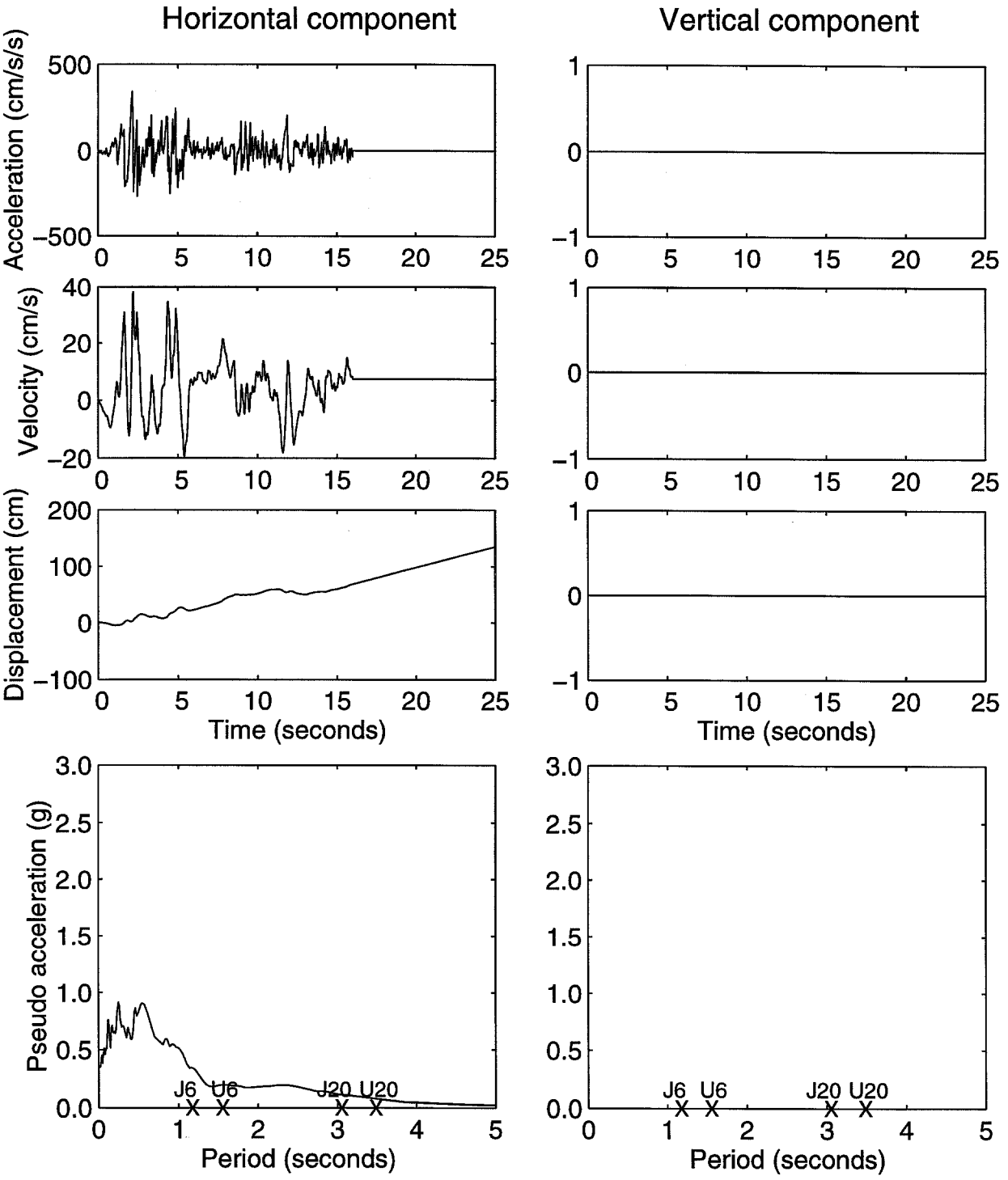

Figure 3.13 ELC ground motion time histories and pseudo acceleration from the 1940 Imperial Valley earthquake.

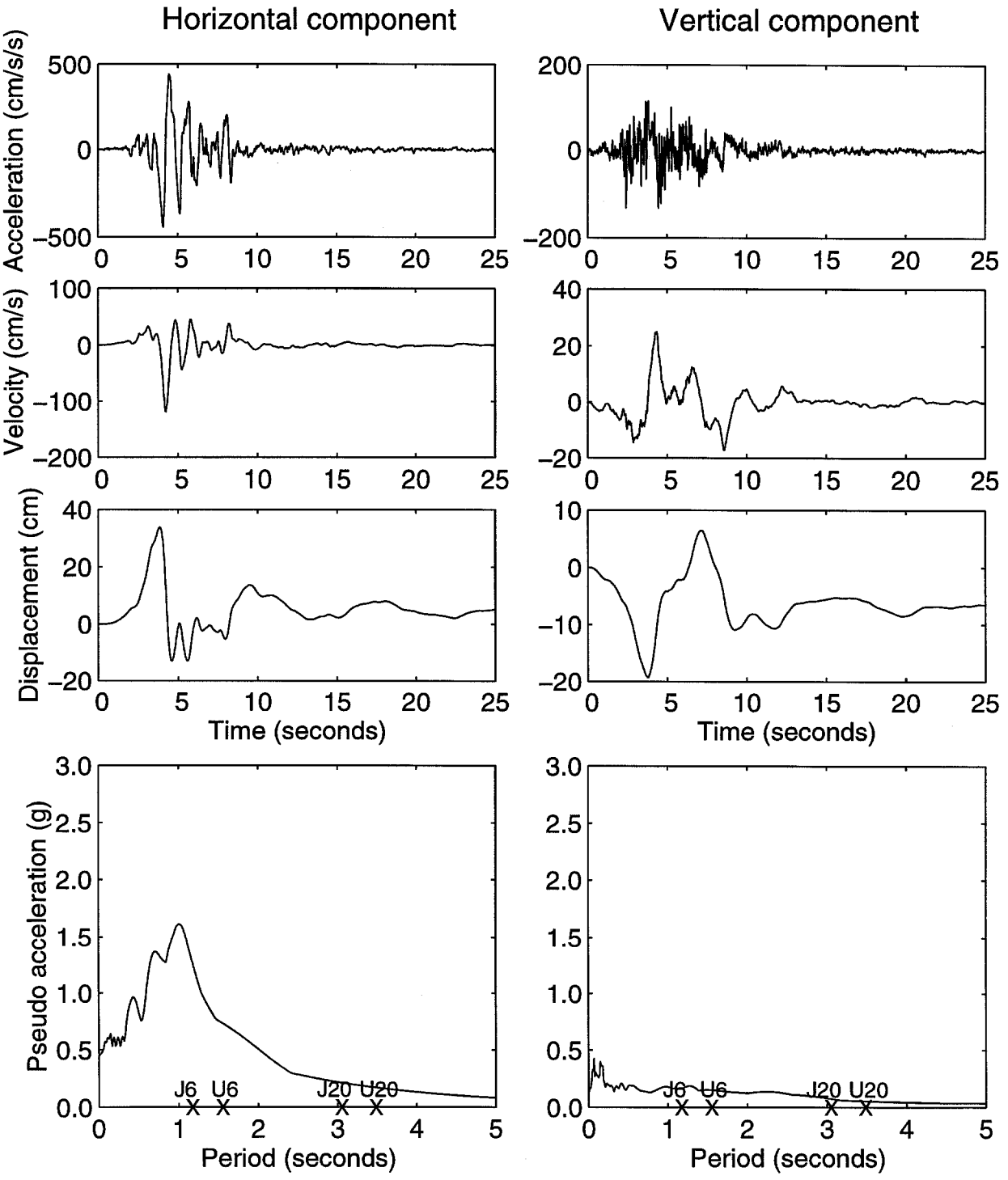

Figure 3.14 LEX ground motion time histories and pseudo acceleration from the 1989 Loma Prieta earthquake.

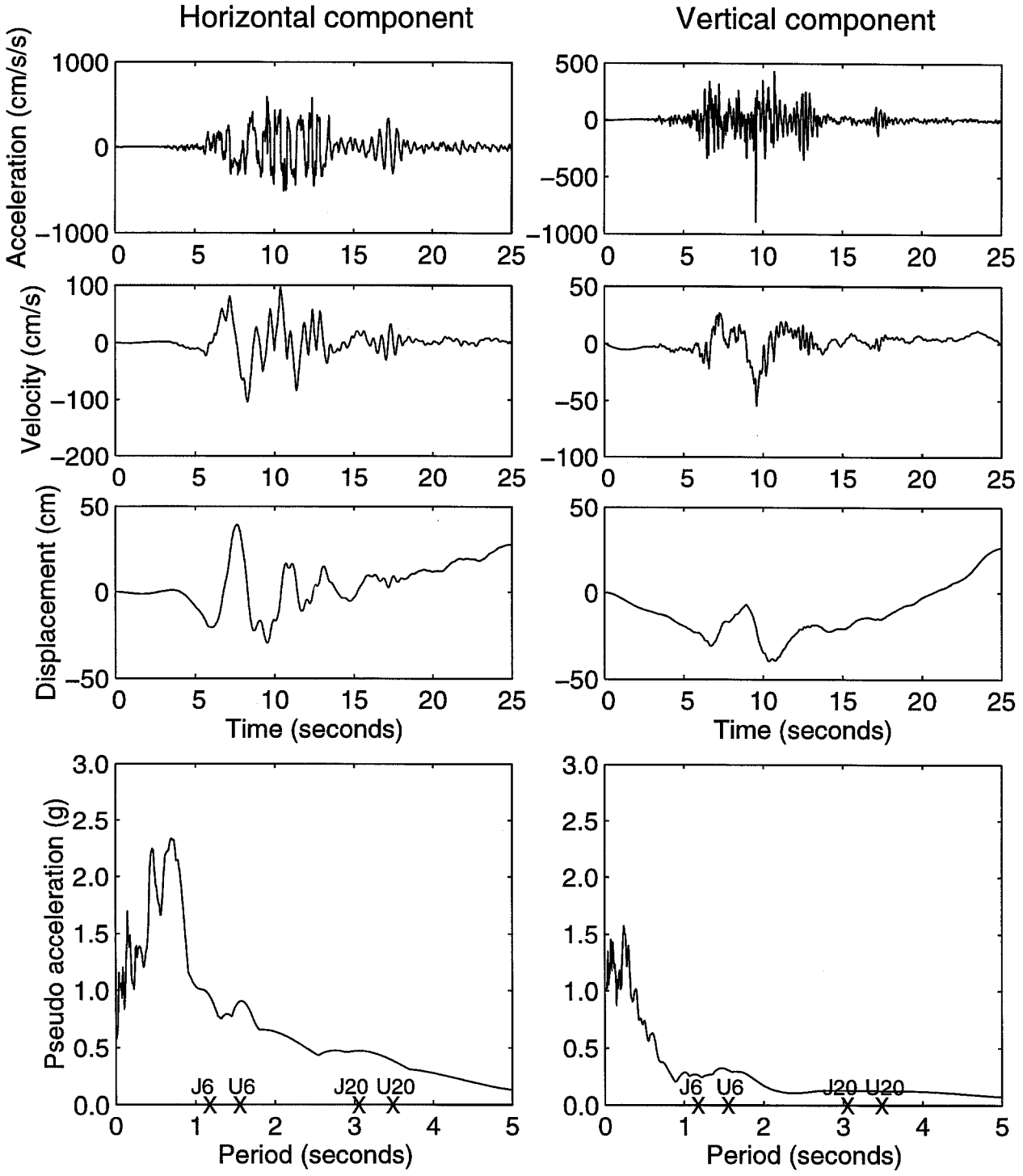

Figure 3.15 LGP ground motion time histories and pseudo acceleration from the 1989 Loma Prieta earthquake.

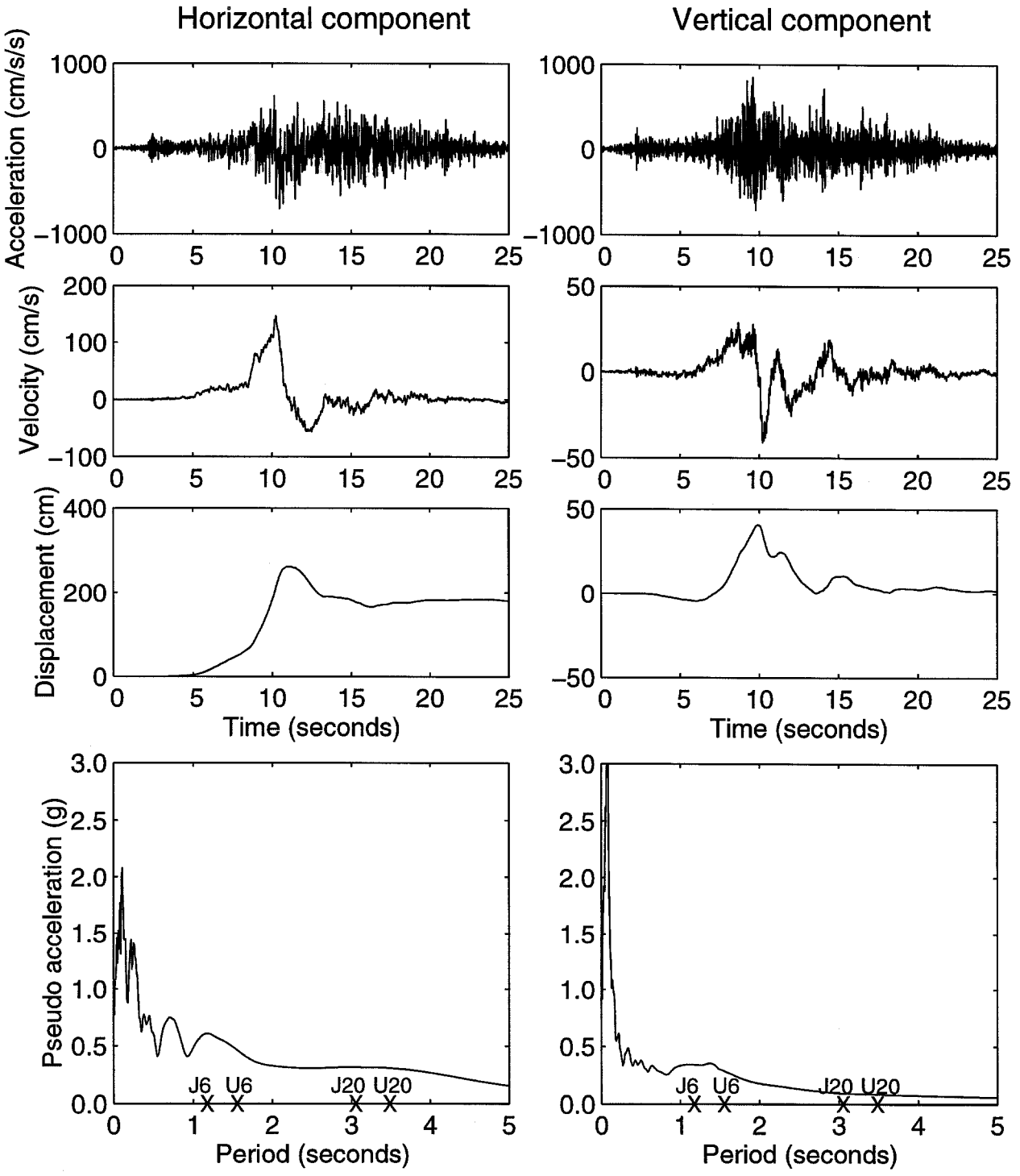

Figure 3.16 LUC ground motion time histories and pseudo acceleration from the 1992 Landers earthquake.

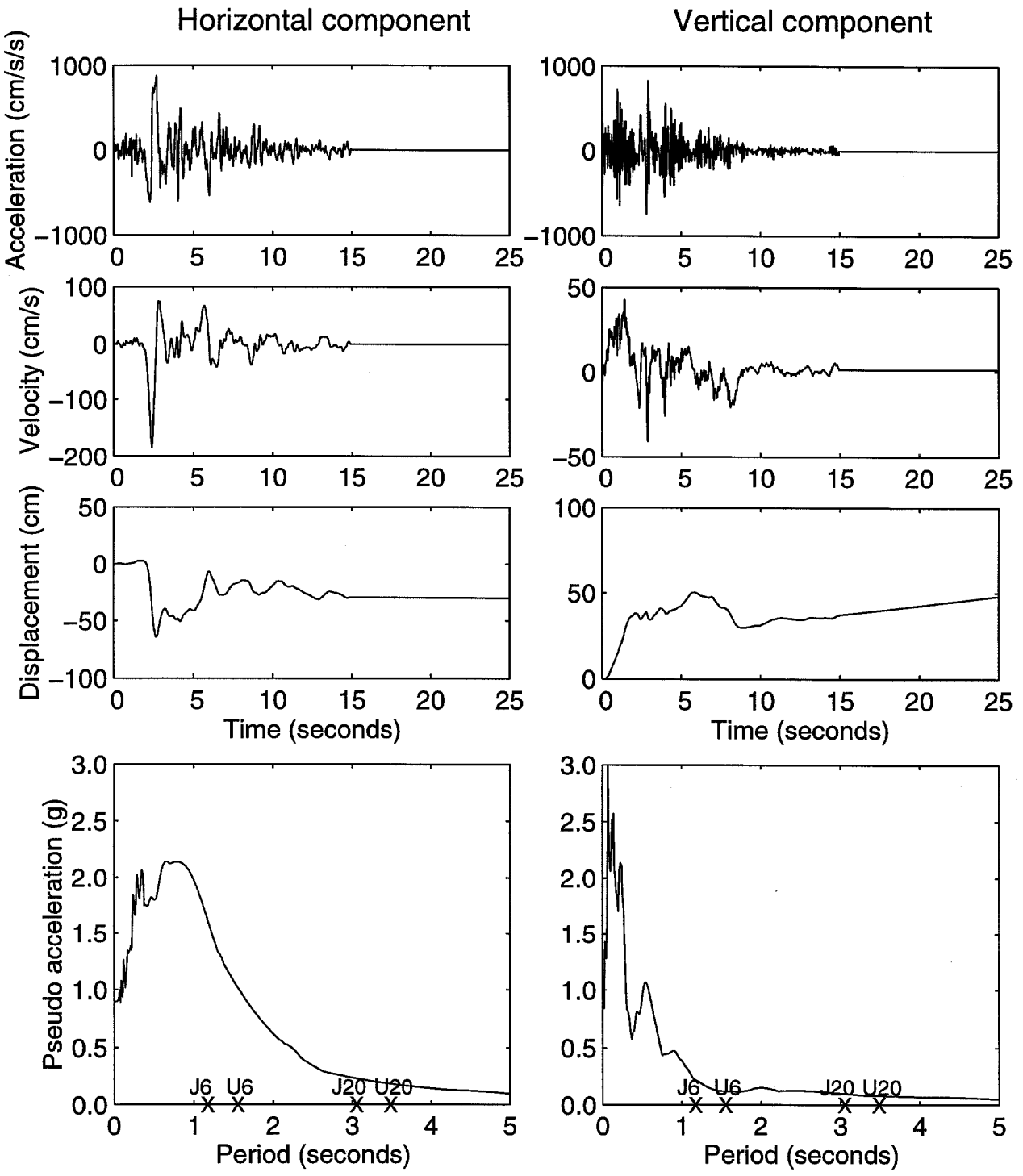

Figure 3.17 RRS ground motion time histories and pseudo acceleration from the 1994 Northridge earthquake.

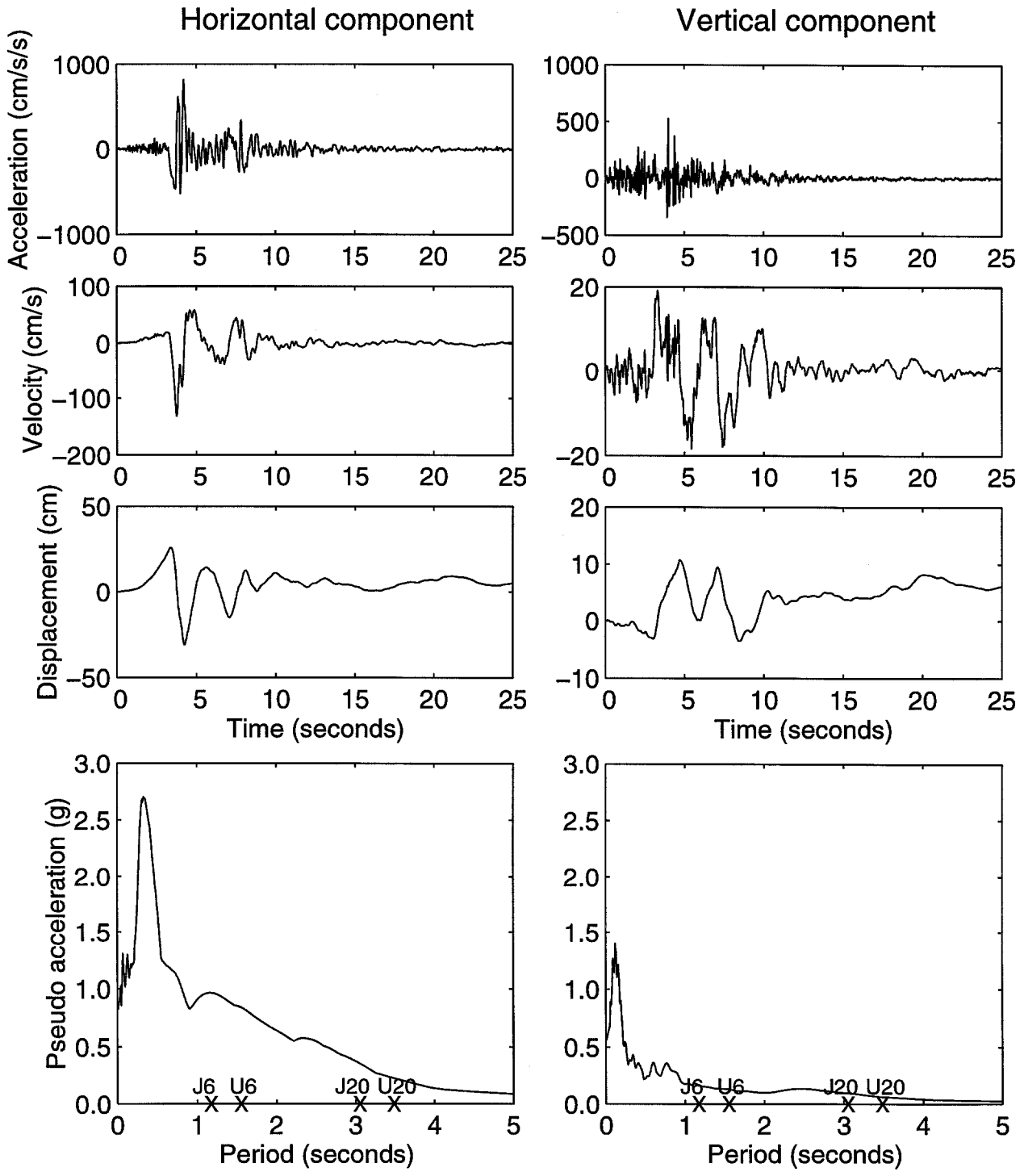

Figure 3.18 OVH ground motion time histories and pseudo acceleration from the 1994 Northridge earthquake.

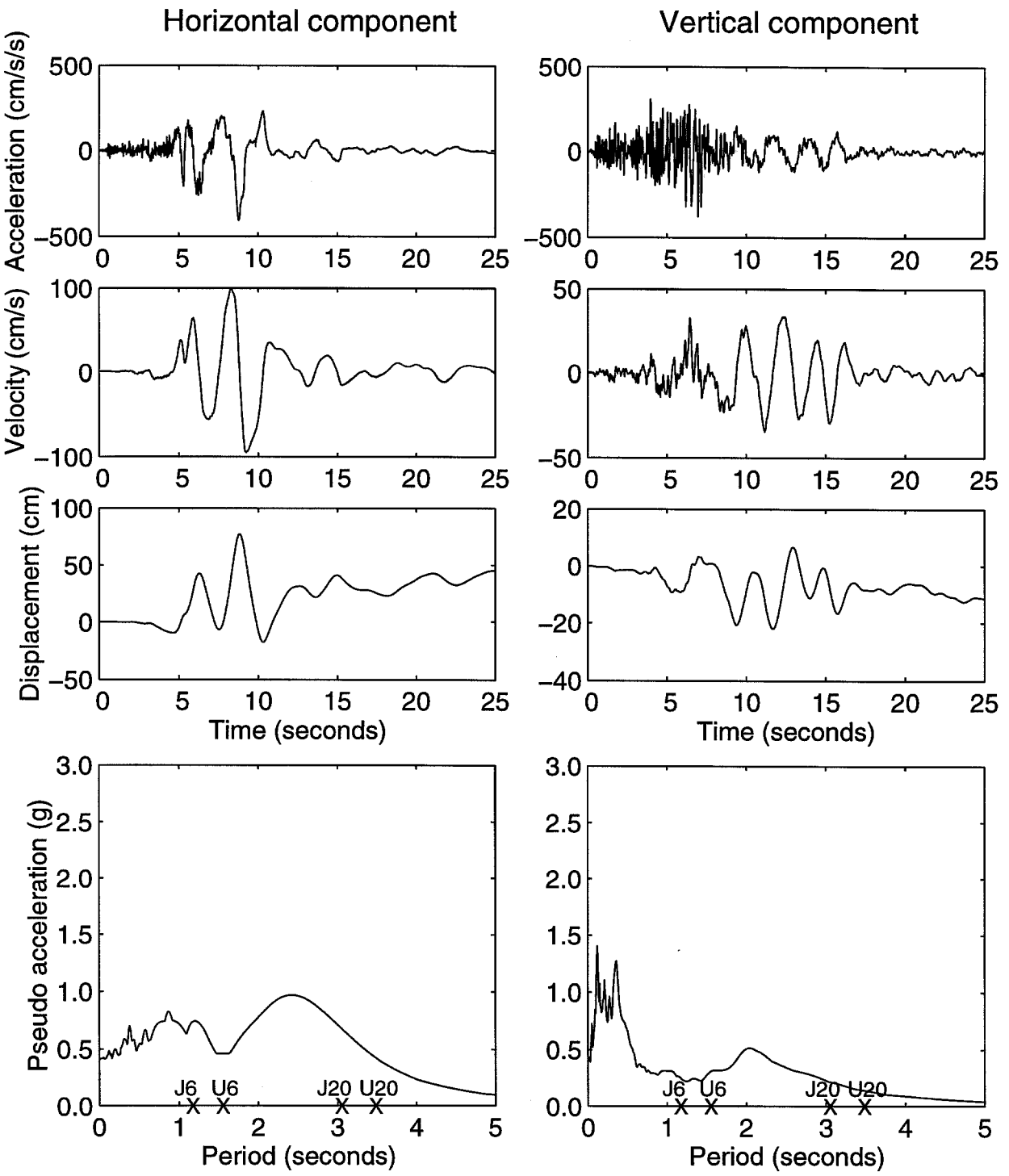

Figure 3.19 EKB ground motion time histories and pseudo acceleration from the 1995 Kobe earthquake.

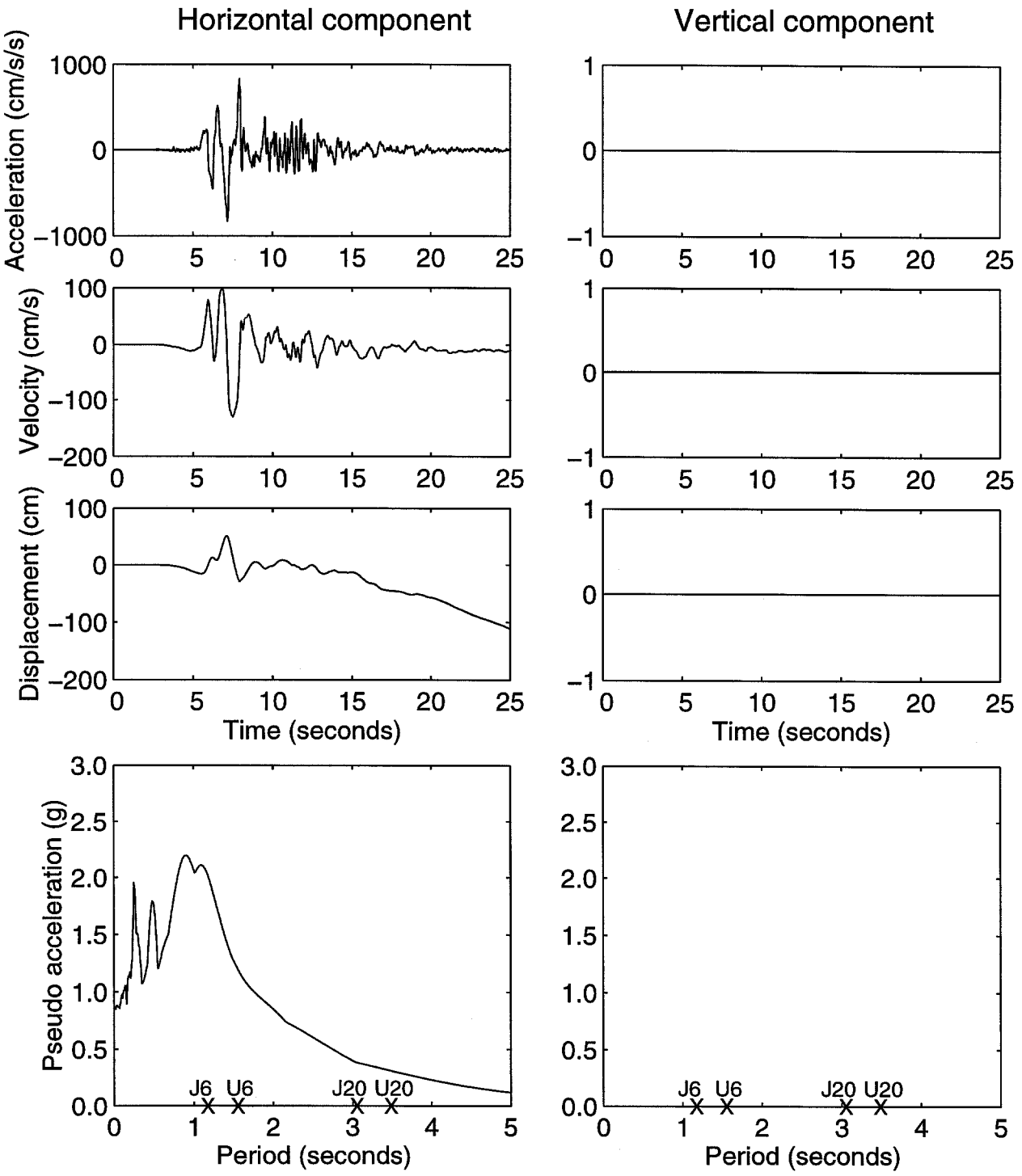

Figure 3.20 FKI ground motion time histories and pseudo acceleration from the 1995 Kobe earthquake.

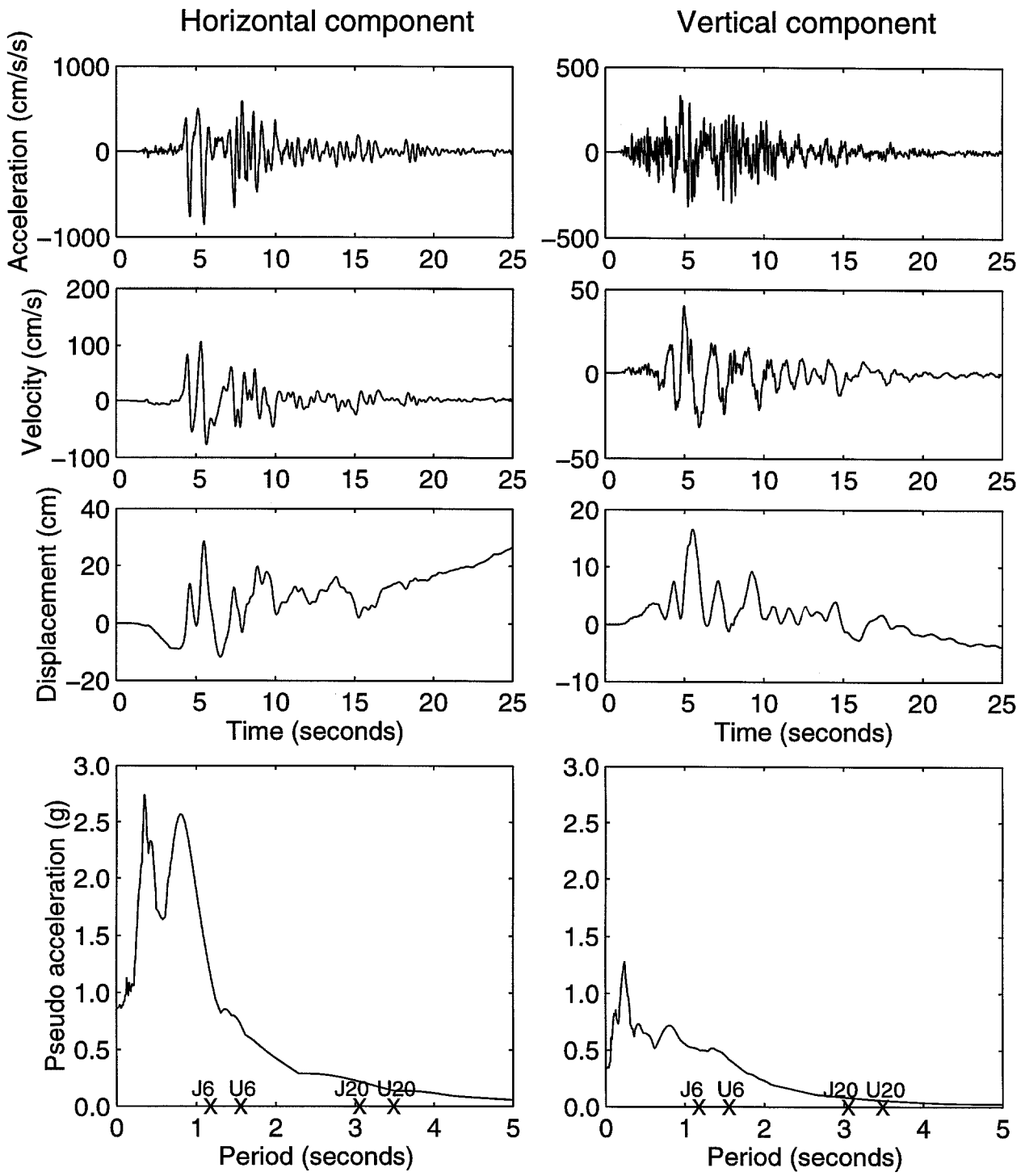

Figure 3.21 JMA ground motion time histories and pseudo acceleration from the 1995 Kobe earthquake.

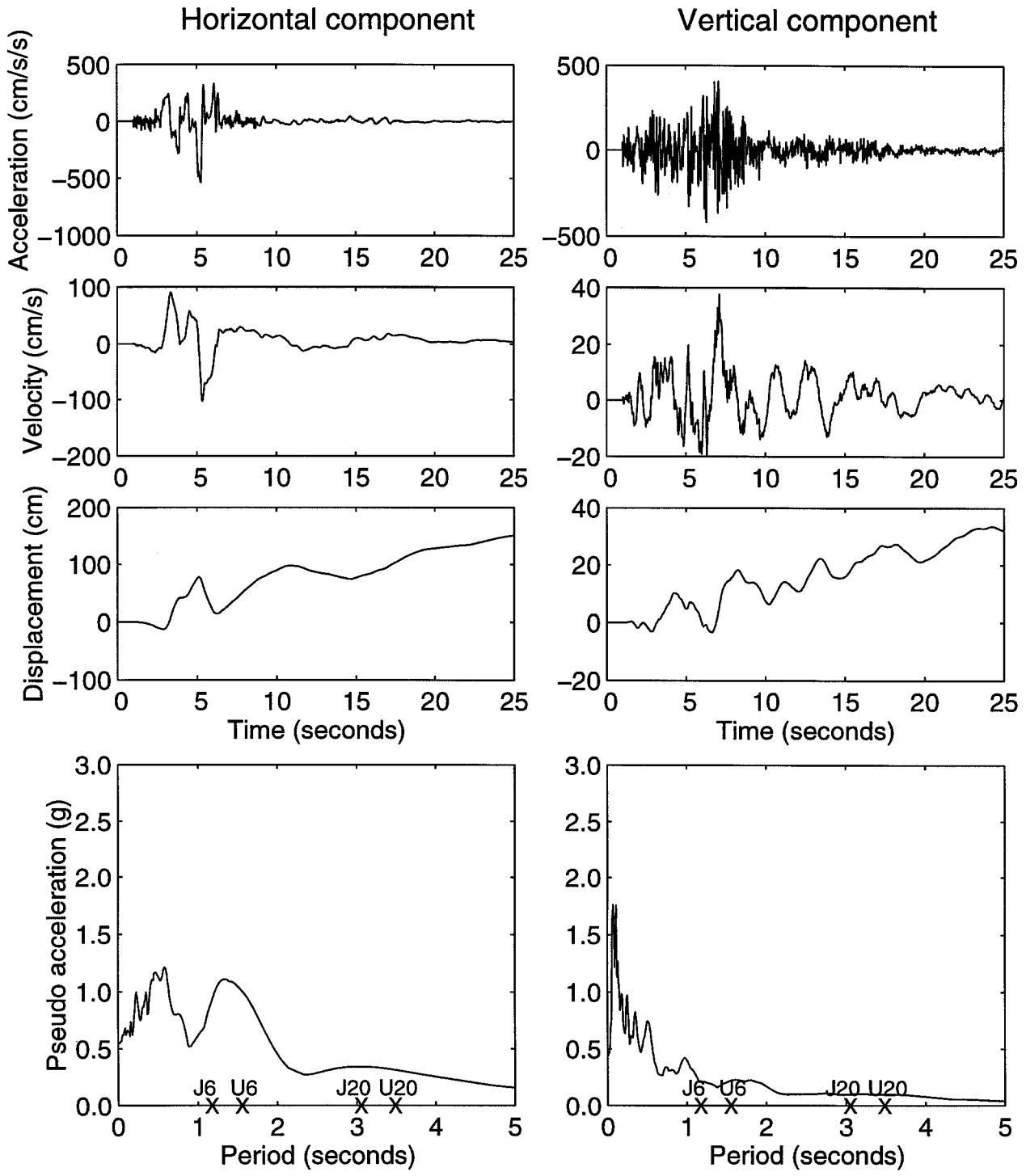

Figure 3.22 KBH ground motion time histories and pseudo acceleration from the 1995 Kobe earthquake.

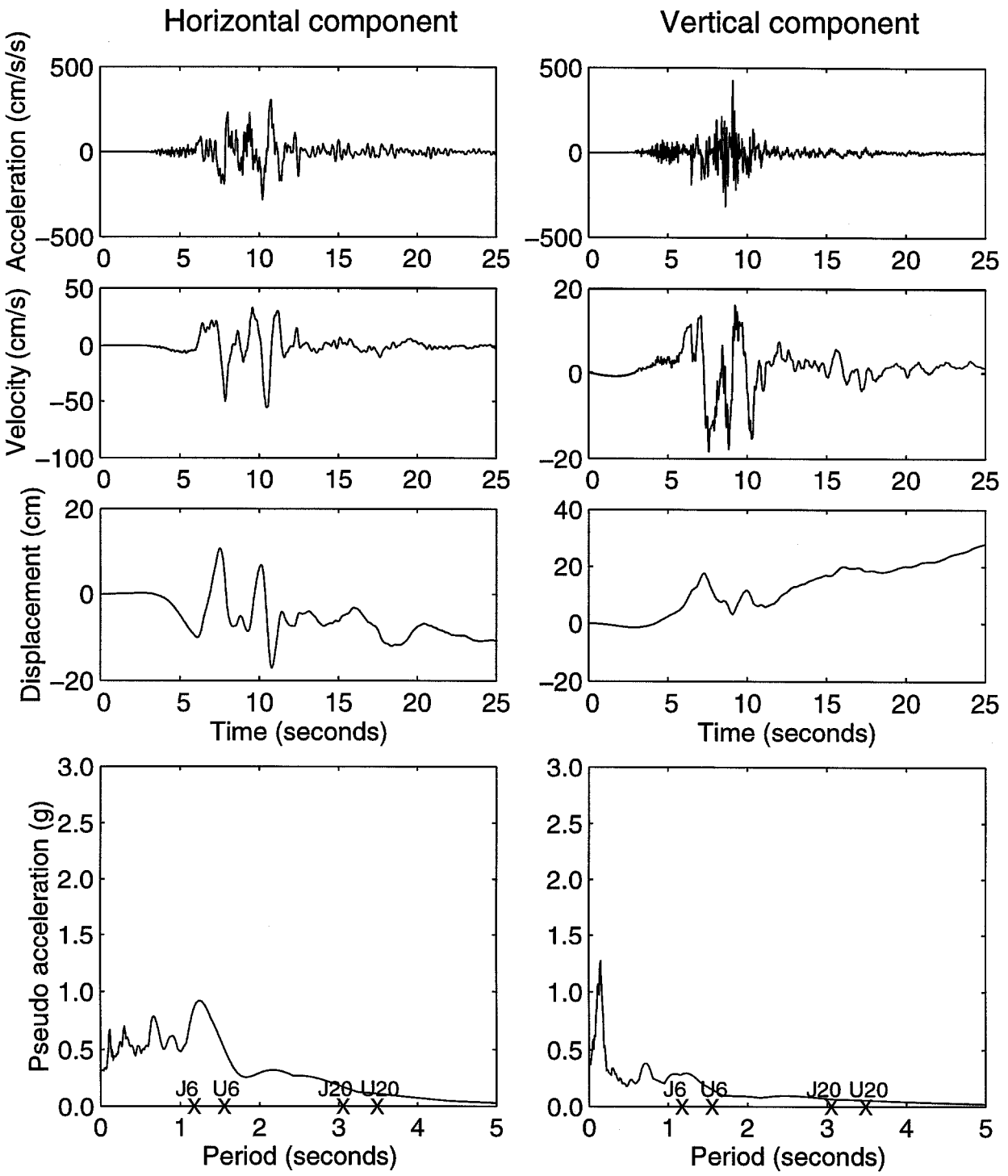

Figure 3.23 KBU ground motion time histories and pseudo acceleration from the 1995 Kobe earthquake.

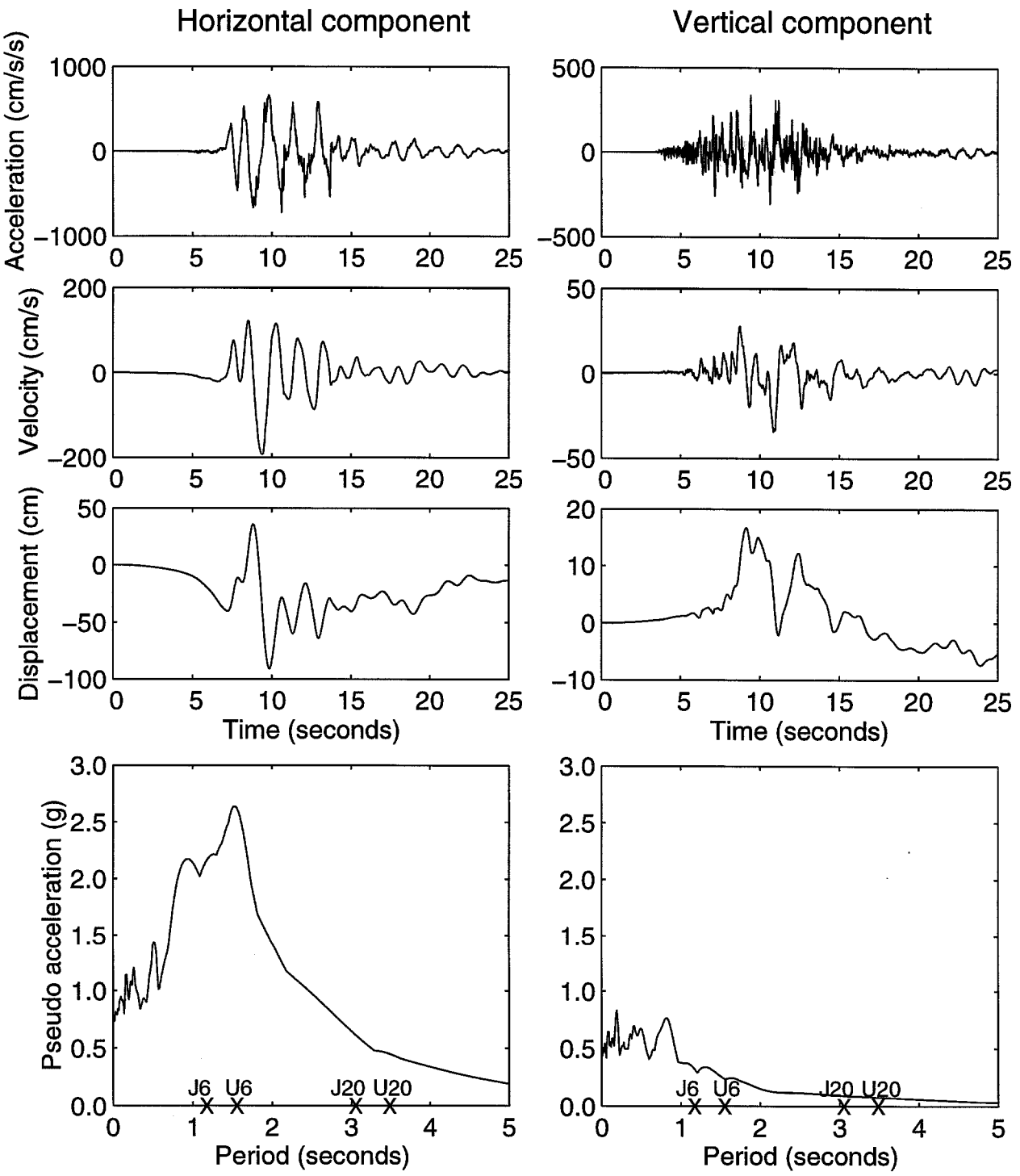

Figure 3.24 KH8 ground motion time histories and pseudo acceleration from the 1995 Kobe earthquake.

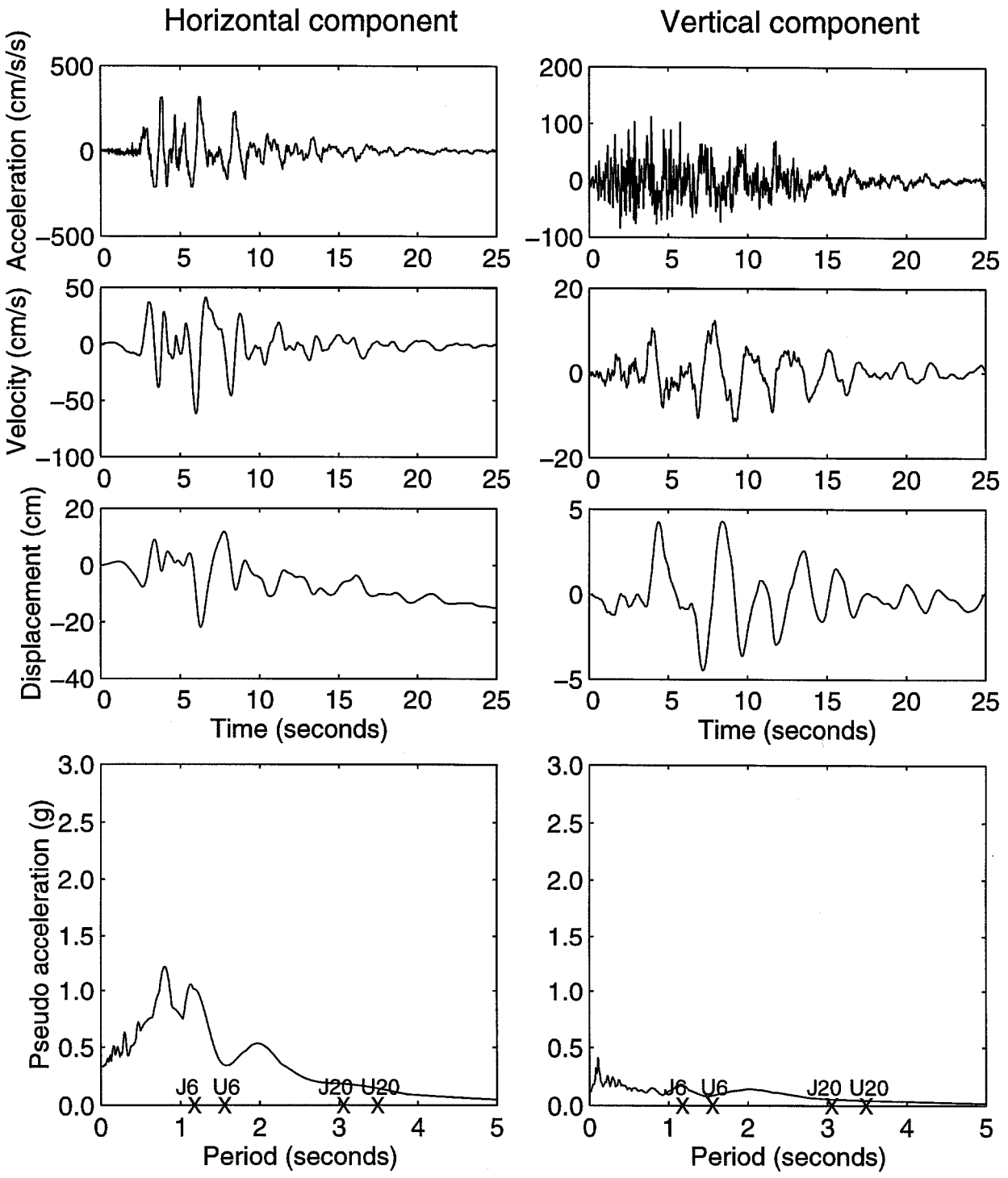

Figure 3.25 NGT ground motion time histories and pseudo acceleration from the 1995 Kobe earthquake.

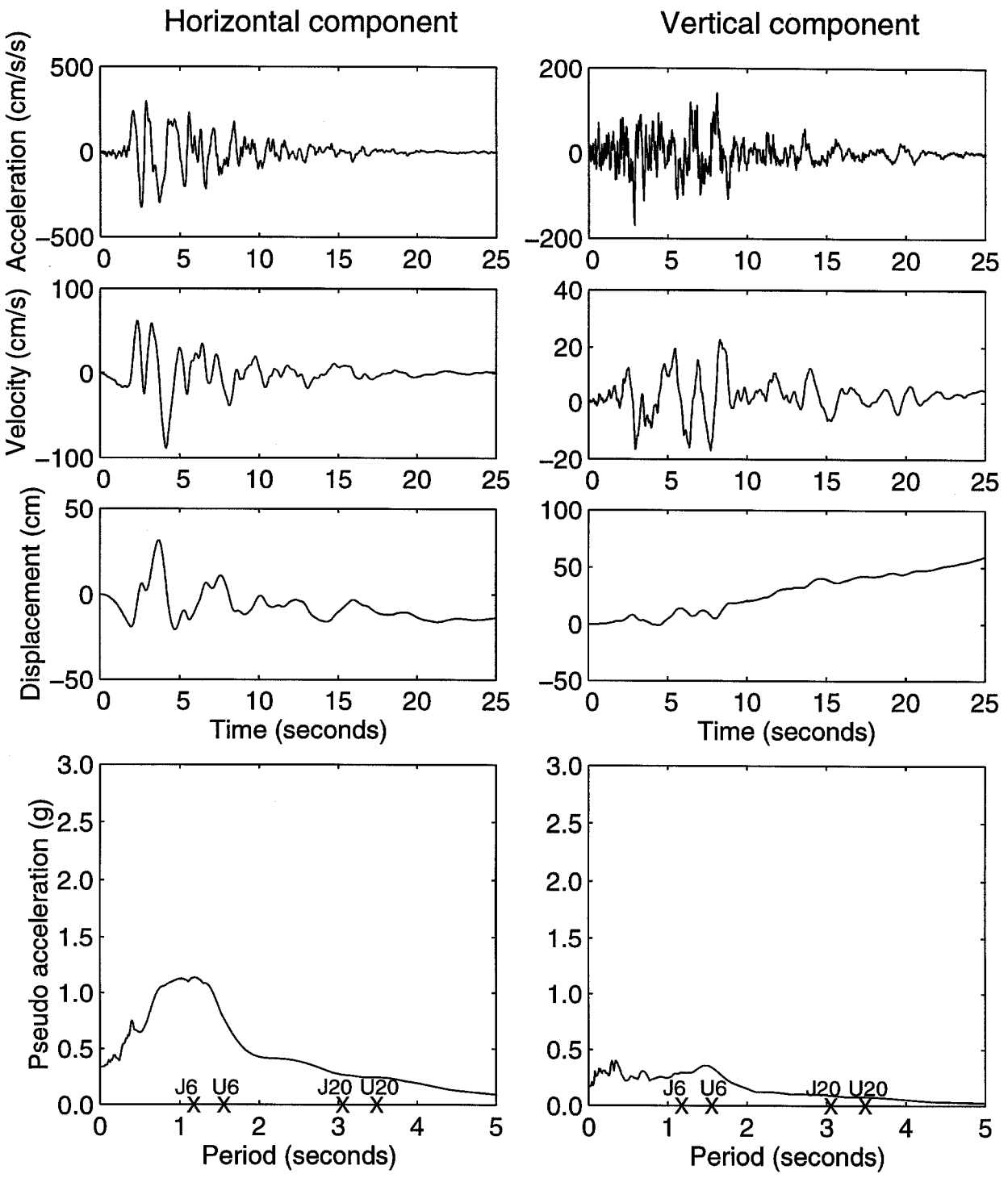

Figure 3.26 NTT ground motion time histories and pseudo acceleration from the 1995 Kobe earthquake.

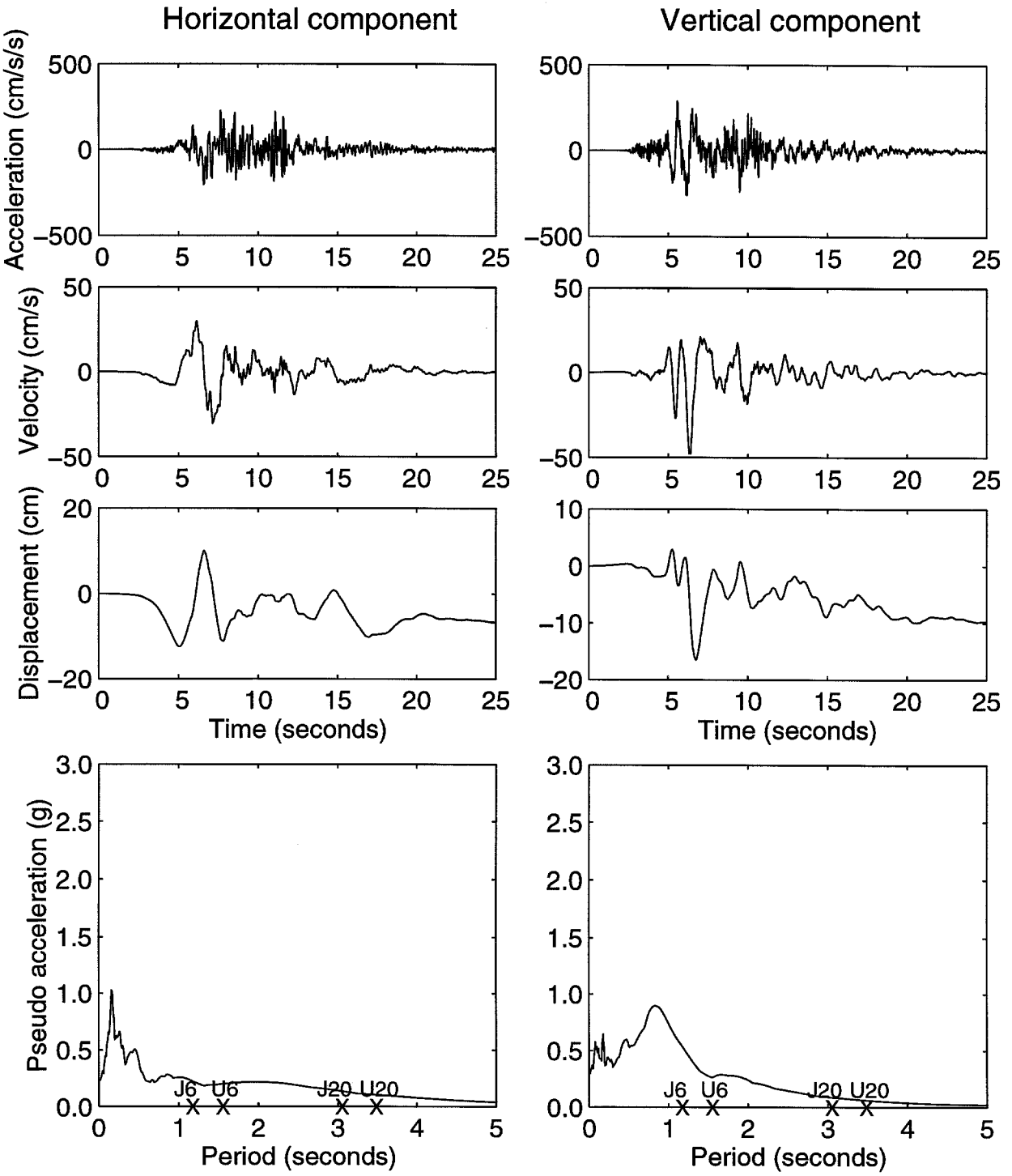

Figure 3.27 SKB ground motion time histories and pseudo acceleration from the 1995 Kobe earthquake.

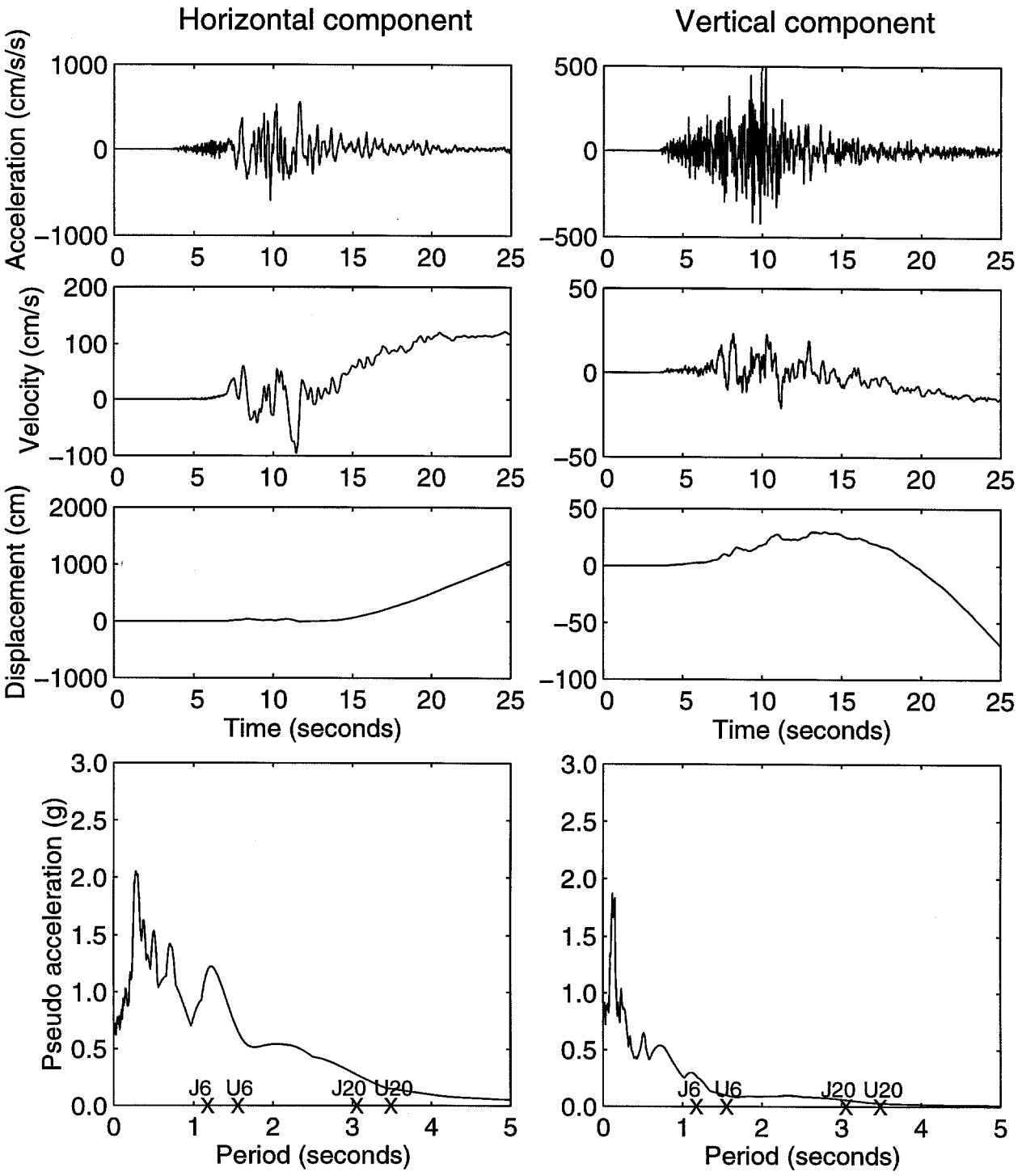

Figure 3.28 SSS ground motion time histories and pseudo acceleration from the 1995 Kobe earthquake.

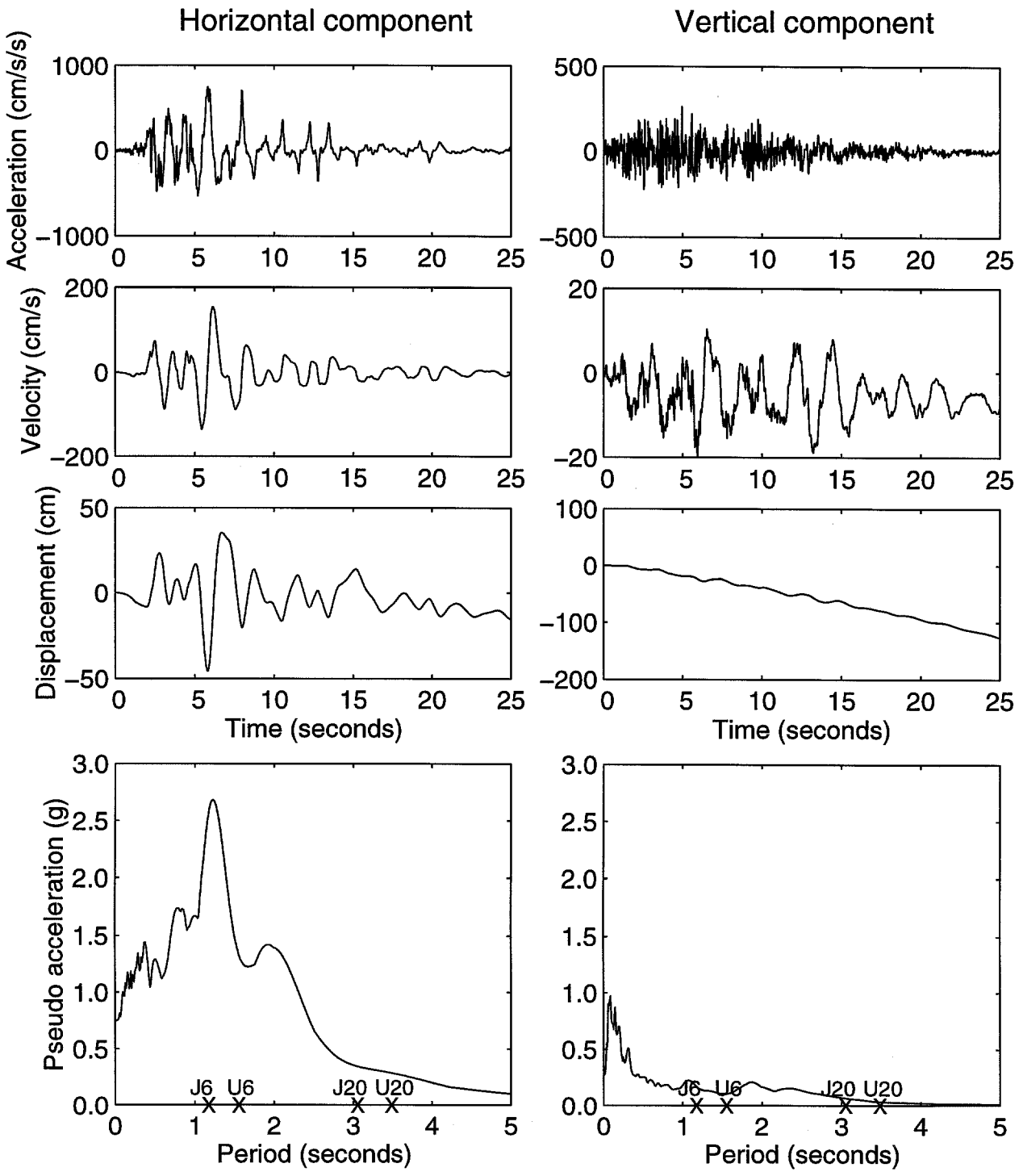

Figure 3.29 TAK ground motion time histories and pseudo acceleration from the 1995 Kobe earthquake.

	2	3	4	5	6	7	8	9	10	11
					PEAK GROUND DISPLACEMENT (cm)					
K	6.7	7.3	9.0	9.5	13.8	10.3	12.3	10.9	9.0	9.4
J	7.7	7.7	10.2	8.9	11.2	14.9	12.3	13.9	7.5	5.2
I	9.0	12.4	16.5	15.9	36.4	28.3	14.3	11.0	8.0	4.8
H	20.4	32.9	52.3	29.8	60.8	37.2	12.6	9.4	6.7	5.6
G	8.0	19.5	16.7	31.1	30.1	35.3	21.2	7.1	4.2	4.3
F	7.6	17.1	20.5	17.2	10.2	21.5	47.9	20.6	5.5	3.9
E	9.2	20.9	19.9	9.2	30.4	29.1	28.8	25.9	10.6	5.7
D	7.6	10.3	10.3	8.5	25.5	20.4	18.3	14.8	3.6	3.2
C	6.4	9.9	9.6	28.3	16.7	14.1	9.0	4.8	5.8	3.9
B	14.7	9.4	10.4	10.4	6.9	6.7	8.0	5.0	4.0	3.5
					PEAK GROUND VELOCITY (cm/sec)					
K	22.	23.	37.	44.	42.	33.	15.	23.	20.	20.
J	29.	35.	38.	52.	46.	50.	38.	39.	21.	13.
I	32.	30.	42.	64.	103.	81.	37.	42.	14.	16.
H	58.	83.	176.	83.	175.	117.	54.	29.	45.	42.
G	23.	35.	37.	37.	50.	58.	54.	34.	35.	43.
F	24.	28.	35.	35.	44.	46.	118.	81.	34.	37.
E	19.	64.	65.	33.	123.	77.	95.	73.	27.	26.
D	24.	33.	29.	22.	68.	82.	41.	43.	27.	17.
C	26.	32.	32.	93.	68.	43.	33.	32.	35.	26.
B	53.	25.	23.	28.	27.	20.	52.	35.	33.	29.
					PEAK GROUND ACCELERATION (cm/sec^2)					
K	181.	208.	414.	488.	414.	395.	134.	127.	126.	218.
J	187.	237.	223.	262.	289.	274.	488.	424.	130.	135.
I	213.	210.	249.	312.	531.	727.	333.	444.	149.	138.
H	326.	445.	754.	334.	854.	774.	450.	432.	460.	448.
G	34.	144.	203.	189.	199.	318.	307.	432.	424.	446.
F	258.	170.	193.	279.	186.	246.	743.	784.	431.	450.
E	164.	523.	540.	238.	690.	634.	499.	600.	222.	347.
D	185.	239.	221.	221.	481.	437.	310.	330.	312.	173.
C	197.	239.	238.	499.	443.	420.	334.	312.	357.	214.
B	304.	151.	130.	258.	183.	126.	391.	320.	233.	213.

Table 3.1 Peak ground displacement, velocity and acceleration for the horizontal component at 100 sites of the Northridge earthquake simulation.

	2	3	4	5	6	7	8	9	10	11
					PEAK GROUND DISPLACEMENT (cm)					
K	3.3	3.6	4.8	5.4	6.1	6.5	6.6	5.0	3.8	5.6
J	4.6	5.2	5.7	7.8	8.5	8.7	8.5	5.9	3.9	2.7
I	6.3	7.9	9.2	12.9	25.1	23.2	8.5	7.6	3.9	2.9
H	11.7	16.9	26.9	22.2	46.4	29.4	10.0	6.8	5.8	4.7
G	8.3	13.4	20.4	32.4	51.9	40.8	14.0	4.9	3.5	4.2
F	7.5	13.0	22.5	33.5	39.3	39.1	27.3	10.3	2.9	3.3
E	6.4	12.9	20.5	23.1	34.3	32.6	26.1	17.6	4.2	2.0
D	5.1	7.3	9.6	13.9	20.5	18.9	14.2	8.8	3.9	1.3
C	3.8	4.3	5.4	9.0	11.4	8.6	6.3	4.1	3.1	2.4
B	2.7	2.2	2.4	3.4	4.3	4.0	3.2	2.6	2.4	2.3
					PEAK GROUND VELOCITY (cm/sec)					
K	10.	10.	14.	17.	16.	14.	11.	7.	5.	11.
J	9.	10.	15.	14.	19.	15.	43.	38.	6.	5.
I	9.	13.	15.	24.	45.	44.	44.	35.	6.	6.
H	17.	22.	42.	24.	73.	50.	38.	41.	37.	36.
G	8.	11.	20.	26.	30.	32.	15.	18.	13.	37.
F	7.	10.	19.	25.	25.	25.	30.	24.	13.	38.
E	10.	33.	36.	15.	31.	34.	24.	16.	11.	12.
D	8.	9.	8.	9.	16.	33.	13.	17.	11.	6.
C	8.	9.	7.	11.	15.	23.	11.	9.	13.	13.
B	10.	9.	10.	7.	7.	4.	10.	11.	8.	10.
					PEAK GROUND ACCELERATION (cm/sec^2)					
K	91.	90.	186.	187.	184.	191.	63.	67.	59.	58.
J	91.	86.	94.	180.	187.	189.	393.	393.	57.	63.
I	89.	90.	85.	188.	241.	353.	435.	401.	59.	67.
H	138.	173.	272.	178.	445.	329.	403.	405.	397.	399.
G	88.	113.	175.	210.	200.	209.	145.	146.	134.	402.
F	87.	117.	163.	123.	177.	124.	199.	182.	132.	404.
E	113.	412.	409.	97.	180.	185.	270.	284.	259.	135.
D	108.	96.	116.	115.	210.	406.	192.	207.	150.	95.
C	110.	106.	118.	184.	161.	394.	151.	140.	145.	102.
B	63.	148.	139.	74.	69.	68.	126.	147.	97.	105.

Table 3.2 Peak ground displacement, velocity and acceleration for the vertical component at 100 sites of the Northridge earthquake simulation.

	A	A2	B1	B3	C1	D	D2	E1	F1	F3	G	G2
						PEAK GROUND DISPLACEMENT (cm)						
1	19.0	15.8	17.1	18.8	19.4	18.6	19.0	18.9	18.9	18.1	14.8	16.1
2	21.0	19.4	20.5	24.2	26.4	22.2	19.3	18.9	20.1	21.4	16.5	19.9
3	23.7	28.2	30.0	31.7	32.6	29.5	26.6	31.4	38.2	31.4	21.9	25.4
4	20.1	24.5	27.0	31.2	33.8	31.9	24.7	25.5	36.4	24.8	15.7	19.6
5	24.0	22.4	26.6	37.1	36.0	36.5	32.0	30.6	51.6	25.8	17.0	22.9
6	27.3	24.2	30.6	41.4	39.1	37.3	44.0	49.7	58.3	32.6	22.1	27.4
7	25.8	28.3	35.4	41.8	38.0	36.6	41.3	55.5	54.2	36.3	23.9	28.2
						PEAK GROUND VELOCITY (cm/sec)						
1	41.	48.	48.	50.	42.	43.	46.	39.	47.	42.	34.	35.
2	44.	50.	49.	60.	54.	49.	52.	32.	36.	45.	38.	43.
3	66.	75.	75.	78.	71.	81.	85.	77.	102.	73.	52.	55.
4	60.	69.	71.	79.	69.	84.	75.	73.	102.	50.	38.	41.
5	57.	67.	73.	104.	88.	99.	106.	86.	135.	53.	37.	46.
6	57.	72.	79.	106.	89.	96.	130.	122.	141.	69.	48.	55.
7	62.	78.	90.	90.	80.	85.	112.	122.	122.	75.	49.	53.
						PEAK GROUND ACCELERATION (cm/sec^2)						
1	133.	169.	188.	204.	170.	175.	184.	155.	176.	132.	110.	121.
2	160.	196.	210.	273.	223.	196.	209.	103.	115.	144.	143.	162.
3	238.	298.	332.	354.	299.	333.	334.	302.	380.	256.	179.	195.
4	194.	251.	290.	356.	309.	353.	321.	294.	421.	166.	139.	156.
5	199.	264.	326.	467.	358.	377.	478.	371.	543.	196.	148.	176.
6	216.	302.	378.	429.	329.	341.	490.	438.	512.	288.	181.	217.
7	246.	347.	402.	363.	292.	303.	408.	414.	403.	301.	179.	198.

Table 3.3 Peak ground displacement, velocity and acceleration for the fault-perpendicular component at 84 sites of the Kobe earthquake simulation.

	1	2	3	4	5	6	7	8	9	10	11
					PEAK GROUND DISPLACEMENT (cm)						
K	26.	28.	36.	47.	57.	56.	44.	34.	23.	12.	12.
J	32.	32.	46.	70.	96.	96.	65.	48.	24.	17.	16.
I	36.	34.	57.	95.	145.	134.	26.	58.	33.	21.	21.
H	35.	36.	62.	109.	168.	152.	41.	67.	39.	33.	30.
G	37.	33.	60.	117.	176.	154.	71.	35.	39.	44.	39.
F	36.	32.	63.	121.	182.	157.	75.	54.	45.	51.	46.
E	35.	31.	65.	129.	194.	183.	49.	58.	52.	58.	61.
D	35.	32.	66.	128.	200.	164.	63.	74.	67.	73.	74.
C	35.	34.	61.	117.	182.	150.	90.	69.	76.	83.	81.
B	35.	36.	53.	96.	150.	146.	91.	67.	89.	88.	81.
A	34.	36.	46.	75.	111.	117.	78.	54.	76.	79.	74.
					PEAK GROUND VELOCITY (cm/sec)						
K	45.	44.	54.	47.	46.	40.	31.	27.	25.	21.	18.
J	48.	54.	63.	72.	91.	66.	48.	37.	31.	31.	22.
I	51.	87.	104.	122.	164.	110.	55.	43.	39.	33.	20.
H	53.	87.	108.	96.	180.	117.	69.	47.	42.	35.	23.
G	49.	88.	92.	103.	174.	121.	78.	39.	46.	33.	26.
F	49.	92.	78.	112.	158.	108.	66.	43.	46.	34.	25.
E	51.	96.	84.	119.	160.	125.	68.	53.	48.	35.	25.
D	52.	88.	78.	118.	158.	111.	76.	76.	58.	38.	27.
C	50.	71.	65.	107.	139.	118.	85.	77.	59.	42.	32.
B	51.	61.	64.	85.	115.	100.	78.	71.	58.	47.	34.
A	47.	52.	56.	67.	82.	80.	85.	76.	60.	45.	33.
					PEAK GROUND ACCELERATION (cm/sec^2)						
K	202.	250.	211.	231.	202.	174.	166.	227.	300.	384.	327.
J	272.	340.	306.	342.	361.	294.	243.	344.	592.	593.	402.
I	532.	820.	834.	984.	1040.	868.	617.	347.	653.	598.	400.
H	549.	811.	836.	845.	914.	846.	568.	385.	649.	590.	353.
G	479.	790.	844.	779.	864.	894.	522.	604.	632.	555.	400.
F	425.	790.	855.	763.	859.	929.	519.	462.	559.	515.	398.
E	395.	692.	855.	640.	746.	796.	599.	440.	519.	531.	352.
D	345.	690.	710.	497.	564.	325.	418.	341.	450.	482.	362.
C	285.	384.	402.	333.	391.	369.	270.	217.	290.	354.	364.
B	226.	273.	299.	245.	299.	287.	218.	213.	222.	276.	286.
A	177.	210.	294.	206.	225.	248.	192.	193.	160.	193.	199.

Table 3.4 Peak ground displacement, velocity and acceleration for the horizontal component at 121 sites of the Elysian Park simulation.

4. RESULTS

All four buildings are analyzed for the ground motions described in the previous section. Connections are considered to be either non-fracturing (Case P) or fracture-prone (Case B for the UBC and Japanese-designed buildings and Case T for the UBC-designed buildings). For Case B, a different random assignment of fracture strains is used for each site in the Northridge, Kobe and Elysian Park simulations.

4.1 Northridge simulation

Results for the simulated Northridge ground motions at the inner 10 by 10 grid of sites are presented in Tables 4.1 to 4.10 as follows.

	Case	Table	Case	Table	Case	Table
U6	P	4.1	B	4.2	T	4.3
J6	P	4.4	B	4.5		
U20	P	4.6	B	4.7	T	4.8
J20	P	4.9	B	4.10		

Each table gives numbers of weld breaks (zero for Case P) and peak story drifts occurring at each site. Weld breaks are for flange welds, and separate totals are listed for girders and columns. The total numbers of girder flange welds (two for each girder-to-column connection: one top flange and one bottom flange) and column flange welds (two for each column splice and base plate) for the computer model of each building are listed below.

	Girder flange welds	Column flange welds
U6	84	64
J6	140	96
U20	252	176
J20	420	264

Story drifts in Tables 4.1 to 4.10 are for the story where the maximum drift occurs. Drifts of 2% or greater are shown in bold type.

A comparison of the peak ground motion parameters in Table 3.1 with the responses in Tables 4.1 to 4.10 shows that building damage (as quantified by the number of weld breaks and maximum drift) correlates best to peak ground displacement. One of the most damaging ground motions is at site H06 where the peak horizontal ground displacement is 61 cm (Figure 3.4). At this site the peak story drift can reach large values, such as the 7.7% for building U6B; collapse occurs for U6T. Although the computer program does not show

collapse at site H06 for building U6B, the large drift is in a range where deterioration mechanisms not included in the computer program, such as local flange buckling, play an important role and so collapse should not be ruled out.

The weld fracture totals in Tables 4.1 to 4.10 show that the percentage of welds that fracture is often quite high for the girder flanges. At site H06 for building U6B, where the 7.7% story drift occurs, 65% of the beam flange welds fracture. Even when the response is much less, often a considerable number of connections still fracture. For building J6B at site F09, 41% of the beam flange welds fracture and the maximum story drift is only 1.7%. Stability of a building in the presence of a high percentage of fractured welds is due to the welds that do not fracture plus the residual strength remaining in the fractured connections. This residual strength as modelled by the program can be significant, especially with composite slab action and axial restraint to beams present. The percentage of welds that fracture is significantly greater for Case-T buildings than Case-B buildings, as expected.

A summary of the story drifts in Tables 4.1 to 4.10 appears in Figure 4.1 for the 6-story buildings and in Figure 4.2 for the 20-story buildings. Plotted are the number of sites where peak story drift exceeds 2%, the data being for 1% increments of drift. Each site represents 25 km^2. From these plots, general conclusions can readily be made regarding the role of building height, the benefits of higher lateral strength, and the effects of connection fracture. Regarding building height, story drifts are much greater for the 6-story buildings than the 20-story buildings. The pseudo-acceleration response spectra in Figures 3.2 to 3.4 show larger ordinates for the shorter buildings, consistent with their greater drifts. These larger drifts occur despite the shorter buildings being much stronger than the taller ones relative to their own weights.

Some benefits are gained by increasing a building's lateral strength, as seen from Figures 4.1 and 4.2 by comparing the Japanese designs to the UBC ones, but they are modest. That increasing a building's lateral strength has only a modest benefit probably has to do with the accompanying increase in stiffness attracting more load. As also seen from Figures 4.1 and 4.2, connection fracture according to the Case-B assumption has a detrimental effect, but it is not catastrophic. Helpful here are the post-fracture residual strength in the connections and the fact that, in the analyses, a significant number of connections are assigned fracture strains high enough so that fracture does not occur. With the "worst-case" Case-T assumption, the collapse of the UBC-designed buildings at 3 sites for U6T and at 4 sites for U20T is a serious matter and shows why it is important that actual behavioral data for fracture-prone connections be obtained and used in assessments.

The trends evident from Figures 4.1 and 4.2 are averages. Individual cases can be found in Tables 4.1 to 4.10 where increasing the lateral strength causes a larger response

and where permitting welds to fracture reduces the response. The results are influenced by many factors such as frequency content of the earthquake, a building's vibrational frequencies, and nonlinear effects.

4.2 Kobe simulation

For the analyses to the simulated Kobe ground motions, 36 sites are selected from the 84 shown in Table 3.3. On each of the 12 fault-perpendicular lines, the three sites containing the smallest, middle and largest peak-to-peak ground velocities are chosen. These ground motions should be representative of those within 3 km of the structural boundary on the seaward side (ie, sediment), with each of these 36 sites corresponding to an area of 2 km^2. Note that the 2 km^2 area associated with each site is much smaller than the 25 km^2 area used for the Northridge earthquake simulation.

Results are presented in Tables 4.11 to 4.20 as follows.

	Case	Table	Case	Table	Case	Table
U6	P	4.11	B	4.12	T	4.13
J6	P	4.14	B	4.15		
U20	P	4.16	B	4.17	T	4.18
J20	P	4.19	B	4.20		

Drifts above 2% are printed bold. Summaries of the story drifts exceeding 2% appear in Figure 4.3 for the 6-story buildings and in Figure 4.4 for the 20-story buildings. The results show that the effects of building height, lateral strengthening and connection fracture are similar to those observed in the Northridge simulation study. Levels of response are on the same order with many sizable drifts occurring for the 6-story buildings, and there are predicted collapses for U6B at site 6/F1 and for U6T at site 6/B3. The 20-story buildings are excited somewhat less by the Kobe ground motions than the Northridge ones. Peak story drifts are in the 3% range for U20B and J20B; however, collapse occurs for U20T at several sites.

4.3 Elysian Park simulation

Results for the Elysian Park motions are obtained at all sites of the 11 by 11 grid and are presented in Tables 4.21 to 4.30 as follows.

	Case	Table	Case	Table	Case	Table
U6	P	4.21	B	4.22	T	4.23
J6	P	4.24	B	4.25		
U20	P	4.26	B	4.27	T	4.28
J20	P	4.29	B	4.30		

Again, drifts above 2% are printed bold. Summaries of the story drifts above 2% appear in Figure 4.5 for the 6-story buildings and in Figure 4.6 for the 20-story buildings.

The level of response for the Elysian Park earthquake significantly exceeds that for the Northridge and Kobe earthquakes because of the much larger ground displacement that occurs in the M_W 7.0 Elysian Park event. This is especially true for the 20-story buildings for which the relatively long forward-and-back displacement pulse that dominates the motion is a very effective excitation. For Case B, both the UBC and Japanese-designed 20-story buildings experience 2% or significantly greater drift at sites representing a huge area of about 1700 km^2, with the large drifts occurring over a third or more of this area. Regarding the 6-story building, the UBC design is also hit hard by the Elysian Park earthquake, but the Japanese design, owing to its higher strength, shows a much improved behavior. For all of the buildings, connection fracture has a significantly detrimental effect for the Elysian Park earthquake, more than what was seen for the smaller Northridge and Kobe earthquakes.

4.4 Various records

Results for the selected U.S., Kobe and simulated records appear in Table 4.31 for the 6-story buildings and in Table 4.32 for the 20-story buildings. Shown are numbers of girder and column flange weld fractures and peak story drifts; the latter include separate values for the first and upper stories. All results for buildings with fracture-prone connections modelled with the Case-B assumption are averages of three runs using different random assignments of fracture strains. Collapse is indicated if it occurs in any of these three runs. The results for the three simulated records (one each from the Northridge, Kobe and Elysian Park earthquakes) have already been discussed and are included in Tables 4.31 and 4.32 for comparison purposes. The ElCentro ground motion is included to show that this commonly used record is very weak in terms of damage potential.

As seen in Tables 4.31 and 4.32, many of the records produce numerous fractures and large drifts. Collapse occurs in some cases. Individually, the results are quite variable, and this indicates complex relationships among the parameters. However, the previous trends regarding building height, lateral strength and connection fracture still hold.

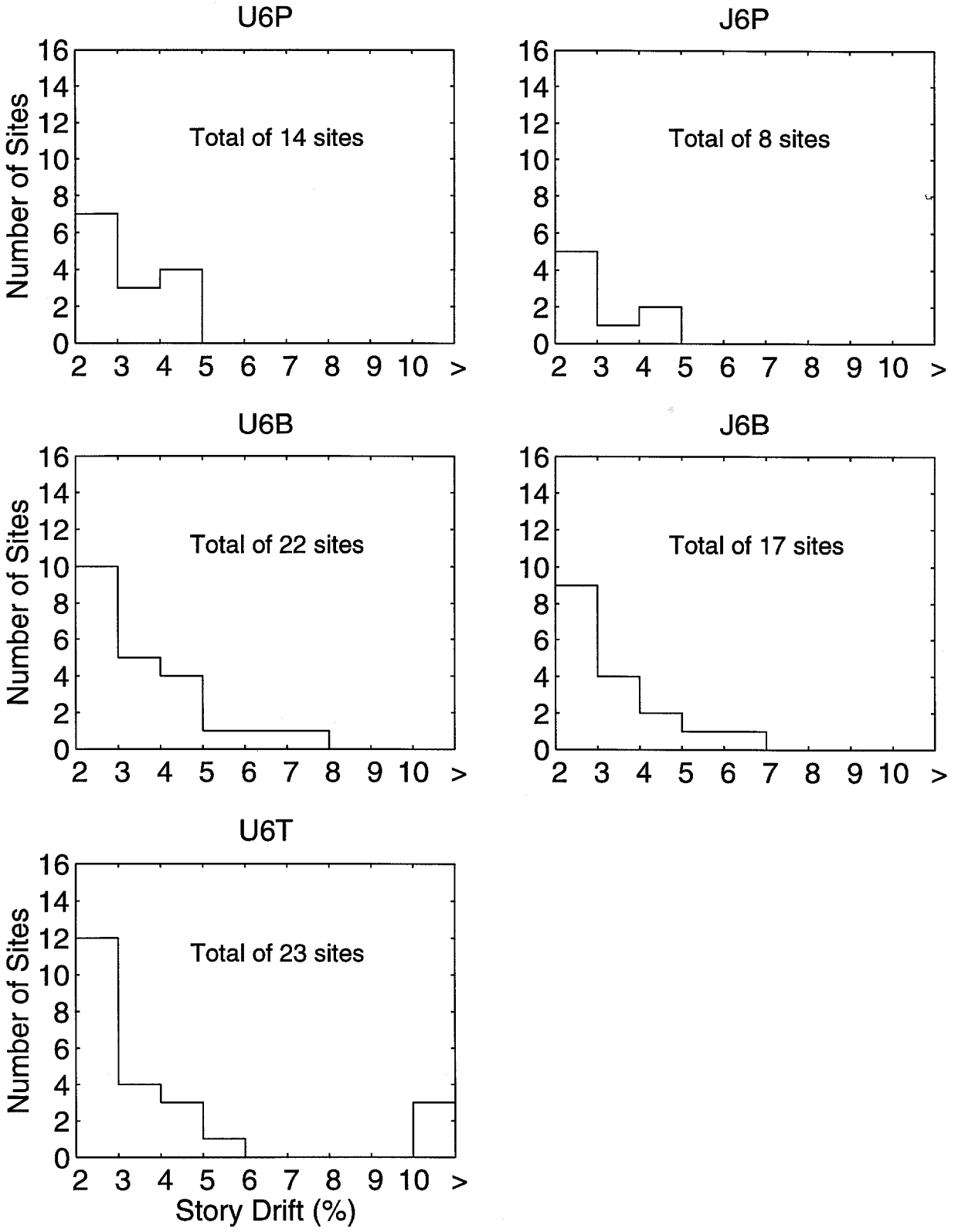

Figure 4.1 Summary of maximum story drifts for the 6–story buildings to the simulated Northridge earthquake. Each site represents an area of 5km by 5km.

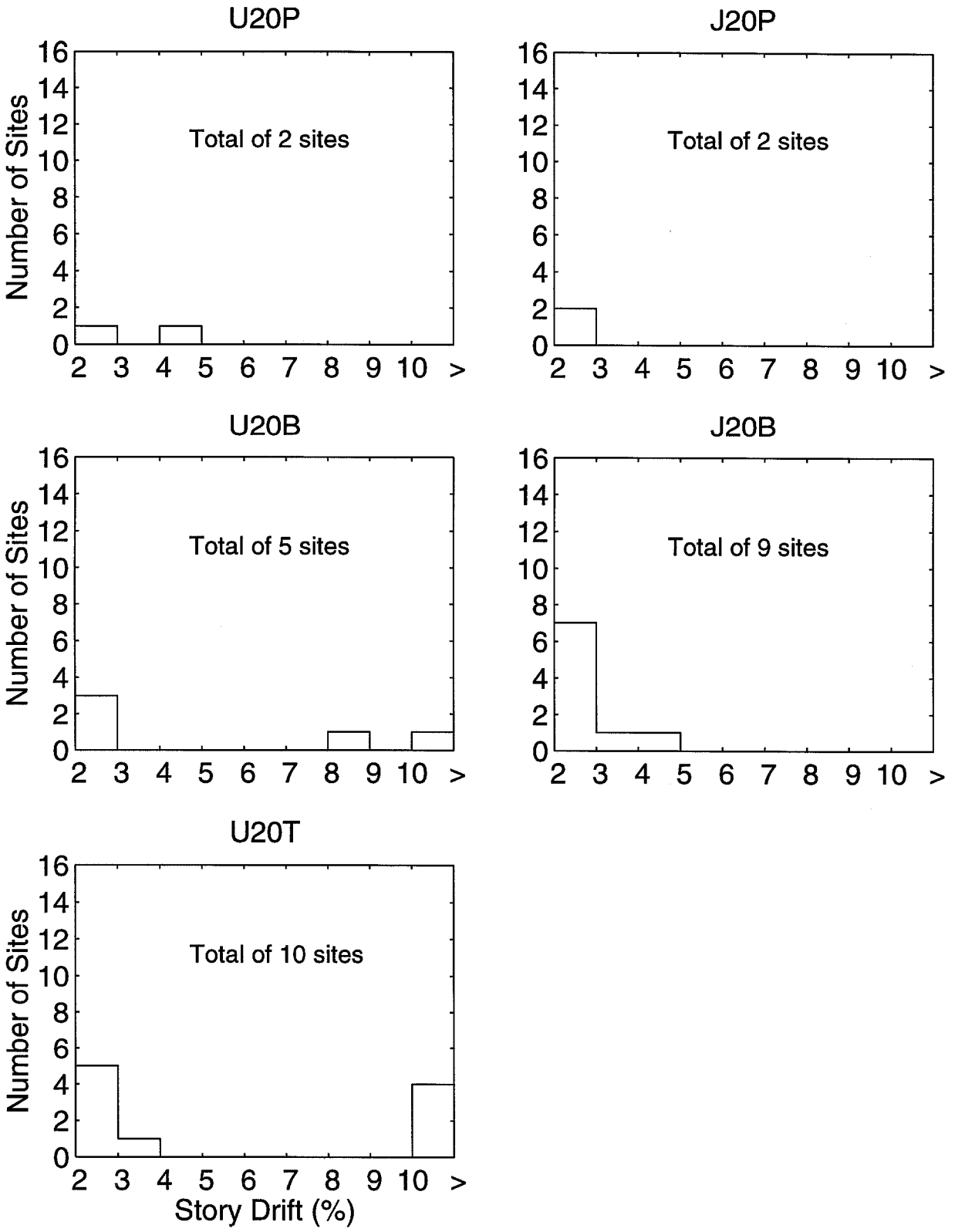

Figure 4.2 Summary of maximum story drifts for the 20–story buildings to the simulated Northridge earthquake. Each site represents an area of 5km by 5km.

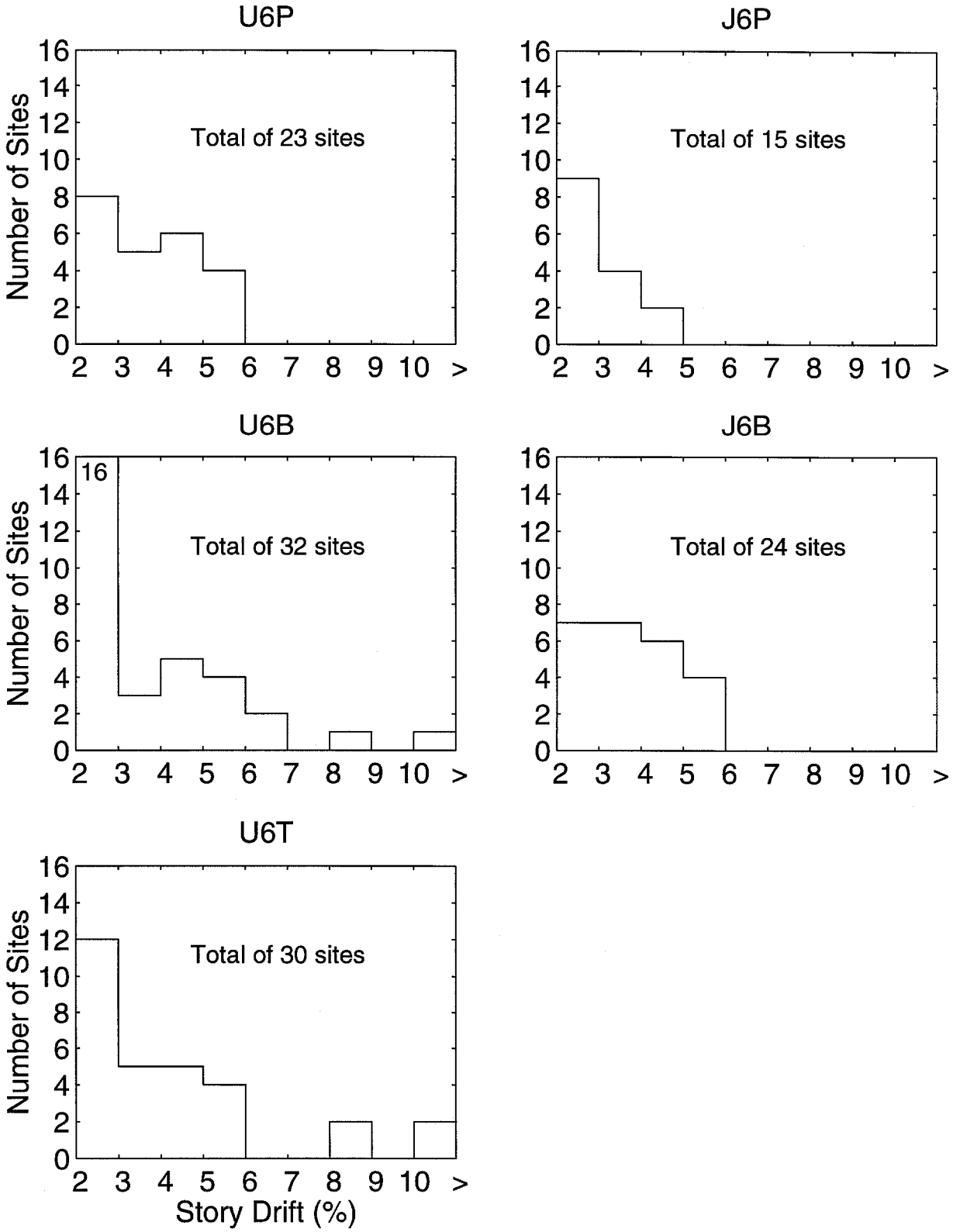

Figure 4.3 Summary of maximum story drifts for the 6–story buildings to the simulated Kobe earthquake. Each site represents an area of 1km by 2km.

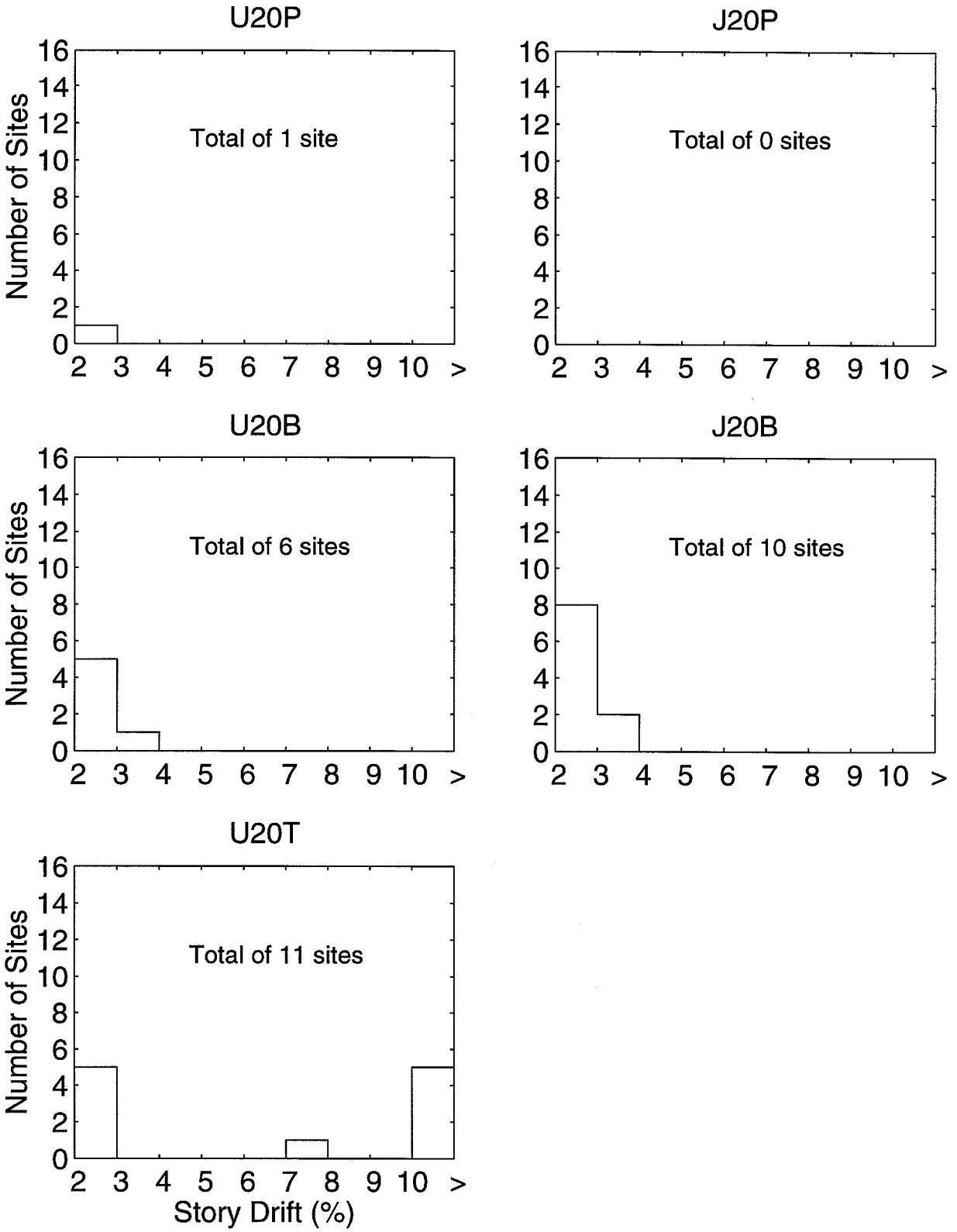

Figure 4.4 Summary of maximum story drifts for the 20–story buildings to the simulated Kobe earthquake. Each site represents an area of 1km by 2km.

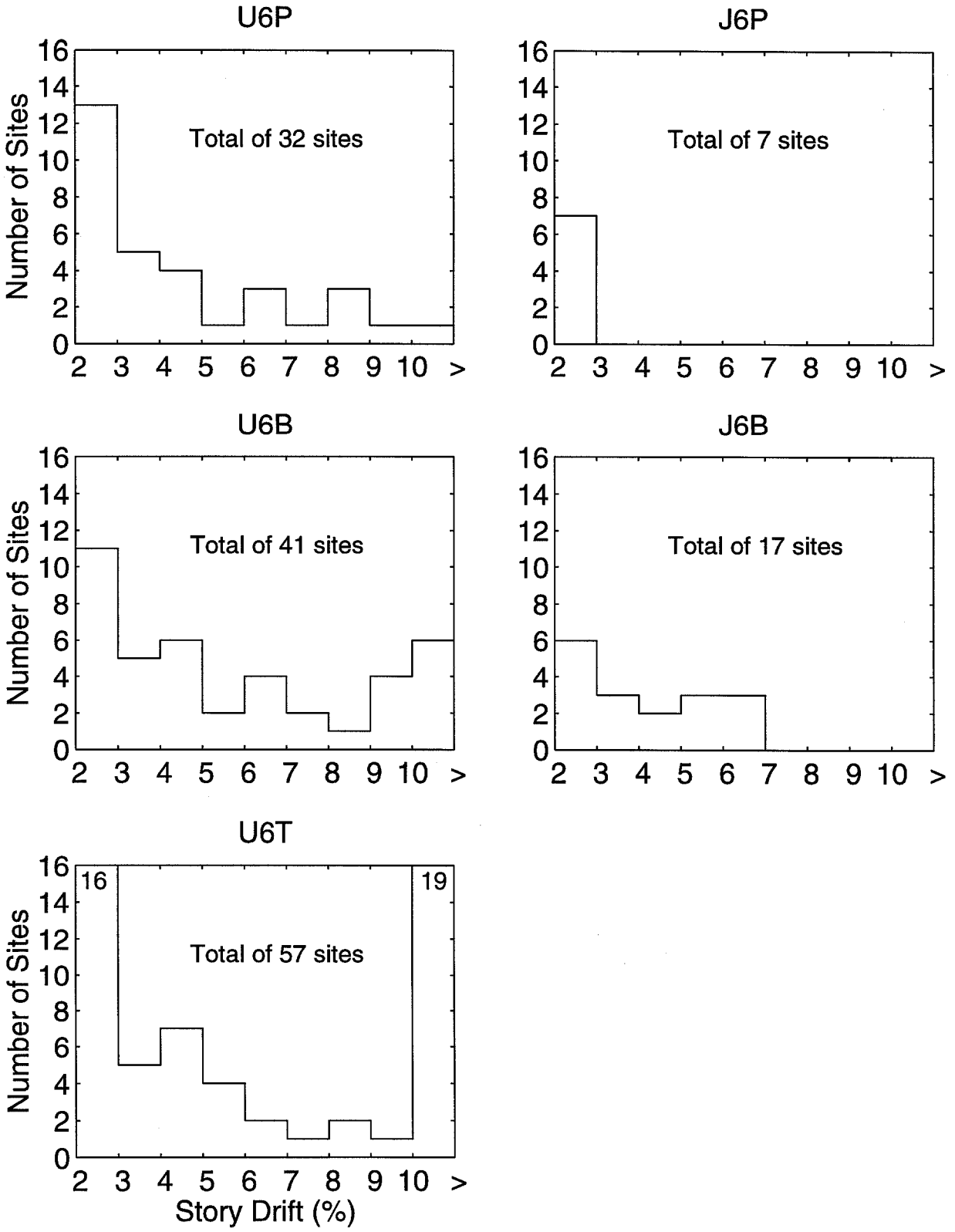

Figure 4.5 Summary of maximum story drifts for the 6–story buildings to the simulated Elysian Park earthquake. Each site represents an area of 5km by 5km.

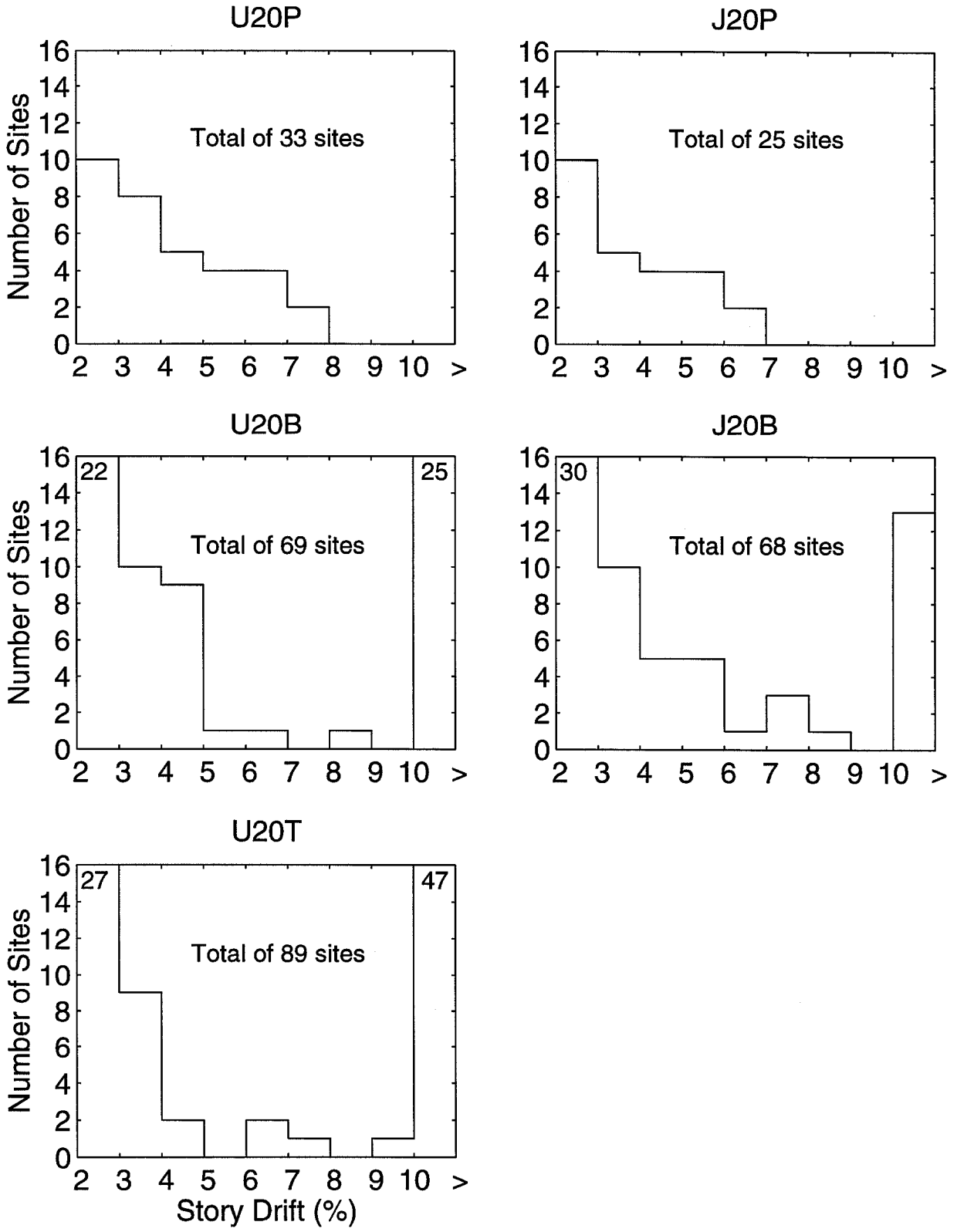

Figure 4.6 Summary of maximum story drifts for the 20–story buildings to the simulated Elysian Park earthquake. Each site represents an area of 5km by 5km.

	2	3	4	5	6	7	8	9	10	11
K	0 0	0 0	0 0	0 0	0 0	0 0	0 0	0 0	0 0	0 0
J	0 0	0 0	0 0	0 0	0 0	0 0	0 0	0 0	0 0	0 0
I	0 0	0 0	0 0	0 0	0 0	0 0	0 0	0 0	0 0	0 0
H	0 0	0 0	0 0	0 0	0 0	0 0	0 0	0 0	0 0	0 0
G	0 0	0 0	0 0	0 0	0 0	0 0	0 0	0 0	0 0	0 0
F	0 0	0 0	0 0	0 0	0 0	0 0	0 0	0 0	0 0	0 0
E	0 0	0 0	0 0	0 0	0 0	0 0	0 0	0 0	0 0	0 0
D	0 0	0 0	0 0	0 0	0 0	0 0	0 0	0 0	0 0	0 0
C	0 0	0 0	0 0	0 0	0 0	0 0	0 0	0 0	0 0	0 0
B	0 0	0 0	0 0	0 0	0 0	0 0	0 0	0 0	0 0	0 0

NUMBER OF FLANGE WELD BREAKS: girders (left) columns (right)

	2	3	4	5	6	7	8	9	10	11
K	0.5	0.4	0.8	0.7	0.5	0.4	0.4	0.3	0.2	0.4
J	0.6	0.6	1.3	1.5	0.6	1.3	0.6	0.5	0.2	0.3
I	0.7	0.6	1.6	**2.3**	**2.8**	1.9	0.8	0.5	0.3	0.4
H	1.3	**2.7**	**4.7**	**3.2**	**4.7**	**3.1**	1.5	0.5	0.4	0.4
G	0.3	1.0	1.1	1.4	1.3	**2.1**	**2.3**	0.6	0.5	0.4
F	0.3	0.7	0.7	0.7	1.7	1.9	**4.5**	1.7	0.5	0.4
E	0.4	1.0	1.1	0.7	**4.5**	**2.3**	1.6	0.8	0.4	0.3
D	0.6	0.8	0.6	0.7	**3.6**	1.6	0.8	0.8	0.4	0.3
C	0.6	1.1	0.9	1.7	**2.1**	1.2	0.6	0.4	0.6	0.3
B	1.1	1.1	0.8	0.5	0.5	0.5	1.0	0.6	0.4	0.3

MAXIMUM STORY DRIFT (%)

Table 4.1 U6P responses to the simulated Northridge earthquake.

	2	3	4	5	6	7	8	9	10	11
K	4 0	2 0	18 0	14 0	11 0	2 0	0 0	0 0	0 0	1 0
J	10 0	7 0	24 0	24 0	9 0	24 0	8 0	5 0	0 0	0 0
I	8 0	9 0	26 0	32 0	52 0	44 0	19 0	3 0	0 0	1 0
H	28 0	36 0	58 1	27 0	55 2	44 1	31 0	4 0	8 0	5 0
G	0 0	25 0	21 0	30 0	25 0	39 0	38 0	13 0	3 0	10 0
F	0 0	20 0	8 0	20 0	23 0	25 0	47 0	32 0	1 0	1 0
E	2 0	27 0	27 0	16 0	51 0	49 0	32 0	34 0	1 0	0 0
D	9 0	15 0	9 0	11 0	45 1	40 0	18 0	23 0	0 0	0 0
C	9 0	22 0	15 0	38 0	52 0	30 0	12 0	0 0	8 0	0 0
B	22 0	23 0	18 0	3 0	3 0	4 0	22 0	12 0	0 0	0 0

NUMBER OF FLANGE WELD BREAKS: girders (left) columns (right)

	2	3	4	5	6	7	8	9	10	11
K	0.5	0.4	1.2	0.7	0.5	0.4	0.4	0.3	0.2	0.5
J	0.7	0.6	1.7	1.6	0.8	1.6	0.6	0.5	0.2	0.3
I	0.7	0.7	**2.2**	**3.3**	**4.0**	**2.4**	1.3	0.5	0.3	0.4
H	1.8	**4.7**	**5.7**	**4.4**	**7.7**	**3.6**	1.5	0.5	0.5	0.5
G	0.3	1.5	1.1	1.6	1.4	**2.7**	**2.0**	0.6	0.5	0.5
F	0.3	0.9	0.7	0.9	**2.1**	1.4	**6.0**	**2.2**	0.5	0.4
E	0.4	1.1	1.3	0.7	**4.3**	**3.3**	**2.2**	1.5	0.5	0.3
D	0.6	1.0	0.8	0.9	**3.4**	**2.7**	1.2	1.0	0.4	0.3
C	0.7	1.1	1.2	**3.5**	**2.7**	**2.1**	0.7	0.4	0.7	0.3
B	1.2	1.1	1.0	0.5	0.5	0.5	1.3	0.7	0.4	0.3

MAXIMUM STORY DRIFT (%)

Table 4.2 U6B responses to the simulated Northridge earthquake.

	2	3	4	5	6	7	8	9	10	11
K	28 0	27 0	52 0	52 0	27 0	19 0	9 0	0 0	0 0	14 0
J	36 0	34 0	50 0	52 0	56 0	59 0	30 0	42 0	0 0	0 0
I	36 0	31 0	62 0	65 0	77 4	74 0	51 0	46 0	0 0	5 0
H	61 0	72 0	***	72 0	***	69 2	54 0	48 0	36 0	34 0
G	0 0	43 0	36 0	50 0	41 0	68 0	60 0	50 0	32 0	34 0
F	0 0	40 0	36 0	48 0	55 0	48 0	***	64 0	18 0	20 0
E	22 0	64 0	64 0	35 0	69 2	76 0	70 0	64 0	18 0	0 0
D	32 0	37 0	42 0	32 0	69 0	74 0	52 0	47 0	5 0	0 0
C	24 0	42 0	44 0	73 0	74 0	64 0	56 0	14 0	29 0	2 0
B	48 0	36 0	42 0	34 0	34 0	34 0	54 0	25 0	22 0	0 0

NUMBER OF FLANGE WELD BREAKS: girders (left) columns (right)

	2	3	4	5	6	7	8	9	10	11
K	0.7	0.6	1.6	0.9	0.5	0.4	0.4	0.3	0.2	0.6
J	0.9	0.9	1.9	1.5	1.2	1.8	0.8	0.7	0.2	0.3
I	1.0	1.1	**2.5**	**3.4**	**4.6**	**3.0**	1.5	1.0	0.3	0.4
H	**2.9**	**5.8**	***	**3.6**	***	**4.3**	**2.3**	0.8	0.6	0.8
G	0.3	1.6	0.8	1.3	1.7	**2.4**	**2.2**	0.8	0.6	0.8
F	0.3	1.2	0.9	1.1	1.8	1.5	***	**3.0**	0.5	0.4
E	0.5	1.1	1.5	1.2	**4.6**	**2.8**	**2.3**	1.7	0.6	0.3
D	0.7	1.5	1.5	0.8	**2.8**	**2.8**	1.8	1.0	0.4	0.3
C	0.8	1.3	1.5	**2.9**	**2.8**	**2.3**	0.9	0.4	0.6	0.4
B	1.3	1.2	1.4	0.8	0.6	0.6	1.4	0.9	0.6	0.3

MAXIMUM STORY DRIFT

Table 4.3 U6T responses to the simulated Northridge earthquake. *** signifies collapse.

	2	3	4	5	6	7	8	9	10	11
K	0 0	0 0	0 0	0 0	0 0	0 0	0 0	0 0	0 0	0 0
J	0 0	0 0	0 0	0 0	0 0	0 0	0 0	0 0	0 0	0 0
I	0 0	0 0	0 0	0 0	0 0	0 0	0 0	0 0	0 0	0 0
H	0 0	0 0	0 0	0 0	0 0	0 0	0 0	0 0	0 0	0 0
G	0 0	0 0	0 0	0 0	0 0	0 0	0 0	0 0	0 0	0 0
F	0 0	0 0	0 0	0 0	0 0	0 0	0 0	0 0	0 0	0 0
E	0 0	0 0	0 0	0 0	0 0	0 0	0 0	0 0	0 0	0 0
D	0 0	0 0	0 0	0 0	0 0	0 0	0 0	0 0	0 0	0 0
C	0 0	0 0	0 0	0 0	0 0	0 0	0 0	0 0	0 0	0 0
B	0 0	0 0	0 0	0 0	0 0	0 0	0 0	0 0	0 0	0 0

NUMBER OF FLANGE WELD BREAKS: girders (left) columns (right)

	2	3	4	5	6	7	8	9	10	11
K	0.3	0.2	0.6	0.5	0.4	0.4	0.3	0.2	0.2	0.5
J	0.6	0.4	0.8	0.9	0.5	1.3	0.4	0.4	0.3	0.2
I	0.6	0.4	0.6	1.4	**2.5**	1.5	0.4	0.4	0.2	0.2
H	1.1	1.6	**4.6**	1.4	**4.1**	**2.6**	0.9	0.4	0.4	0.4
G	0.2	0.6	0.7	1.0	0.8	1.7	1.1	0.5	0.4	0.4
F	0.3	0.5	0.4	0.4	1.0	1.1	**2.5**	1.0	0.4	0.4
E	0.5	0.8	0.6	0.4	**3.4**	**2.0**	1.8	0.8	0.5	0.3
D	0.7	0.5	0.2	0.5	**2.1**	1.6	0.4	0.8	0.5	0.3
C	0.7	0.7	0.3	1.7	1.3	0.5	0.5	0.5	0.5	0.3
B	1.5	0.6	0.3	0.4	0.5	0.3	0.7	0.7	0.6	0.4

MAXIMUM STORY DRIFT (%)

Table 4.4 J6P responses to the simulated Northridge earthquake.

	2	3	4	5	6	7	8	9	10	11
K	0 0	0 0	30 0	21 0	2 0	2 0	0 0	0 0	0 0	14 0
J	15 0	0 0	35 0	53 0	12 0	52 0	5 0	16 0	0 0	0 0
I	24 0	4 0	20 0	64 0	81 1	71 0	8 0	3 0	0 0	0 0
H	49 0	56 0	102 5	56 0	95 3	87 0	38 0	7 0	5 0	2 0
G	0 0	25 0	42 0	45 0	54 0	66 0	61 0	5 0	0 0	0 0
F	0 0	15 0	10 0	6 0	42 0	39 0	74 3	58 0	1 0	0 0
E	18 0	38 0	29 0	12 0	82 2	77 2	64 0	53 0	11 0	0 0
D	28 0	21 0	0 0	6 0	94 0	67 0	5 0	43 0	6 0	0 0
C	28 0	30 0	0 0	55 1	61 0	35 0	11 0	18 0	4 0	0 0
B	51 0	41 0	0 0	0 0	21 0	0 0	45 0	26 0	24 0	8 0

NUMBER OF FLANGE WELD BREAKS: girders (left) columns (right)

	2	3	4	5	6	7	8	9	10	11
K	0.3	0.2	0.8	0.6	0.4	0.4	0.3	0.2	0.2	0.6
J	0.7	0.4	1.0	1.3	0.5	1.4	0.4	0.5	0.3	0.2
I	0.9	0.4	0.8	1.9	**3.0**	**2.7**	0.4	0.4	0.2	0.2
H	1.5	**2.2**	**6.9**	**2.4**	**4.5**	**2.7**	1.2	0.4	0.4	0.4
G	0.2	0.9	1.1	1.3	1.7	**3.0**	**2.2**	0.5	0.4	0.4
F	0.3	0.6	0.5	0.4	1.6	1.5	**5.0**	1.7	0.4	0.4
E	0.6	1.1	0.7	0.5	**4.8**	**3.4**	**2.0**	1.0	0.5	0.3
D	0.9	0.7	0.2	0.5	**3.8**	**2.1**	0.5	1.2	0.5	0.3
C	0.8	1.0	0.3	**2.7**	**2.2**	0.7	0.5	0.6	0.5	0.3
B	1.9	1.1	0.3	0.4	0.8	0.3	1.2	0.7	0.8	0.4

MAXIMUM STORY DRIFT (%)

Table 4.5 J6B responses to the simulated Northridge earthquake.

	2	3	4	5	6	7	8	9	10	11
K	0 0	0 0	0 0	0 0	0 0	0 0	0 0	0 0	0 0	0 0
J	0 0	0 0	0 0	0 0	0 0	0 0	0 0	0 0	0 0	0 0
I	0 0	0 0	0 0	0 0	0 0	0 0	0 0	0 0	0 0	0 0
H	0 0	0 0	0 0	0 0	0 0	0 0	0 0	0 0	0 0	0 0
G	0 0	0 0	0 0	0 0	0 0	0 0	0 0	0 0	0 0	0 0
F	0 0	0 0	0 0	0 0	0 0	0 0	0 0	0 0	0 0	0 0
E	0 0	0 0	0 0	0 0	0 0	0 0	0 0	0 0	0 0	0 0
D	0 0	0 0	0 0	0 0	0 0	0 0	0 0	0 0	0 0	0 0
C	0 0	0 0	0 0	0 0	0 0	0 0	0 0	0 0	0 0	0 0
B	0 0	0 0	0 0	0 0	0 0	0 0	0 0	0 0	0 0	0 0

NUMBER OF FLANGE WELD BREAKS: girders (left) columns (right)

	2	3	4	5	6	7	8	9	10	11
K	0.2	0.3	0.3	0.4	0.4	0.3	0.3	0.2	0.1	0.3
J	0.3	0.3	0.4	0.5	0.4	0.5	0.3	0.4	0.2	0.1
I	0.3	0.4	0.6	0.7	1.6	1.0	0.4	0.3	0.2	0.2
H	0.8	1.3	**2.3**	1.0	**4.4**	1.3	0.4	0.2	0.3	0.2
G	0.1	0.4	0.4	0.7	0.5	0.5	0.6	0.2	0.2	0.2
F	0.2	0.3	0.3	0.3	0.4	0.6	1.7	0.8	0.2	0.2
E	0.2	0.6	0.7	0.2	1.2	1.9	0.9	0.6	0.4	0.2
D	0.3	0.3	0.2	0.2	0.8	1.5	0.7	0.4	0.3	0.2
C	0.3	0.2	0.2	0.8	0.6	0.5	0.3	0.3	0.3	0.2
B	0.7	0.2	0.2	0.2	0.3	0.2	0.4	0.3	0.3	0.2

MAXIMUM STORY DRIFT (%)

Table 4.6 U20P responses to the simulated Northridge earthquake.

	2	3	4	5	6	7	8	9	10	11
K	0 0	3 0	8 0	14 0	18 0	3 0	1 0	0 0	0 0	0 0
J	2 0	7 0	21 0	29 0	34 0	48 0	0 0	5 0	0 0	0 0
I	11 0	27 0	23 0	40 0	111 0	79 0	14 0	9 0	0 0	0 0
H	69 0	95 0	98 0	53 0	110 0	89 0	16 0	1 0	1 0	0 0
G	0 0	17 0	17 0	38 0	41 0	29 0	38 0	0 0	0 0	1 0
F	0 0	9 0	11 0	0 0	9 0	43 0	90 0	71 0	0 0	0 0
E	0 0	31 0	47 0	0 0	67 0	79 0	72 0	66 0	17 0	0 0
D	2 0	0 0	0 0	0 0	92 0	66 0	45 0	11 0	2 0	0 0
C	1 0	0 0	0 0	62 0	48 0	26 0	4 0	0 0	0 0	0 0
B	51 0	0 0	0 0	0 0	0 0	0 0	24 0	4 0	0 0	0 0

NUMBER OF FLANGE WELD BREAKS: girders (left) columns (right)

	2	3	4	5	6	7	8	9	10	11
K	0.2	0.3	0.4	0.5	0.6	0.3	0.3	0.2	0.1	0.3
J	0.3	0.3	0.4	0.6	0.4	1.0	0.3	0.5	0.2	0.1
I	0.5	0.6	0.7	0.9	**2.0**	1.4	0.4	0.4	0.2	0.2
H	1.0	1.8	**10.3**	1.5	**8.2**	**2.2**	0.4	0.2	0.3	0.2
G	0.1	0.6	0.5	1.1	0.7	0.5	0.6	0.2	0.2	0.2
F	0.2	0.4	0.3	0.3	0.4	0.9	**2.7**	1.1	0.2	0.2
E	0.2	1.2	1.4	0.2	1.8	1.5	1.1	0.9	0.5	0.2
D	0.3	0.3	0.2	0.2	1.7	1.8	1.5	0.4	0.3	0.2
C	0.3	0.2	0.2	1.0	1.0	0.7	0.3	0.3	0.3	0.2
B	0.9	0.2	0.2	0.2	0.3	0.2	0.6	0.3	0.3	0.2

MAXIMUM STORY DRIFT (%)

Table 4.7 U20B responses to the simulated Northridge earthquake.

	2	3	4	5	6	7	8	9	10	11
K	0 0	11 0	43 0	47 0	52 0	53 0	42 0	0 0	0 0	0 0
J	26 0	36 0	61 0	74 0	74 0	140 0	35 0	32 0	0 0	0 0
I	47 0	90 0	83 0	63 0	161 0	113 0	74 0	43 0	0 0	0 0
H	77 0	134 0	***	94 0	***	***	108 0	7 0	13 0	2 0
G	0 0	90 0	75 0	97 0	156 0	165 0	110 0	0 0	0 0	2 0
F	0 0	36 0	16 0	44 0	65 0	129 0	***	121 0	0 0	0 0
E	0 0	82 0	107 0	0 0	99 0	112 0	112 0	83 0	52 0	0 0
D	19 0	0 0	0 0	0 0	178 0	73 0	61 0	71 0	25 0	0 0
C	21 0	0 0	0 0	124 0	78 0	66 0	38 0	21 0	0 0	0 0
B	86 0	0 0	0 0	0 0	0 0	0 0	78 0	11 0	5 0	0 0

NUMBER OF FLANGE WELD BREAKS: girders (left) columns (right)

	2	3	4	5	6	7	8	9	10	11
K	0.2	0.3	0.4	0.9	1.1	0.8	0.8	0.2	0.1	0.3
J	0.4	0.5	0.8	0.7	0.8	0.7	0.7	0.5	0.2	0.1
I	0.4	0.6	0.9	1.2	**3.1**	1.2	0.8	0.5	0.2	0.2
H	1.6	**2.4**	***	**2.2**	***	***	0.6	0.3	0.3	0.2
G	0.1	0.9	1.1	1.3	1.5	1.2	1.1	0.2	0.2	0.3
F	0.2	0.5	0.4	0.9	0.4	1.4	***	1.5	0.2	0.2
E	0.2	1.2	1.3	0.2	1.8	**2.1**	1.8	1.5	0.8	0.2
D	0.4	0.3	0.2	0.2	1.5	1.7	**2.1**	0.6	0.5	0.2
C	0.4	0.2	0.2	**2.9**	1.5	0.8	0.4	0.4	0.3	0.2
B	1.3	0.2	0.2	0.2	0.3	0.2	0.9	0.3	0.3	0.2

MAXIMUM STORY DRIFT

Table 4.8 U20T responses to the simulated Northridge earthquake. *** signifies collapse.

	2	3	4	5	6	7	8	9	10	11
K	0 0	0 0	0 0	0 0	0 0	0 0	0 0	0 0	0 0	0 0
J	0 0	0 0	0 0	0 0	0 0	0 0	0 0	0 0	0 0	0 0
I	0 0	0 0	0 0	0 0	0 0	0 0	0 0	0 0	0 0	0 0
H	0 0	0 0	0 0	0 0	0 0	0 0	0 0	0 0	0 0	0 0
G	0 0	0 0	0 0	0 0	0 0	0 0	0 0	0 0	0 0	0 0
F	0 0	0 0	0 0	0 0	0 0	0 0	0 0	0 0	0 0	0 0
E	0 0	0 0	0 0	0 0	0 0	0 0	0 0	0 0	0 0	0 0
D	0 0	0 0	0 0	0 0	0 0	0 0	0 0	0 0	0 0	0 0
C	0 0	0 0	0 0	0 0	0 0	0 0	0 0	0 0	0 0	0 0
B	0 0	0 0	0 0	0 0	0 0	0 0	0 0	0 0	0 0	0 0

NUMBER OF FLANGE WELD BREAKS: girders (left) columns (right)

	2	3	4	5	6	7	8	9	10	11
K	0.2	0.3	0.4	0.5	0.3	0.3	0.2	0.1	0.1	0.3
J	0.3	0.3	0.3	0.5	0.5	0.5	0.3	0.3	0.2	0.1
I	0.3	0.3	0.5	0.6	1.7	1.0	0.4	0.3	0.2	0.1
H	0.6	1.1	**2.1**	0.9	**2.9**	1.0	0.4	0.3	0.3	0.3
G	0.1	0.3	0.3	0.5	0.4	0.4	0.6	0.3	0.2	0.3
F	0.2	0.3	0.3	0.3	0.4	0.4	1.8	1.0	0.2	0.2
E	0.2	0.5	0.7	0.2	0.8	1.6	0.8	0.6	0.4	0.2
D	0.3	0.2	0.3	0.2	0.8	1.5	0.6	0.3	0.2	0.2
C	0.3	0.1	0.2	1.0	0.7	0.7	0.4	0.3	0.2	0.3
B	0.5	0.1	0.2	0.3	0.2	0.2	0.5	0.3	0.3	0.2

MAXIMUM STORY DRIFT (%)

Table 4.9 J20P responses for the simulated Northridge earthquake.

	2	3	4	5	6	7	8	9	10	11
K	0 0	0 0	23 0	39 0	10 0	2 0	0 0	0 0	0 0	5 0
J	0 0	9 0	16 0	39 0	52 0	50 0	2 0	6 0	0 0	0 0
I	1 0	17 0	50 0	63 0	163 0	137 0	21 0	3 0	0 0	0 0
H	108 0	131 0	129 0	80 0	163 2	123 0	34 0	3 0	1 0	5 0
G	0 0	1 0	26 0	60 0	21 0	24 0	67 0	0 0	0 0	4 0
F	0 0	3 0	5 0	4 0	15 0	19 0	141 0	97 0	0 0	0 0
E	0 0	61 0	91 0	0 0	138 0	122 0	90 0	109 0	15 0	0 0
D	0 0	0 0	0 0	0 0	132 0	98 0	83 0	4 0	0 0	0 0
C	0 0	0 0	0 0	108 0	96 0	48 0	31 0	9 0	0 0	0 0
B	34 0	0 0	0 0	6 0	0 0	0 0	33 0	0 0	0 0	0 0

NUMBER OF FLANGE WELD BREAKS: girders (left) columns (right)

	2	3	4	5	6	7	8	9	10	11
K	0.2	0.3	0.5	0.6	0.4	0.3	0.2	0.1	0.1	0.3
J	0.3	0.3	0.4	0.6	0.7	0.6	0.3	0.3	0.2	0.1
I	0.3	0.4	0.7	0.9	**2.2**	1.4	0.4	0.3	0.2	0.1
H	1.0	**2.9**	**3.5**	1.3	**4.9**	**2.0**	0.5	0.3	0.3	0.3
G	0.1	0.3	0.4	0.6	0.5	0.6	0.9	0.3	0.2	0.3
F	0.2	0.3	0.3	0.3	0.4	0.5	**2.6**	1.4	0.2	0.2
E	0.2	0.9	0.7	0.2	**2.0**	**2.3**	1.5	1.0	0.4	0.2
D	0.3	0.2	0.3	0.2	1.6	**2.0**	1.3	0.3	0.2	0.2
C	0.3	0.1	0.2	1.1	0.9	0.9	0.4	0.3	0.2	0.3
B	0.5	0.1	0.2	0.3	0.2	0.2	0.6	0.3	0.3	0.2

MAXIMUM STORY DRIFT (%)

Table 4.10 J20B responses to the simulated Northridge earthquake.

	A	A2	B1	B3	C1	D	D2	E1	F1	F3	G	G2
1	0 0	0 0	0 0	0 0	0 0	0 0	0 0			0 0	0 0	0 0
2								0 0	0 0		0 0	
3	0 0			0 0	0 0		0 0	0 0			0 0	
4						0 0			0 0			
5	0 0	0 0	0 0			0 0				0 0		0 0
6				0 0	0 0		0 0		0 0			0 0
7		0 0	0 0					0 0		0 0		

NUMBER OF FLANGE WELD BREAKS: beams (left) columns (right)

	A	A2	B1	B3	C1	D	D2	E1	F1	F3	G	G2
1	1.4	1.8	1.9	**2.2**	1.8	1.8	**2.0**			1.9	1.6	1.6
2								1.3	1.4		1.8	
3	**2.7**			**4.1**	**3.7**		**4.0**	**3.2**			**2.1**	
4						**4.4**			**3.9**			
5	**2.0**	**2.5**	**3.2**			**5.2**				**2.0**		1.6
6				**5.5**	**4.9**		**5.6**		**4.8**			1.9
7		**3.4**	**4.7**					**5.0**		**2.8**		

MAXIMUM STORY DRIFT

Table 4.11 U6P responses to the simulated Kobe earthquake.

	A	A2	B1	B3	C1	D	D2	E1	F1	F3	G	G2
1	25 0	26 0	31 0	28 0	24 0	31 0	40 0			28 0	24 0	33 0
2								23 0	25 0		33 0	
3	38 0			43 0	39 0		43 2	45 0			39 0	
4						47 0			53 0			
5	27 0	30 0	40 0			52 1				25 0		30 0
6				54 3	51 0		55 1		***			38 0
7		46 0	43 0					60 2		35 0		

NUMBER OF FLANGE WELD BREAKS: beams (left) columns (right)

	A	A2	B1	B3	C1	D	D2	E1	F1	F3	G	G2
1	1.8	**2.1**	**2.5**	**2.8**	**2.7**	**2.5**	**2.7**			**2.2**	**2.1**	1.5
2								1.8	1.6		**2.1**	
3	**3.3**			**4.5**	**5.0**		**5.5**	**4.0**			**2.8**	
4						**4.8**			**4.7**			
5	**2.1**	**2.6**	**3.3**			**5.8**				**2.3**		**2.2**
6				**6.9**	**5.3**		**6.1**		***			**2.3**
7		**3.8**	**4.5**					**8.0**		**2.7**		

MAXIMUM STORY DRIFT

Table 4.12 U6B responses to the simulated Kobe earthquake. *** signifies collapse.

	A	A2	B1	B3	C1	D	D2	E1	F1	F3	G	G2
1	50 0	51 0	61 0	64 0	65 0	65 0	65 0			61 0	53 0	50 0
2								50 0	50 0		54 0	
3	67 0			71 0	68 1		68 3	66 2			65 0	
4						71 1			73 3			
5	54 0	67 0	72 0			72 4				64 0		61 0
6				***	72 1		76 8		75 8			63 0
7		74 0	76 2					75 8		71 0		

NUMBER OF FLANGE WELD BREAKS: beams (left) columns (right)

	A	A2	B1	B3	C1	D	D2	E1	F1	F3	G	G2
1	1.8	**2.0**	**2.4**	**2.7**	**2.9**	**2.9**	**3.0**			1.9	1.8	1.9
2								**2.0**	1.9		**2.3**	
3	**2.3**			**4.4**	**5.0**		**4.5**	**4.8**			**3.1**	
4						**4.9**			**4.4**			
5	1.6	**2.1**	**3.6**			**5.8**				**2.6**		**2.4**
6				***	**5.4**		**8.4**		**8.5**			**2.6**
7		**3.0**	**5.7**					**11.3**		**3.6**		

MAXIMUM STORY DRIFT

Table 4.13 U6T responses to the simulated Kobe earthquake. *** signifies collapse.

	A	A2	B1	B3	C1	D	D2	E1	F1	F3	G	G2
1	0 0	0 0	0 0	0 0	0 0	0 0	0 0			0 0	0 0	0 0
2								0 0	0 0		0 0	
3	0 0			0 0	0 0		0 0	0 0			0 0	
4						0 0			0 0			
5	0 0	0 0	0 0			0 0				0 0		0 0
6				0 0	0 0		0 0		0 0			0 0
7		0 0	0 0					0 0		0 0		

NUMBER OF FLANGE WELD BREAKS: beams (left) columns (right)

	A	A2	B1	B3	C1	D	D2	E1	F1	F3	G	G2
1	0.7	1.0	1.0	1.2	0.9	1.0	1.4			0.7	0.6	0.8
2								0.4	0.6		0.9	
3	1.7			***2.7***	1.9		**2.6**	**2.6**			1.3	
4						**2.4**			**3.4**			
5	1.5	1.8	**2.3**			**2.6**				1.4		1.4
6				**3.4**	**2.4**		**4.2**		**4.5**			1.6
7		**2.6**	**3.1**					**3.5**		**2.1**		

MAXIMUM STORY DRIFT

Table 4.14 J6P responses to the simulated Kobe earthquake.

	A	A2	B1	B3	C1	D	D2	E1	F1	F3	G	G2
1	33 0	40 0	53 0	58 0	49 0	56 0	62 0			50 0	21 0	56 0
2								6 0	18 0		49 0	
3	61 0			66 5	73 0		90 2	86 0			66 0	
4						65 1			73 1			
5	55 0	58 0	57 1			73 2				57 0		61 0
6				84 2	73 3		91 1		100 3			72 1
7		70 0	83 1					79 2		63 1		

NUMBER OF FLANGE WELD BREAKS: beams (left) columns (right)

	A	A2	B1	B3	C1	D	D2	E1	F1	F3	G	G2
1	1.0	1.6	1.6	1.9	1.4	1.6	**2.5**			1.4	0.8	1.5
2								0.5	0.7		1.8	
3	**3.1**			**4.3**	**3.4**		**3.6**	**4.0**			**2.4**	
4						**4.1**			**3.7**			
5	**2.1**	**2.3**	**3.5**			**4.7**				**2.3**		**2.3**
6				**5.8**	**4.0**		**5.0**		**5.1**			**2.7**
7		**3.7**	**4.6**					**5.5**		**3.6**		

MAXIMUM STORY DRIFT

Table 4.15 J6B responses to the simulated Kobe earthquake.

	A	A2	B1	B3	C1	D	D2	E1	F1	F3	G	G2
1	0 0	0 0	0 0	0 0	0 0	0 0	0 0			0 0	0 0	0 0
2								0 0	0 0		0 0	
3	0 0			0 0	0 0		0 0	0 0			0 0	
4						0 0			0 0			
5	0 0	0 0	0 0			0 0				0 0		0 0
6				0 0	0 0		0 0		0 0			0 0
7		0 0	0 0					0 0		0 0		

NUMBER OF FLANGE WELD BREAKS: beams (left) columns (right)

	A	A2	B1	B3	C1	D	D2	E1	F1	F3	G	G2
1	0.4	0.5	0.5	0.5	0.5	0.5	0.5			0.3	0.3	0.3
2								0.3	0.3		0.4	
3	0.6			1.3	1.1		1.4	1.1			0.5	
4						1.5			1.3			
5	0.6	1.1	1.3			1.8				0.5		0.5
6				1.9	1.6		1.9		**2.0**			0.5
7		1.0	1.6					1.8		0.5		

MAXIMUM STORY DRIFT

Table 4.16 U20P responses to the simulated Kobe earthquake.

	A	A2	B1	B3	C1	D	D2	E1	F1	F3	G	G2
1	14 0	29 0	44 0	42 0	33 0	29 0	32 0			4 0	5 0	1 0
2								2 0	4 0		4 0	
3	61 0			93 0	90 0		95 0	89 0			31 0	
4						85 0			100 0			
5	42 0	80 0	72 0			90 0				14 0		40 0
6				101 0	99 0		107 0		127 0			47 0
7		67 0	89 0					127 0		74 0		

NUMBER OF FLANGE WELD BREAKS: beams (left) columns (right)

	A	A2	B1	B3	C1	D	D2	E1	F1	F3	G	G2
1	0.5	0.6	0.7	0.7	0.7	0.6	0.8			0.3	0.4	0.3
2								0.3	0.3		0.4	
3	0.9			1.4	1.2		**2.2**	1.6			0.9	
4						1.3			1.6			
5	1.1	1.3	1.7			**2.2**				0.6		0.9
6				**2.1**	1.6		**2.9**		**2.7**			1.4
7		1.5	1.4					**3.3**		1.3		

MAXIMUM STORY DRIFT

Table 4.17 U20B responses to the simulated Kobe earthquake.

	A	A2	B1	B3	C1	D	D2	E1	F1	F3	G	G2
1	99 0	108 0	79 0	76 0	112 0	114 0	122 0			79 0	49 0	33 0
2								59 0	45 0		89 0	
3	72 0			109 0	99 0		135 0	147 0			139 0	
4						107 0			169 0			
5	131 0	106 0	120 0			131 11				174 0		157 0
6				132 2	139 14		***		***			163 0
7		95 0	115 0					***		159 0		

NUMBER OF FLANGE WELD BREAKS: beams (left) columns (right)

	A	A2	B1	B3	C1	D	D2	E1	F1	F3	G	G2
1	0.5	0.7	0.7	0.8	0.8	0.7	1.4			0.6	0.4	0.4
2								0.5	0.4		0.8	
3	1.5			1.7	1.4		**2.2**	**2.5**			1.4	
4						**2.3**			**2.5**			
5	1.2	1.5	1.6			**12.3**				1.5		1.4
6				**7.6**	**16.3**		***		***			1.8
7		1.8	**2.0**					***		1.9		

MAXIMUM STORY DRIFT

Table 4.18 U20T responses to the simulated Kobe earthquake.

	A	A2	B1	B3	C1	D	D2	E1	F1	F3	G	G2
1	0 0	0 0	0 0	0 0	0 0	0 0	0 0			0 0	0 0	0 0
2								0 0	0 0		0 0	
3	0 0			0 0	0 0		0 0	0 0			0 0	
4						0 0			0 0			
5	0 0	0 0	0 0			0 0				0 0		0 0
6				0 0	0 0		0 0		0 0			0 0
7		0 0	0 0					0 0		0 0		

NUMBER OF FLANGE WELD BREAKS: beams (left) columns (right)

	A	A2	B1	B3	C1	D	D2	E1	F1	F3	G	G2
1	0.3	0.4	0.4	0.5	0.5	0.5	0.4			0.3	0.3	0.3
2								0.3	0.2		0.3	
3	0.5			1.0	0.9		0.9	0.8			0.4	
4						1.1			0.9			
5	0.5	0.6	0.7			1.3				0.4		0.3
6				1.5	1.4		1.4		1.3			0.4
7		0.8	1.3					1.0		0.5		

MAXIMUM STORY DRIFT

Table 4.19 J20P responses to the simulated Kobe earthquake.

	A	A2	B1	B3	C1	D	D2	E1	F1	F3	G	G2
1	13 0	30 0	30 0	60 0	65 0	59 0	30 0			0 0	0 0	0 0
2								7 0	0 0		3 0	
3	75 0			147 0	127 0		137 0	134 0			33 0	
4						134 0			141 0			
5	71 0	102 0	132 0			162 0				10 0		29 0
6				200 0	179 0		190 0		196 0			7 0
7		108 0	143 0					174 0		71 0		

NUMBER OF FLANGE WELD BREAKS: beams (left) columns (right)

	A	A2	B1	B3	C1	D	D2	E1	F1	F3	G	G2
1	0.4	0.4	0.4	0.6	0.7	0.7	0.6			0.3	0.3	0.3
2								0.4	0.2		0.3	
3	0.6			**2.0**	**2.1**		**2.4**	**2.1**			0.5	
4						1.7			1.7			
5	0.9	1.1	1.4			**3.0**				0.4		0.4
6				**2.5**	**2.1**		**2.5**		**2.6**			0.4
7		1.5	1.5					**3.1**		0.8		

MAXIMUM STORY DRIFT

Table 4.20 J20B responses to the simulated Kobe earthquake.

	1	2	3	4	5	6	7	8	9	10	11
K	0 0	0 0	0 0	0 0	0 0	0 0	0 0	0 0	0 0	0 0	0 0
J	0 0	0 0	0 0	0 0	0 0	0 0	0 0	0 0	0 0	0 0	0 0
I	0 0	0 0	0 0	0 0	0 0	0 0	0 0	0 0	0 0	0 0	0 0
H	0 0	0 0	0 0	0 0	0 0	0 0	0 0	0 0	0 0	0 0	0 0
G	0 0	0 0	0 0	0 0	0 0	0 0	0 0	0 0	0 0	0 0	0 0
F	0 0	0 0	0 0	0 0	0 0	0 0	0 0	0 0	0 0	0 0	0 0
E	0 0	0 0	0 0	0 0	0 0	0 0	0 0	0 0	0 0	0 0	0 0
D	0 0	0 0	0 0	0 0	0 0	0 0	0 0	0 0	0 0	0 0	0 0
C	0 0	0 0	0 0	0 0	0 0	0 0	0 0	0 0	0 0	0 0	0 0
B	0 0	0 0	0 0	0 0	0 0	0 0	0 0	0 0	0 0	0 0	0 0
A	0 0	0 0	0 0	0 0	0 0	0 0	0 0	0 0	0 0	0 0	0 0

NUMBER OF FLANGE WELD BREAKS: beams (left) columns (right)

	1	2	3	4	5	6	7	8	9	10	11
K	0.5	0.7	1.1	1.1	0.9	0.5	0.4	0.4	0.3	0.3	0.2
J	0.5	0.8	1.0	**2.2**	**2.2**	0.9	0.7	0.5	0.4	0.3	0.2
I	0.7	1.1	**2.2**	**3.7**	**6.0**	**2.5**	0.6	0.6	0.5	0.3	0.2
H	0.6	1.0	**2.3**	**3.6**	**8.3**	**3.0**	1.1	0.5	0.4	0.4	0.2
G	0.6	1.0	1.9	**4.3**	**8.0**	**2.9**	1.3	0.4	0.4	0.3	0.2
F	0.7	1.3	**2.0**	**5.0**	**7.9**	**2.8**	0.7	0.5	0.5	0.4	0.2
E	0.6	1.7	**2.3**	**6.5**	**9.5**	**4.2**	0.6	0.6	0.5	0.4	0.3
D	0.9	1.5	**2.1**	**6.4**	**10.4**	**3.7**	0.7	0.5	0.4	0.4	0.2
C	0.8	1.1	1.6	**4.8**	**8.0**	**3.3**	0.9	0.5	0.5	0.3	0.2
B	0.6	0.8	1.0	**2.5**	**4.7**	**2.4**	0.9	0.5	0.4	0.3	0.2
A	0.6	0.6	0.8	1.7	**2.2**	1.9	1.1	0.6	0.4	0.3	0.2

MAXIMUM STORY DRIFT

Table 4.21 U6P responses to the simulated Elysian Park earthquake.

	1	2	3	4	5	6	7	8	9	10	11
K	3 0	18 0	20 0	21 0	19 0	1 0	3 0	0 0	0 0	0 0	0 0
J	8 0	23 0	21 0	37 0	27 0	9 0	2 0	1 0	1 0	1 0	0 0
I	8 0	25 0	34 0	38 1	32 3	43 0	8 0	12 0	7 0	1 0	0 0
H	13 0	38 0	38 0	38 1	***	41 1	24 0	11 0	6 0	1 0	0 0
G	8 0	21 0	25 0	28 0	31 2	37 1	40 0	8 0	2 0	0 0	0 0
F	15 0	41 0	33 0	41 1	***	42 0	17 0	8 0	3 0	0 0	0 0
E	11 0	31 0	33 0	44 0	***	34 0	7 0	9 0	1 0	1 0	0 0
D	16 0	31 0	40 0	44 2	***	44 1	6 0	3 0	2 0	3 0	0 0
C	12 0	14 0	27 0	46 3	43 3	43 0	29 0	0 0	4 0	0 0	0 0
B	8 0	19 0	22 0	37 0	32 1	35 0	5 0	12 0	2 0	0 0	0 0
A	9 0	9 0	17 0	28 0	36 0	25 0	30 0	7 0	1 0	0 0	0 0

NUMBER OF FLANGE WELD BREAKS: beams (left) columns (right)

	1	2	3	4	5	6	7	8	9	10	11
K	0.5	0.9	1.1	1.4	1.2	0.5	0.4	0.4	0.3	0.3	0.2
J	0.5	1.1	1.7	**3.4**	**4.3**	1.0	0.7	0.5	0.4	0.3	0.2
I	0.6	1.6	**2.8**	**5.8**	**9.8**	**4.4**	0.6	0.6	0.5	0.3	0.2
H	0.6	1.4	**2.9**	**6.2**	***	**6.2**	1.8	0.6	0.5	0.4	0.2
G	0.7	1.4	**2.5**	**7.5**	**19.2**	**4.6**	**2.8**	0.4	0.4	0.3	0.2
F	0.9	1.8	**2.9**	**7.8**	***	**5.1**	0.9	0.5	0.5	0.4	0.2
E	0.8	**2.1**	**3.3**	**9.7**	***	**6.7**	0.7	0.6	0.5	0.4	0.3
D	1.2	**2.3**	**3.2**	**9.7**	***	**6.0**	0.8	0.5	0.4	0.4	0.2
C	1.0	1.4	**2.6**	**8.0**	**12.4**	**4.2**	**2.0**	0.5	0.6	0.3	0.2
B	0.7	1.0	1.5	**3.9**	**9.9**	**4.0**	1.0	0.7	0.4	0.3	0.2
A	0.7	0.7	1.1	**2.4**	**4.6**	**3.2**	**2.7**	0.7	0.5	0.3	0.2

MAXIMUM STORY DRIFT

Table 4.22 U6B responses to the simulated Elysian Park earthquake. *** signifies collapse.

	1	2	3	4	5	6	7	8	9	10	11
K	40 0	42 0	54 0	62 0	53 0	29 0	23 0	8 0	0 0	0 0	0 0
J	43 0	55 0	64 0	57 3	57 3	56 0	39 0	34 0	6 0	6 0	0 0
I	50 0	68 0	65 1	***	***	59 4	54 0	32 0	37 0	5 0	0 0
H	54 0	66 0	67 3	***	***	***	65 1	34 0	22 0	7 0	0 0
G	39 0	62 0	60 2	***	***	58 4	74 1	31 0	10 0	7 0	0 0
F	42 0	65 0	62 2	***	***	59 7	69 0	22 0	15 0	4 0	0 0
E	54 0	65 0	63 1	***	***	***	52 0	38 0	20 0	2 0	0 0
D	47 0	74 0	63 2	***	***	***	55 0	17 0	19 0	14 0	0 0
C	42 0	65 0	59 2	***	***	***	72 0	36 0	22 0	0 0	0 0
B	39 0	60 0	60 0	60 4	***	58 5	76 0	30 0	16 0	0 0	0 0
A	34 0	40 0	42 0	56 0	57 4	57 3	74 0	53 0	18 0	0 0	0 0

NUMBER OF FLANGE WELD BREAKS: beams (left) columns (right)

	1	2	3	4	5	6	7	8	9	10	11
K	1.6	1.6	1.8	1.9	1.8	0.8	0.6	0.4	0.3	0.3	0.2
J	1.8	**2.1**	**2.6**	**4.9**	**5.9**	**2.5**	1.0	0.7	0.4	0.3	0.2
I	1.9	**2.8**	**4.7**	***	***	**7.3**	**2.1**	0.9	0.5	0.3	0.2
H	1.8	**2.7**	**5.0**	***	***	***	**4.1**	0.8	0.5	0.4	0.2
G	1.3	**2.3**	**3.8**	***	***	**8.4**	**5.5**	0.5	0.4	0.3	0.2
F	1.5	**2.1**	**4.0**	***	***	**9.1**	**3.0**	0.5	0.4	0.4	0.2
E	**2.1**	**2.5**	**4.4**	***	***	***	**2.1**	0.7	0.5	0.4	0.3
D	1.7	**2.2**	**4.6**	***	***	***	1.7	0.5	0.5	0.5	0.2
C	1.5	**2.3**	**3.7**	***	***	***	**3.2**	0.9	0.7	0.3	0.2
B	1.6	1.9	**2.4**	**6.3**	***	**8.1**	**3.0**	0.9	0.6	0.3	0.2
A	1.4	1.2	1.5	**4.0**	**6.0**	**5.5**	**2.9**	**2.4**	0.6	0.3	0.2

MAXIMUM STORY DRIFT

Table 4.23 U6T responses to the simulated Elysian Park earthquake. *** signifies collapse.

	1	2	3	4	5	6	7	8	9	10	11
K	0 0	0 0	0 0	0 0	0 0	0 0	0 0	0 0	0 0	0 0	0 0
J	0 0	0 0	0 0	0 0	0 0	0 0	0 0	0 0	0 0	0 0	0 0
I	0 0	0 0	0 0	0 0	0 0	0 0	0 0	0 0	0 0	0 0	0 0
H	0 0	0 0	0 0	0 0	0 0	0 0	0 0	0 0	0 0	0 0	0 0
G	0 0	0 0	0 0	0 0	0 0	0 0	0 0	0 0	0 0	0 0	0 0
F	0 0	0 0	0 0	0 0	0 0	0 0	0 0	0 0	0 0	0 0	0 0
E	0 0	0 0	0 0	0 0	0 0	0 0	0 0	0 0	0 0	0 0	0 0
D	0 0	0 0	0 0	0 0	0 0	0 0	0 0	0 0	0 0	0 0	0 0
C	0 0	0 0	0 0	0 0	0 0	0 0	0 0	0 0	0 0	0 0	0 0
B	0 0	0 0	0 0	0 0	0 0	0 0	0 0	0 0	0 0	0 0	0 0
A	0 0	0 0	0 0	0 0	0 0	0 0	0 0	0 0	0 0	0 0	0 0

NUMBER OF FLANGE WELD BREAKS: beams (left) columns (right)

	1	2	3	4	5	6	7	8	9	10	11
K	0.2	0.3	0.4	0.4	0.3	0.3	0.2	0.2	0.3	0.4	0.3
J	0.3	0.5	0.5	0.7	0.8	0.3	0.3	0.3	0.5	0.5	0.3
I	0.6	1.3	1.5	1.4	1.9	1.1	0.5	0.4	0.6	0.5	0.3
H	0.7	1.3	1.5	1.2	**2.1**	1.1	0.5	0.4	0.6	0.5	0.3
G	0.6	1.3	1.2	1.3	**2.1**	1.3	0.6	0.6	0.5	0.5	0.3
F	0.5	1.3	1.1	1.5	**2.3**	1.1	0.5	0.6	0.6	0.4	0.3
E	0.4	1.3	1.1	**2.0**	**2.3**	1.2	0.6	0.5	0.5	0.5	0.3
D	0.6	1.2	1.1	1.9	**2.8**	0.9	0.4	0.5	0.5	0.4	0.3
C	0.5	0.6	0.8	1.5	**2.2**	0.7	0.4	0.3	0.3	0.3	0.3
B	0.4	0.4	0.4	0.7	1.2	0.6	0.4	0.2	0.3	0.3	0.2
A	0.4	0.4	0.3	0.6	0.7	0.5	0.4	0.3	0.2	0.2	0.2

MAXIMUM STORY DRIFT

Table 4.24 J6P responses to the simulated Elysian Park earthquake.

	1	2	3	4	5	6	7	8	9	10	11
K	0 0	0 0	3 0	5 0	0 0	0 0	0 0	0 0	0 0	0 0	0 0
J	0 0	6 0	19 0	38 0	40 0	1 0	2 0	0 0	10 0	3 0	0 0
I	26 0	47 0	63 0	57 0	79 1	58 0	7 0	0 0	15 0	3 0	0 0
H	32 0	54 0	63 0	60 0	68 2	57 0	16 0	3 0	8 0	3 0	0 0
G	19 0	40 0	53 0	61 1	55 2	50 0	27 0	9 0	2 0	5 0	0 0
F	26 0	67 0	50 0	72 3	56 2	61 0	6 0	7 0	4 0	3 0	0 0
E	5 0	59 0	52 0	67 1	61 2	62 0	2 0	7 0	5 0	4 0	0 0
D	21 0	57 0	52 0	64 2	65 4	41 0	0 0	3 0	4 0	6 0	0 0
C	17 0	21 0	24 0	65 0	63 2	32 0	2 0	0 0	0 0	0 0	0 0
B	6 0	5 0	2 0	44 0	49 0	24 0	3 0	0 0	0 0	0 0	0 0
A	0 0	2 0	0 0	31 0	23 0	27 0	4 0	0 0	0 0	0 0	0 0

NUMBER OF FLANGE WELD BREAKS: beams (left) columns (right)

	1	2	3	4	5	6	7	8	9	10	11
K	0.2	0.3	0.4	0.4	0.3	0.3	0.2	0.2	0.3	0.4	0.3
J	0.3	0.5	0.5	1.4	1.6	0.3	0.3	0.3	0.5	0.5	0.3
I	0.6	1.2	**2.4**	1.9	**3.6**	1.5	0.5	0.4	0.6	0.5	0.3
H	0.6	1.2	**2.1**	**2.5**	**6.0**	1.7	0.6	0.4	0.6	0.5	0.3
G	0.6	1.1	1.5	**2.5**	**4.8**	1.7	1.0	0.6	0.5	0.5	0.3
F	0.6	1.6	1.2	**3.4**	**6.2**	1.4	0.5	0.6	0.6	0.4	0.3
E	0.4	1.7	1.5	**4.3**	**5.3**	**2.4**	0.6	0.5	0.6	0.5	0.3
D	0.6	1.2	1.3	**5.3**	**6.4**	1.6	0.4	0.5	0.5	0.5	0.3
C	0.5	0.6	0.8	**3.1**	**5.2**	1.5	0.4	0.3	0.3	0.3	0.3
B	0.5	0.4	0.4	1.0	**2.7**	0.9	0.4	0.2	0.3	0.3	0.2
A	0.4	0.4	0.3	0.8	0.9	0.6	0.4	0.3	0.2	0.2	0.2

MAXIMUM STORY DRIFT

Table 4.25 J6B responses to the simulated Elysian Park earthquake.

	1	2	3	4	5	6	7	8	9	10	11
K	0 0	0 0	0 0	0 0	0 0	0 0	0 0	0 0	0 0	0 0	0 0
J	0 0	0 0	0 0	0 0	0 0	0 0	0 0	0 0	0 0	0 0	0 0
I	0 0	0 0	0 0	0 0	0 0	0 0	0 0	0 0	0 0	0 0	0 0
H	0 0	0 0	0 0	0 0	0 0	0 0	0 0	0 0	0 0	0 0	0 0
G	0 0	0 0	0 0	0 0	0 0	0 0	0 0	0 0	0 0	0 0	0 0
F	0 0	0 0	0 0	0 0	0 0	0 0	0 0	0 0	0 0	0 0	0 0
E	0 0	0 0	0 0	0 0	0 0	0 0	0 0	0 0	0 0	0 0	0 0
D	0 0	0 0	0 0	0 0	0 0	0 0	0 0	0 0	0 0	0 0	0 0
C	0 0	0 0	0 0	0 0	0 0	0 0	0 0	0 0	0 0	0 0	0 0
B	0 0	0 0	0 0	0 0	0 0	0 0	0 0	0 0	0 0	0 0	0 0
A	0 0	0 0	0 0	0 0	0 0	0 0	0 0	0 0	0 0	0 0	0 0

NUMBER OF FLANGE WELD BREAKS: beams (left) columns (right)

	1	2	3	4	5	6	7	8	9	10	11
K	1.0	1.0	0.8	0.8	1.0	0.7	0.4	0.5	0.3	0.3	0.3
J	1.2	1.1	0.9	1.6	**2.3**	1.9	0.7	0.6	0.4	0.4	0.3
I	1.4	1.2	1.1	**2.8**	**5.1**	**3.9**	1.1	0.7	0.5	0.4	0.2
H	1.3	1.1	1.2	**3.2**	**6.0**	**4.6**	1.8	1.0	0.6	0.5	0.3
G	1.3	1.0	1.2	**3.2**	**6.3**	**4.3**	1.8	0.3	0.7	0.6	0.2
F	1.3	0.9	1.4	**3.1**	**6.3**	**4.3**	1.6	0.5	0.7	0.5	0.2
E	1.3	1.0	1.5	**3.5**	**7.8**	**5.7**	1.5	1.0	0.7	0.4	0.2
D	1.2	1.1	1.5	**3.5**	**7.8**	**5.8**	1.7	1.8	0.8	0.4	0.2
C	1.1	1.2	1.1	**3.0**	**6.2**	**5.4**	**2.7**	1.8	1.0	0.4	0.2
B	1.1	1.1	0.9	**2.1**	**4.5**	**4.6**	**2.4**	**2.4**	1.2	0.5	0.3
A	1.1	1.2	0.8	1.4	**2.8**	**3.2**	**2.1**	**2.6**	**2.0**	0.6	0.3

MAXIMUM STORY DRIFT

Table 4.26 U20P responses to the simulated Elysian Park earthquake.

	1	2	3	4	5	6	7	8	9	10	11
K	46 0	51 0	57 0	70 0	58 0	43 0	32 0	33 0	10 0	4 0	2 0
J	62 0	60 0	84 0	84 0	93 0	75 0	54 0	47 0	26 0	14 0	0 0
I	55 0	56 0	65 0	89 6	***	***	58 0	55 0	33 0	11 0	0 0
H	56 0	57 0	75 0	***	***	***	74 0	62 0	42 0	30 0	2 0
G	54 0	41 0	81 0	87 3	***	***	73 0	9 0	45 0	33 0	0 0
F	71 0	59 0	91 0	***	***	***	67 0	54 0	51 0	38 0	0 0
E	72 0	53 0	85 0	***	***	***	48 0	56 0	42 0	20 0	0 0
D	59 0	54 0	74 0	***	***	***	58 0	66 0	53 0	9 0	0 0
C	56 0	70 0	86 1	***	***	***	***	69 0	59 0	26 0	0 0
B	60 0	60 0	64 0	94 0	***	***	68 1	73 0	71 0	24 0	1 0
A	54 0	59 0	70 0	87 0	***	90 1	58 0	69 0	70 0	36 0	1 0

NUMBER OF FLANGE WELD BREAKS: beams (left) columns (right)

	1	2	3	4	5	6	7	8	9	10	11
K	1.7	1.4	1.3	**2.2**	**2.5**	1.7	0.7	0.7	0.4	0.3	0.3
J	**2.1**	**2.0**	1.6	**4.0**	**5.4**	**4.3**	1.6	1.3	0.6	0.5	0.3
I	1.6	1.5	**4.0**	**19.9**	***	***	**2.5**	1.9	0.7	0.4	0.2
H	1.7	**2.2**	**2.6**	***	***	***	**2.6**	**2.0**	1.0	0.6	0.3
G	**2.2**	1.3	**3.3**	**18.2**	***	***	**3.9**	0.4	1.2	1.3	0.2
F	**2.5**	**2.1**	**3.4**	***	***	***	**3.7**	0.9	1.1	1.1	0.2
E	1.8	1.5	**4.3**	***	***	***	**2.7**	1.9	1.5	0.8	0.2
D	**2.2**	**2.1**	**3.0**	***	***	***	**4.4**	**2.8**	**2.2**	0.5	0.2
C	**2.6**	1.5	**4.7**	***	***	***	***	**3.5**	**2.2**	0.8	0.2
B	1.9	**2.0**	1.9	**4.3**	***	***	**6.1**	**3.8**	**3.9**	1.0	0.3
A	**2.2**	1.6	**2.2**	**3.9**	***	**8.3**	**4.9**	**3.1**	**4.0**	1.4	0.3

MAXIMUM STORY DRIFT

Table 4.27 U20B responses to the simulated Elysian Park earthquake. *** signifies collapse.

	1	2	3	4	5	6	7	8	9	10	11
K	100 0	110 0	100 0	126 0	132 0	109 0	96 0	60 0	50 0	42 0	17 0
J	119 0	123 0	117 2	***	***	***	106 0	100 0	57 0	41 0	30 0
I	92 0	97 0	132 7	***	***	***	85 0	103 0	72 0	54 0	0 0
H	90 0	98 0	129 9	***	***	***	77 0	108 0	74 0	65 0	40 0
G	90 0	95 0	125 7	***	***	***	***	60 0	65 0	83 0	0 0
F	90 0	98 0	125 10	***	***	***	***	73 0	89 0	62 0	0 0
E	88 0	89 0	131 10	***	***	***	***	116 0	91 0	66 0	0 0
D	84 0	88 0	142 14	***	***	***	***	88 0	88 0	62 0	0 0
C	90 0	94 0	124 7	***	***	***	***	***	103 0	78 0	0 0
B	113 0	101 0	98 0	***	***	***	***	***	109 0	125 8	17 0
A	98 0	94 0	103 0	***	***	***	***	110 12	109 0	97 0	38 0

NUMBER OF FLANGE WELD BREAKS: beams (left) columns (right)

	1	2	3	4	5	6	7	8	9	10	11
K	1.6	**2.0**	**3.7**	**6.0**	**6.7**	**2.6**	1.6	1.1	1.3	1.0	0.4
J	1.5	**3.2**	**7.9**	***	***	***	**2.7**	1.8	1.5	1.1	0.7
I	**2.0**	**2.8**	**12.1**	***	***	***	**2.5**	**2.4**	1.3	1.4	0.2
H	**2.0**	**3.6**	**10.7**	***	***	***	**2.9**	**4.2**	**2.2**	1.1	0.6
G	**2.2**	**3.2**	**10.6**	***	***	***	***	1.3	**2.3**	1.3	0.2
F	1.9	**2.9**	**12.9**	***	***	***	***	**2.3**	**2.3**	1.4	0.2
E	**2.1**	**2.5**	**14.8**	***	***	***	***	**3.1**	**2.5**	1.4	0.2
D	**2.0**	**2.4**	**17.2**	***	***	***	***	**3.8**	**2.5**	1.5	0.2
C	**2.2**	**2.1**	**9.6**	***	***	***	***	***	**2.5**	1.6	0.2
B	1.9	**2.1**	**3.1**	***	***	***	***	***	**2.6**	**10.8**	0.4
A	1.8	**2.9**	**3.5**	***	***	***	***	**15.9**	**3.2**	**4.9**	0.6

MAXIMUM STORY DRIFT

Table 4.28 U20T responses to the simulated Elysian Park earthquake. *** signifies collapse.

	1	2	3	4	5	6	7	8	9	10	11
K	0 0	0 0	0 0	0 0	0 0	0 0	0 0	0 0	0 0	0 0	0 0
J	0 0	0 0	0 0	0 0	0 0	0 0	0 0	0 0	0 0	0 0	0 0
I	0 0	0 0	0 0	0 0	0 0	0 0	0 0	0 0	0 0	0 0	0 0
H	0 0	0 0	0 0	0 0	0 0	0 0	0 0	0 0	0 0	0 0	0 0
G	0 0	0 0	0 0	0 0	0 0	0 0	0 0	0 0	0 0	0 0	0 0
F	0 0	0 0	0 0	0 0	0 0	0 0	0 0	0 0	0 0	0 0	0 0
E	0 0	0 0	0 0	0 0	0 0	0 0	0 0	0 0	0 0	0 0	0 0
D	0 0	0 0	0 0	0 0	0 0	0 0	0 0	0 0	0 0	0 0	0 0
C	0 0	0 0	0 0	0 0	0 0	0 0	0 0	0 0	0 0	0 0	0 0
B	0 0	0 0	0 0	0 0	0 0	0 0	0 0	0 0	0 0	0 0	0 0
A	0 0	0 0	0 0	0 0	0 0	0 0	0 0	0 0	0 0	0 0	0 0

NUMBER OF FLANGE WELD BREAKS: beams (left) columns (right)

	1	2	3	4	5	6	7	8	9	10	11
K	0.8	0.8	1.1	0.9	0.9	0.6	0.5	0.4	0.3	0.3	0.2
J	1.0	1.0	0.9	1.1	1.8	1.2	0.5	0.5	0.4	0.4	0.2
I	1.1	1.3	1.0	**2.4**	**4.5**	**2.9**	0.8	0.5	0.4	0.3	0.2
H	1.0	1.2	1.0	**2.6**	**5.4**	**3.3**	1.6	0.6	0.4	0.4	0.2
G	0.9	1.1	1.1	**2.6**	**5.4**	**3.1**	**2.8**	0.3	0.6	0.4	0.2
F	1.0	1.1	1.2	**2.6**	**5.3**	**3.0**	1.7	0.5	0.6	0.4	0.2
E	0.9	1.1	1.3	**2.9**	**6.4**	**4.5**	1.3	0.7	0.4	0.3	0.3
D	1.0	1.2	1.3	**2.8**	**6.5**	**4.3**	1.1	0.8	0.4	0.3	0.2
C	0.9	1.3	0.9	**2.4**	**5.5**	**4.1**	1.5	1.2	0.5	0.3	0.1
B	0.8	1.1	0.9	1.6	**3.7**	**3.3**	1.5	1.1	0.5	0.3	0.2
A	0.8	1.0	0.9	1.0	1.9	**2.1**	1.3	1.9	0.9	0.4	0.2

MAXIMUM STORY DRIFT

Table 4.29 J20P responses to the simulated Elysian Park earthquake.

	1	2	3	4	5	6	7	8	9	10	11
K	85 0	86 0	93 0	97 0	78 0	58 0	40 0	28 0	7 0	6 0	0 0
J	83 0	97 0	106 0	117 0	104 0	96 0	61 0	52 0	12 0	15 0	0 0
I	85 0	104 0	114 0	146 0	***	121 0	94 0	58 0	22 0	2 0	0 0
H	97 0	111 0	140 0	125 1	***	121 1	104 0	81 0	37 0	18 0	0 0
G	84 0	74 0	129 0	136 0	***	104 1	116 0	4 0	48 0	30 0	0 0
F	90 0	88 0	110 0	***	***	114 1	105 0	51 0	47 0	30 0	0 0
E	82 0	89 0	129 0	***	***	***	104 0	70 0	22 0	1 0	1 0
D	86 0	102 0	124 0	159 2	***	***	88 0	78 0	27 0	0 0	0 0
C	85 0	95 0	112 0	***	***	119 1	116 0	100 0	25 0	0 0	0 0
B	93 0	99 0	97 0	137 0	***	124 1	97 0	109 1	56 0	8 0	0 0
A	77 0	90 0	76 0	101 0	110 1	114 0	105 0	131 0	70 0	19 0	0 0

NUMBER OF FLANGE WELD BREAKS: beams (left) columns (right)

	1	2	3	4	5	6	7	8	9	10	11
K	1.7	**2.3**	1.8	1.5	1.9	0.8	0.6	0.4	0.3	0.4	0.2
J	**2.5**	**2.6**	1.8	**3.6**	**3.8**	**2.2**	0.7	0.9	0.4	0.4	0.2
I	**2.2**	**2.8**	**3.1**	**4.5**	***	**5.7**	1.8	0.9	0.5	0.3	0.2
H	**2.2**	**2.3**	**2.9**	**5.5**	***	**5.4**	**3.8**	1.4	0.6	0.4	0.2
G	**2.0**	**2.4**	1.9	**5.3**	***	**8.1**	**3.6**	0.3	0.7	0.6	0.2
F	**2.4**	**2.0**	**2.8**	***	***	**7.2**	**2.0**	0.7	0.7	0.5	0.2
E	**2.4**	**2.1**	**3.2**	***	***	***	**2.1**	1.0	0.5	0.3	0.3
D	**2.4**	1.9	**2.8**	**7.7**	***	***	**2.4**	**2.1**	0.6	0.3	0.2
C	**2.3**	**2.0**	**2.7**	***	***	**7.6**	**4.0**	**3.0**	0.6	0.3	0.1
B	**2.3**	**2.4**	1.5	**3.3**	***	**6.4**	**3.5**	**4.2**	1.3	0.4	0.2
A	**2.1**	1.8	1.5	**3.1**	**5.1**	**4.2**	**2.7**	**4.2**	**2.9**	0.5	0.2

MAXIMUM STORY DRIFT

Table 4.30 J20B responses to the simulated Elysian Park earthquake

Number of Flange Weld Breaks

Record	U6P		U6B		U6T		J6P		J6B	
	Grd	Col	Grd	Col	Grd	Col	Grd	Col	Grd	Col
Sim Nridge H06	0	0	58	3	***	***	0	0	93	4
Sim Kobe 6/F1	0	0	53	1	75	8	0	0	91	3
Sim ElPark C05	0	0	***	***	***	***	0	0	61	2
Imp Val ELC	0	0	15	0	40	0	0	0	20	0
Lom Pri LEX	0	0	44	0	76	0	0	0	63	0
Lom Pri LGP	0	0	52	0	***	***	0	0	79	1
Landers LUC	0	0	35	0	***	***	0	0	49	1
Nridge RRS	0	0	57	2	70	8	0	0	85	0
Nridge OVH	0	0	48	1	73	2	0	0	73	0
Kobe EKB	0	0	51	0	74	5	0	0	88	4
Kobe FKI	0	0	50	1	76	6	0	0	80	1
Kobe JMA	0	0	46	0	75	2	0	0	75	0
Kobe KBH	0	0	50	0	75	0	0	0	75	0
Kobe KBU	0	0	32	0	66	0	0	0	55	0
Kobe KH8	0	0	59	2	***	***	0	0	84	5
Kobe NGT	0	0	38	0	67	0	0	0	60	0
Kobe NTT	0	0	41	0	71	0	0	0	68	0
Kobe SKB	0	0	17	0	43	0	0	0	4	0
Kobe SSS	0	0	47	0	73	0	0	0	65	0
Kobe TAK	0	0	61	3	76	9	0	0	91	4

Maximum Story Drifts (%)

Record	U6P		U6B		U6T		J6P		J6B	
	1st	Upr	1st	Upr	1st	Upr	1st	Upr	1st	Upr
Sim Nridge H06	**3.9**	**4.7**	**4.9**	**7.9**	***	***	**3.6**	**4.1**	**2.7**	**5.0**
Sim Kobe 6/F1	**4.3**	**4.8**	**3.9**	**6.5**	**4.0**	**8.5**	**4.3**	**4.5**	**3.3**	**5.6**
Sim ElPark C05	**7.3**	**8.0**	***	***	***	***	**2.2**	**2.1**	**3.5**	**4.9**
Imp Val ELC	0.6	0.6	0.6	0.7	0.6	1.1	0.6	0.5	0.6	0.7
Lom Pri LEX	**2.0**	**2.4**	1.6	**2.9**	1.8	**2.8**	**2.5**	**2.5**	1.8	**2.7**
Lom Pri LGP	**2.3**	**2.7**	**2.7**	**3.9**	***	***	1.6	1.6	**2.1**	**3.1**
Landers LUC	**2.6**	**2.8**	**2.8**	**3.9**	***	***	1.6	1.5	**2.1**	**3.0**
Nridge RRS	**2.7**	**3.0**	**2.8**	**3.7**	**3.0**	**4.1**	**3.0**	**3.2**	1.8	**3.9**
Nridge OVH	**2.2**	**2.6**	**2.1**	**3.2**	**2.2**	**3.5**	**2.0**	**2.1**	**2.4**	**3.5**
Kobe EKB	**5.4**	**6.0**	**3.7**	**5.6**	**2.1**	**6.0**	**2.0**	**2.0**	**5.2**	**6.9**
Kobe FKI	**4.0**	**4.6**	**2.8**	**6.5**	**3.7**	**10.3**	**3.7**	**4.0**	**2.8**	**4.7**
Kobe JMA	1.3	**2.5**	1.5	**2.9**	**2.0**	**3.4**	1.0	1.7	1.1	**2.7**
Kobe KBH	**2.4**	**2.9**	1.6	**3.2**	1.9	**4.6**	**2.8**	**3.1**	**2.0**	**3.5**
Kobe KBU	1.3	1.5	0.9	1.7	1.2	**2.4**	1.6	1.5	1.3	**2.0**
Kobe KH8	**6.6**	**7.6**	**7.8**	**14.4**	***	***	**5.5**	**5.8**	**5.0**	**7.4**
Kobe NGT	1.8	**2.1**	1.2	**2.4**	1.0	**2.1**	1.7	1.7	1.4	**2.2**
Kobe NTT	1.9	**2.3**	1.4	**2.7**	1.8	**3.8**	**2.6**	**2.6**	1.7	**2.6**
Kobe SKB	0.8	0.7	0.8	1.0	0.9	1.5	0.4	0.4	0.4	0.4
Kobe SSS	**2.1**	**2.3**	**2.1**	**3.8**	1.2	**3.3**	**2.0**	**2.1**	**2.0**	**2.7**
Kobe TAK	**4.5**	**5.3**	**2.9**	**5.7**	**3.0**	**9.6**	**4.6**	**5.0**	**3.1**	**5.8**

Table 4.31 Responses of the 6-story buildings to various actual and simulated earthquake records: number of weld breaks (top) in girders and columns, and maximum story drift (bottom) in 1st and upper stories. *** signifies collapse.

Number of Flange Weld Breaks

Record	U6P		U6B		U6T		J6P		J6B	
	Grd	Col	Grd	Col	Grd	Col	Grd	Col	Grd	Col
Sim Nridge H06	0	0	***	***	***	***	0	0	167	0
Sim Kobe 6/F1	0	0	116	0	***	***	0	0	186	0
Sim ElPark C05	0	0	***	***	***	***	0	0	***	***
Imp Val ELC	0	0	19	0	48	0	0	0	39	0
Lom Pri LEX	0	0	54	0	***	***	0	0	106	0
Lom Pri LGP	0	0	74	0	131	0	0	0	133	0
Landers LUC	0	0	***	***	131	0	0	0	***	***
Nridge RRS	0	0	81	0	***	***	0	0	127	0
Nridge OVH	0	0	60	0	***	***	0	0	122	0
Kobe EKB	0	0	86	0	***	***	0	0	159	0
Kobe FKI	0	0	96	0	148	17	0	0	166	0
Kobe JMA	0	0	78	0	136	0	0	0	128	0
Kobe KBH	0	0	98	0	131	0	0	0	132	0
Kobe KBU	0	0	53	0	107	0	0	0	69	0
Kobe KH8	0	0	***	***	151	0	0	0	190	1
Kobe NGT	0	0	70	0	137	0	0	0	98	0
Kobe NTT	0	0	94	0	157	0	0	0	146	0
Kobe SKB	0	0	34	0	91	0	0	0	51	0
Kobe SSS	0	0	74	0	121	0	0	0	112	0
Kobe TAK	0	0	113	0	***	***	0	0	187	0

Maximum Story Drift (%)

Record	U6P		U6B		U6T		J6P		J6B	
	1st	Upr	1st	Upr	1st	Upr	1st	Upr	1st	Upr
Sim Nridge H06	**3.7**	**4.4**	***	***	***	***	**2.7**	**2.9**	**3.5**	**4.9**
Sim Kobe 6/F1	1.0	**2.0**	1.2	**2.4**	***	***	0.5	1.3	1.4	**2.4**
Sim ElPark C05	**4.5**	**6.2**	***	***	***	***	**4.8**	**5.5**	***	***
Imp Val ELC	0.4	0.4	0.4	0.5	0.5	0.9	0.4	0.4	0.4	0.5
Lom Pri LEX	1.1	1.4	1.4	**2.5**	***	***	1.1	1.2	1.1	1.8
Lom Pri LGP	1.5	1.8	1.9	**4.2**	1.1	**2.6**	1.3	1.5	**2.1**	**3.5**
Landers LUC	**3.6**	**4.4**	***	***	1.6	**5.3**	**2.4**	**2.6**	***	***
Nridge RRS	1.6	1.9	1.6	**2.7**	***	***	1.3	1.5	1.5	**2.1**
Nridge OVH	1.2	1.4	1.2	**2.5**	***	***	1.0	1.1	1.1	1.7
Kobe EKB	0.8	1.1	0.9	**4.2**	***	***	0.9	1.3	1.0	**2.6**
Kobe FKI	1.9	**2.5**	1.3	**3.2**	**3.5**	**17.8**	**2.3**	**2.6**	**2.2**	**3.3**
Kobe JMA	1.0	1.2	0.9	1.6	1.0	1.9	1.3	1.5	1.0	1.6
Kobe KBH	1.7	**2.0**	1.2	**3.7**	1.0	**3.0**	1.2	1.2	1.7	**3.1**
Kobe KBU	0.5	0.5	0.5	0.8	0.8	1.7	0.5	0.6	0.6	0.8
Kobe KH8	**2.7**	**3.3**	***	***	**2.1**	**3.9**	**2.5**	**2.7**	**4.0**	**6.2**
Kobe NGT	0.7	0.7	0.6	1.3	0.7	1.3	0.5	0.7	0.7	1.0
Kobe NTT	1.1	1.4	1.1	**2.5**	1.1	**2.5**	0.9	1.0	1.2	**2.1**
Kobe SKB	0.4	0.5	0.4	1.1	0.6	1.6	0.5	0.5	0.5	0.7
Kobe SSS	0.8	1.0	0.6	1.3	1.6	**3.7**	0.7	0.8	0.8	1.3
Kobe TAK	1.6	**2.0**	1.3	**2.9**	***	***	1.4	**2.2**	1.6	**2.7**

Table 4.32 Responses of the 20-story buildings to various actual and simulated earthquake records: number of weld breaks (top) in girders and columns, and maximum story drift (bottom) in 1st and upper stories. *** signifies collapse.

5. SUMMARY AND CONCLUSIONS

U.S.-designed buildings have considerably greater strength than indicated by the code lateral force coefficient V/W. For the 6-story building U6P (P: perfect connections) designed according to the UBC, V = 0.044W, but the push-over analysis shows an ultimate lateral strength of 0.23W (with perfect connections). For the 20-story UBC-designed building U20P, the values are V = 0.03W (code) and 0.11W (push-over with perfect connections). The extra strength is due to the drift requirements in the code, the code's safety factor, and the contributions from higher-than-nominal steel strength, strain hardening, composite slab action, and the adjacent gravity frames.

The strongest of the ground motions from the simulated M_W 6.7 Northridge and M_W 6.9 Kobe earthquakes hits the 6-story buildings hard, not only the UBC-designed U6P, but the stronger J6P. The push-over strength of J6P is 0.40W, and this increase in strength has only a modest benefit in reducing story drift. For example, for the Northridge earthquake simulation, building U6P experiences story drifts of 2% or greater at 14 sites (25 km^2 per site) with a peak drift of 4.7%, and the stronger J6P experiences such drift at 8 sites with a peak drift of 4.6%. The 20-story buildings are hit less hard. For the Northridge simulation, both U20P and J20P (push-over strength of 0.15W) experience drifts of 2% or greater at only 2 sites.

The M_W 7.0 Elysian Park earthquake, with its large displacement pulse, severely affects the UBC-designed buildings, both the 6-story and 20-story ones. Drifts of 2% or greater occur at 32 sites for U6P and at 33 sites for U20P. Maximum drifts are 10.4% and 7.8%, respectively. Strengthening is beneficial for the Elysian Park earthquake, especially for the 6-story building. J6P experiences story drifts of 2% or greater at only 7 sites (maximum of 2.8%), but J20P still experiences such drifts at 25 sites (maximum of 6.5%). The 25 sites for J20P represent an area of 625 km^2, a large area for a strengthened design to receive significant damage in a M_W 7.0 earthquake.

Weld fracture is detrimental because it increases story drifts and the possibility of collapse. The model for connection fracture employed here that uses the Case-B assumption reduces the push-over strengths by about 40%; even so, the residual strength is still above the code-design level. For the Northridge earthquake simulation, story drifts of 2% or greater are experienced by U6B, J6B, U20B and J20B at 22, 17, 5, and 9 sites, respectively, compared to 14, 8, 2 and 2 sites, respectively, with perfect connections. Story drifts in the Case-B buildings that are above 6%, for which collapse can not be ruled out, occur

at a few sites. For the Elysian Park simulation, U6B, J6B, U20B and J20B experience story drifts of 2% or greater at 41, 17, 69 and 68 sites, respectively, compared to 32, 7, 33 and 25 sites, respectively, with perfect connections. Many of these sites show either large story drifts or collapse, and this result is quite alarming. For example, for U20B there are 27 sites with story drifts at or above 6%, and at 23 of these the computer program actually predicts collapse. The 23 sites represent a large area of 575 km^2. Furthermore, the "worst-case" connection-fracture scenario (Case-T assumption) is far worse. Assuming the present modelling scheme is valid, these results indicate that the connection fracture problem in existing buildings significantly increases the risk of collapse in large earthquakes.

Several of the actual ground motions from the set of various records produce responses comparable to or even greater than the strongest ground motions from the Northridge and Kobe simulations. Especially notable are LUC from Landers and FKI, KH8 and TAK from the Kobe earthquake. These records contain either large displacement pulses from a magnitude 7+ earthquake (LUC) or soft soil effects (the Kobe records). The large displacement pulse effect was well demonstrated by the results for the Elysian Park earthquake, but potential damaging effects of soft soils need further study.

In summary, this investigation has quantified near-source effects on buildings during moderate earthquakes such as Northridge and Kobe and during a larger M_W 7.0 earthquake on a blind-thrust fault. These earthquakes are capable of causing significant wide-spread damage to existing steel buildings in the U.S., including collapse, especially for the larger earthquake and if the connections in the buildings are fracture-prone. The strongest ground motions from such earthquakes present a challenge to designers who want to limit story drifts to 2%. Stouter connections and stronger buildings are beneficial, but the accompanying increase in stiffness can attract more load and offset some of the expected gain in performance. However, the best design philosophy for large earthquakes such as the M_W 7.0 event considered here does appear to be strong, short buildings. The economics of improved designs can be evaluated by weighing the extra construction costs with the estimates of damage from studies like the present one.

If the alarming increment in damage and collapse potential from a M_W 6.7 to a M_W 7.0 earthquake, as demonstrated here, is not intuitive, perhaps it is because of the lack of actual experience with a large earthquake directly striking a major city. Or perhaps the ground motions from the simulated Elysian Park earthquake have been overestimated. Realistic simulation of ground motion from large earthquakes is a critical area that needs to develop further. Other future work that verifies and extends the present study is needed to:

- improve the structural models, especially with regards to nonstructural contributions to strength and stiffness, structural degradation mechanisms including weld fracture, and foundation interaction;
- examine buildings of other heights, including very tall buildings;
- incorporate 3-dimensional structural modeling capabilities to capture torsion and effects of building irregularity;
- quantify the effects of even greater earthquakes that have not only large ground displacements but long durations of shaking.

6. REFERENCES

1. International Conference of Building Officials, *Uniform Building Code*, Whittier CA, May 1994.

2. International Association of Earthquake Engineering, "Earthquake Resistant Design Method for Buildings,"*Earthquake Resistant Regulations A World List - 1992*, Chapter 23, Part 2, pp. 23-55 to 23-71, Tokyo Japan, July 1992.

3. Anderson, J.C. and V.V. Bertero, "Uncertainties in Establishing Design Earthquakes," *Journal of Structural Engineering*, ASCE, Vol. 113, No. 8, pp. 1709-1724, August 1987.

4. Bertero, V.V., S.A. Mahin and R.A. Herrera, "Aseismic Design Implications of Near-Fault San Fernando Earthquake Records," *International Journal of Earthquake Engineering and Structural Dynamics*, Vol. 6, No. 1, pp. 31-42, January-February 1978.

5. Roeder, C.W., S.P.Schneider and J.E. Carpenter, "Seismic Behavior of Moment-Resisting Steel Frames: Analytical Study," *Journal of Structural Engineering*, Vol. 119, No. 6, pp. 1866-1884, June 1993.

6 Hall, J.F., T.H. Heaton, M.W. Halling and D.J. Wald, "Near-Source Ground Motion and Its Effects on Flexible Buildings," *Earthquake Spectra*, EERI, Vol. 11, No. 4, November 1995.

7. Hall, J.F., "Parameter Study of the Response of Moment-Resisting Steel Frame Buildings to Near-Source Ground Motions," Report No. EERL 95-08, Earthquake Engineering Research Laboratory, Caltech, Pasadena CA, December 1995.

8. Wald, D.J., T.H. Heaton and K.W. Hudnut, "The Slip History of the 1994 Northridge, California, Earthquake Determined from Strong-Motion, Teleseismic, GPS, and Leveling Data," *Bulletin of the Seismological Society of America*, Vol. 86, No. 1B, pp. S49-S70, February 1996.

9. Wald, D.J., "A Preliminary Dislocation Model for the 1995 Kobe (Hyogo-ken Nanbu), Japan, Earthquake Determined from Strong Motion and Teleseismic Waveforms," *Seismological Research Letters*, Vol. 66, No.4, pp. 22-28, July-August 1995.

10. Yamada, A., et.al., "Near-Source Ground Motion Studies for Northridge and Hanshin Earthquakes," Kajima-CUREe Project Phase 2, September 1996.

APPENDIX: COMPUTER PROGRAM

Computations in this report were carried out with a planar frame analysis computer program based on the fiber method. The program was written especially for steel structures and can handle either moment frames or braced frames. Details of the formulation can be found in references 1A and 2A; only an overview is presented here. Since braces are not used in the present study, no details of their formulation are provided.

A.1 Planar frame model

A frame consists of a planar arrangement of beams, columns and panel zones (Figure A.1), all of which can exhibit nonlinear behavior. The panel zones occupy the joint regions and to them are connected the beams (at the sides) and the columns (top and bottom). Each panel zone is a rectangular element that deforms in shear, and its actual dimensions are represented. The shear strain in the panel zone is the difference between the end rotation of the connected beams and the end rotation of the connected columns. Two connected beams have the same end rotation as do two connected columns. Beam and column members are modeled by the fiber method wherein each member is subdivided along its length into segments (Figures A.1 and A.2) and within its cross-section into fibers (Figure A.2). Associated with each segment is a linear shear stiffness and associated with each fiber is an axial stress-strain relation.

Degrees of freedom in the frame model are a horizontal and vertical translation of each joint plus the beam-ends and column-ends rotations, a total of four at each joint. Mass

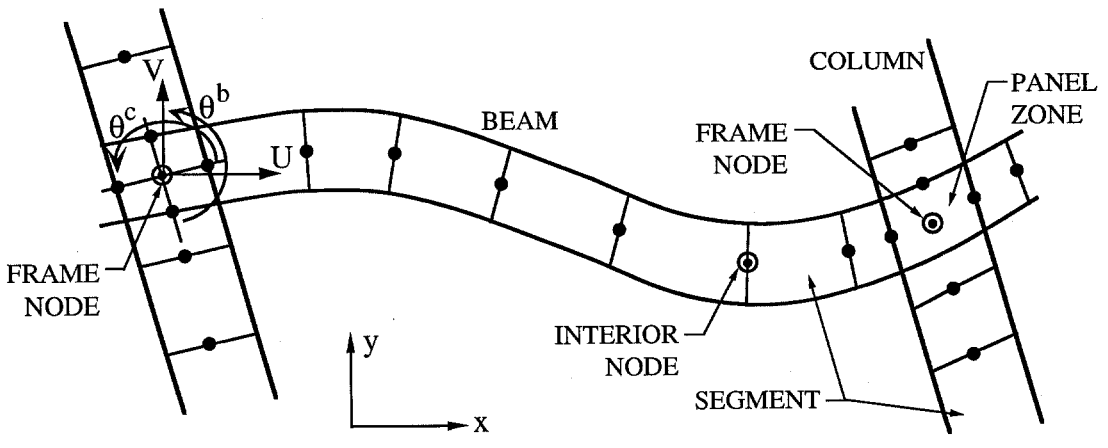

Figure A.1 Details of planar frame model

is lumped into the translational degrees of freedom. Interior degrees of freedom in the beam and column members are massless, and this allows them to be dealt with locally and left out of the frame matrices.

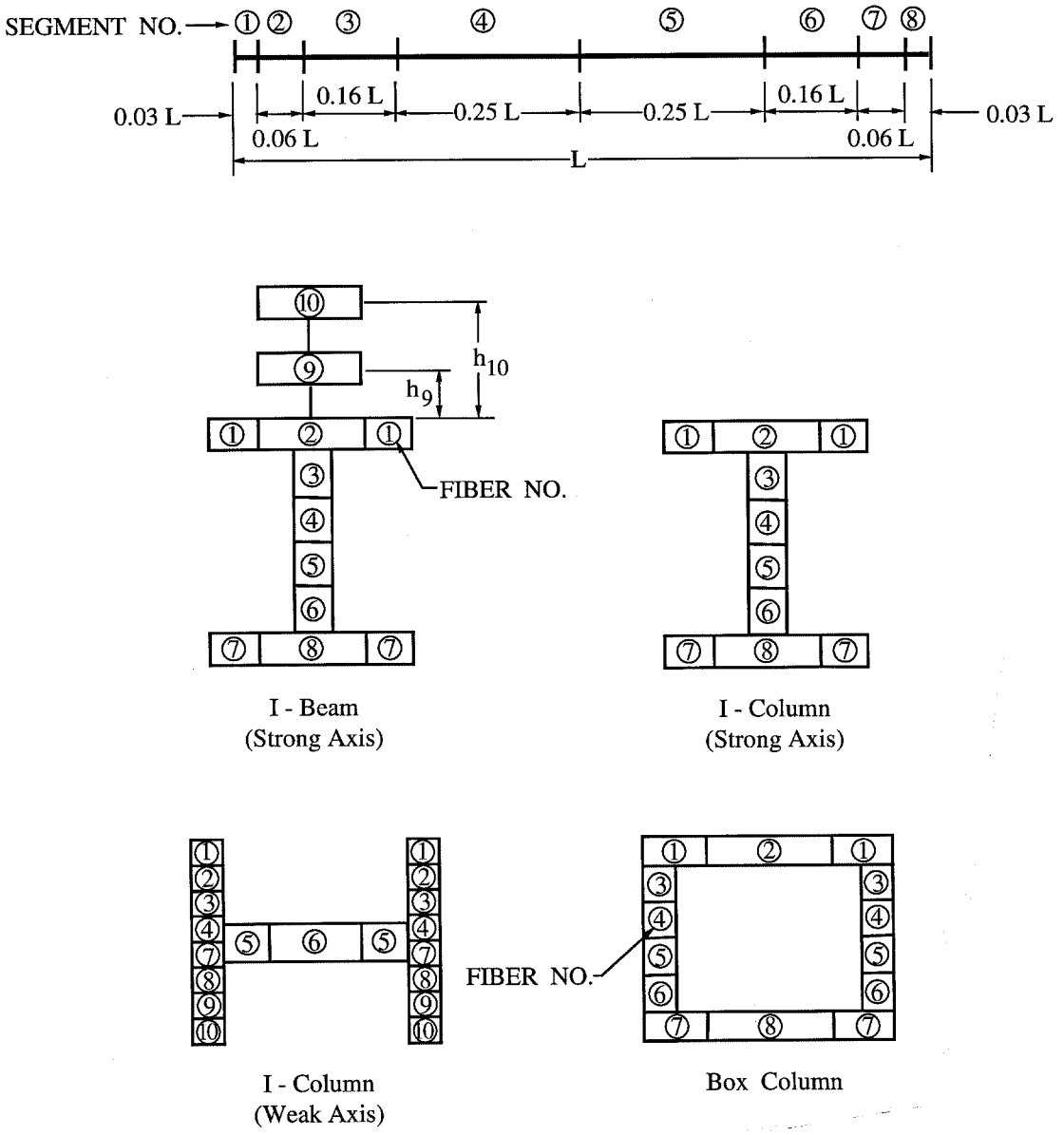

Figure A.2 Segment layout (top) and fiber layout (bottom) for beams and columns.

A.2 Panel zone

The load on a panel zone is a double-couple derived from the end moments and shears of the connected beams and columns, one couple coming from the beam end moments and column shears and the other coming from the column end moments and beam shears. This double-couple is self-equilibrating; that is, the moments of each couple are equal and opposite. Behavior of a panel zone is defined by the relation between this moment M^{pz} and the resulting shear strain γ^{pz}. The relation used is nonlinear and hysteretic as shown in Figure A.3. The elastic panel zone stiffness for moment-shear strain is given by the product of the volume of the panel zone and the shear modulus of steel G. The panel zone yields when the moment reaches 0.8 times the theoretical yield moment which is defined as the product of the panel zone volume and the steel shear strength τ_Y. No degradation in strength is included in the hysteretic model.

A capability exists to account for the addition of doubler plates by increasing the thickness of the panel zone. Without doubler plates, the panel zone thickness is the same as the column web thickness. One criteria used to determine the panel zone thickness is that the panel zone strength (ie, the yield moment) be at least 0.8 times the plastic moment capacity of the connected beams.

A.3 Beam and column elements

These elements are divided into segments along their length and into fibers within their cross-section (Figure A.2). Columns can be oriented either by their strong or weak axis. Eight segments and ten fibers are used as shown in Figure A.2. Fibers 9 and 10 in the strong-axis orientation are used only for a beam to represent composite slab action and are discussed in Section A.5.

Associated with each segment is a linear shear stiffness and associated with each fiber is an axial stress-strain relation. The shear stiffness is based on the area of the plates in the plane of the frame and the shear modulus of steel G. The fiber stress-strain relation is that of a steel bar subjected to axial stress and is nonlinear and hysteretic (Figure A.3). The behavior is fully defined by the following parameters of the skeleton curve:

E, initial elastic (Young's) modulus
E_{SH}, initial modulus at strain-hardening
σ_Y, yield stress
σ_U, ultimate stress
ε_{SH}, strain at strain-hardening
ε_U, strain at ultimate strength.

Identical behavior is assumed for tension and compression. In addition, a residual stress

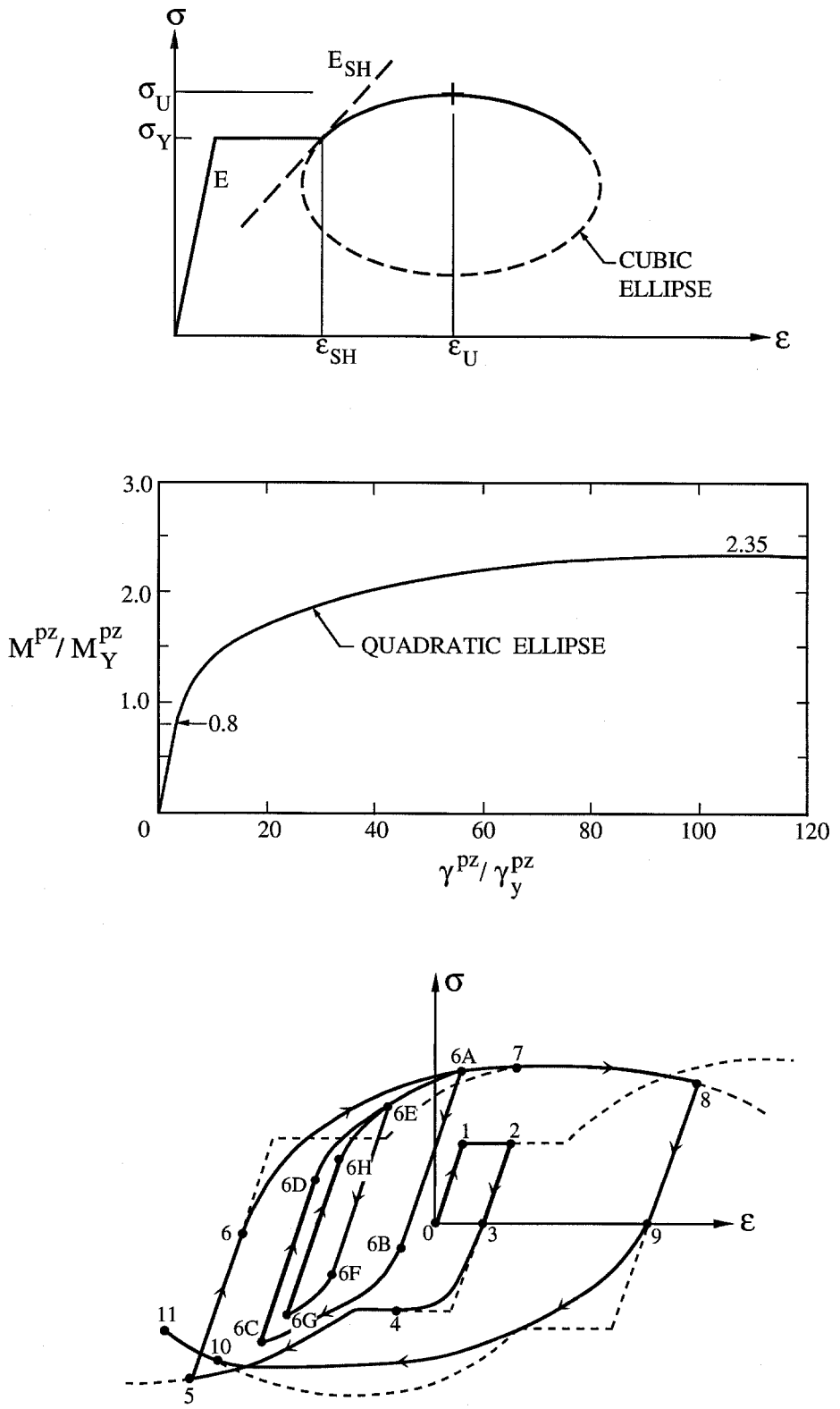

Figure A.3 Backbone curves for beam or column fiber (top) and panel zone (middle); axial stress-strain hysteretic relation for steel fiber (bottom). Panel zone hysteresis is similar to that of the fiber.

σ_{RES} can be distributed over the cross-section as tensile in the flange-web junction area and as compressive in the mid-web and flange-tip areas. The behavior shown in Figure A.3 is augmented by a weld fracture capability as described in Section A.4. This is the only degradation mechanism included.

A simple connection (non-moment-resisting) is modeled by reducing the areas of the fibers in the two adjacent segments at the end of the beam where the connection is located - either segments 1 and 2 or segments 7 and 8 or both pairs. The areas of the flange fibers 1, 2, 7 and 8 are zeroed, and the areas of the web fibers 3 through 6 are reduced to an amount appropriate to represent the flexibility of a bolted web plate, say, 0.3 of the original areas. This technique greatly reduces the moment capacity of the joint and still retains sufficient shear stiffness which is based on the web area.

A.4 Weld fracture

Fibers in the end segments 1 or 8 (Figure A.2) of a beam are given the capability to fracture when the strain reaches some specified value. A fractured fiber releases its tensile stress and loses its ability to carry tension in the future, but it can carry future compression if contact is regained. The nonlinear features shown in Figure A.3 are retained for compression. For a column (segment 1 is at the bottom; segment 8 is at the top), the fiber fracture capability is used for splice welds and welds to base plates. Column segment 4 is used for the splice weld and segment 1 for the base plate weld.

A fracture strain ε_F is assigned to a fiber using a randomized process. Sets of fracture strains are established with associated percentages in units of 10%. An example of a set is

$$\varepsilon_F = 0.7\ \varepsilon_Y \text{ at } 20\%$$
$$\varepsilon_F = 1.0\ \varepsilon_Y \text{ at } 50\%$$
$$\varepsilon_F = 2.0\ \varepsilon_Y \text{ at } 30\%, \quad \text{where } \varepsilon_Y = \text{yield strain.}$$

Fibers to be assigned fracture strains are placed into groups of which there are four types: column splice, column base plate, beam top flange and beam bottom flange. A group of column splice fibers consists of all eight fibers of segment 4 in a column containing a splice. A group of column base plate fibers consists of all eight fibers of segment 1 in a column attached to a base plate. A group of beam top flange fibers consists of fibers 1 to 4 in segment 1 or 8 where a moment connection exists, similar for a beam bottom flange group except that the fibers are 5 to 8. Each group type is associated with a set of fracture strains. For example, the beam bottom flange type could be associated with a set that has higher percentages of lower fracture strains, compared to the set used for the beam top flange type. Once the sets of fracture strains and the groups of fibers are established, the

fracture strains are assigned randomly to the groups within each type using the specified percentages of the associated set. All fibers in a group receive the same fracture strain, but the fracture strain would vary from group to group within each type throughout the building.

If all fibers of a column splice fracture, the column is assumed not to carry any load thereafter. The assumption here is that the lateral offset of the story would be sufficient to bring the flange and web plates out of alignment, and so the load carrying capacity would be reduced dramatically. If all beam fibers of a beam-to-column connection fracture, the shear transfer capacity is assumed to remain intact. In addition, for a beam or a partially cracked column splice, axial fiber stresses can be transferred through parts of the cross-section that later reestablish contact. The column-to-base-plate connection is handled similarly to the beam-to-column connection.

A.5 Composite slab action

A deck-slab system is represented as two additional fibers located on top of a beam as shown in Figure A.2. Fiber #9 represents the deck and is assumed to have the same axial stress-strain behavior as the steel fibers of the member (#'s 1 through 8). The area A_9 of the deck fiber is an effective area equal to the deck thickness times an appropriate width in the direction perpendicular to the axis of the beam. If the ribs of the deck lie perpendicular to the beam axis, then A_9 should be set to zero. The distance h_9 is to the centroid of the deck. Area A_{10} and distance h_{10} are for the concrete slab. A_{10} is again computed as the product of a thickness and an appropriate width. The stress-strain behavior of the concrete fiber is linearly elastic-perfectly plastic in compression (yield stress σ_{CY}) and linear to cracking in tension (cracking strength σ_{CF}) as shown in Figure A.4. Cracking releases the tensile stress and no tension can be subsequently carried. Once formed, a crack can later close and carry compression. The concrete elastic (Young's) modulus is denoted as E_C.

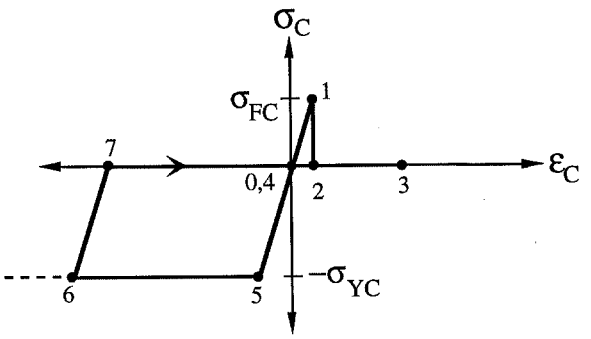

Figure A.4 Axial stress-strain hysteretic relation for concrete fiber.

A.6 Wall and foundation elements

Each basement story bay can be constrained against lateral motion by a wall element that connects the top and bottom joint nodes of two adjacent columns. The wall element resists shear deformation and does not oppose rigid body rotations. In addition, some axial stiffness is provided to the beam and column members of the frame on the perimeter of the wall element. All of these features are linearly elastic.

Foundation interaction is included through a horizontal and vertical spring attached to the bottom of each column line. Each spring is bilinear, and the hardening behavior is kinematic (Figure A.5). Parameters of the springs are as follows:

K_H, initial stiffness of horizontal spring

K_V, initial stiffness of vertical spring

α, ratio of secondary stiffness to initial stiffness

F_{YH}, D_{YH}, yield strength, displacement of horizontal spring

F_{YU}, D_{YU}, yield strength, displacement of vertical spring in upward direction

F_{YD}, D_{YD}, yield strength, displacement of vertical spring in downward direction.

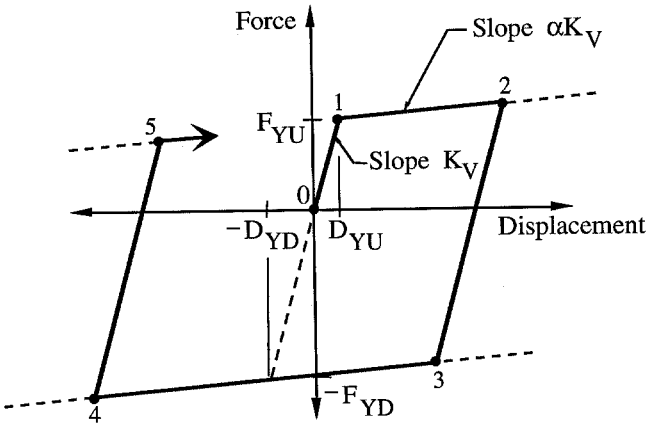

Figure A.5 Vertical load-deflection hysteretic relation for vertical foundation spring.

A.7 Solution technique

In the analysis, gravity loads are applied first followed by the earthquake loading. Ground motions can have both a horizontal and a vertical component present. The equations of motion involving the frame joint degrees of freedom are integrated implicitly with iterations in each time step until convergence is achieved. The tangent stiffness matrix is used in this process. The matrix solution in each iteration produces increments in the displacements of the four degrees of freedom at each frame joint. From these, the increments

in the end displacements of each beam and column are computed and applied to these members. Each beam and column is then solved individually for their end forces and shears which are fed back to the frame equations and assembled into the right-side residual vector. The individual beam and column solutions also yield contributions to the frame tangent stiffness matrix. Because the beams and columns exhibit nonlinear behavior, their individual solutions are iterative as well. Contributions to the right-side residual vector and the tangent stiffness matrix in the frame iterations also come from the panel zones, foundations springs and basement walls.

Several options are available for providing viscous damping. The usual mass and stiffness-proportional damping matrices can be used. In this case, the stiffness matrix employed is the initial elastic one. Such damping should be used with caution, however, because when yielding occurs in a building, large relative velocities can take place, and stiffness-proportional damping forces can then reach unrealistically high values. Use of the tangent stiffness matrix is not a suitable remedy. The preferred practice to using mass and stiffness-proportional damping is to provide capped viscous dampers placed alongside each column so as to oppose the relative floor-to-floor horizontal velocity. The capping is on the force carried by these inter-story dampers. The cap values can be set so that the capacity of all dampers in a story is a specified fraction, say 0.01 to 0.02, of the seismic design shear for that story computed with a seismic design coefficient of one. The damper "stiffness" can be set by specifying the story shear velocity at which the cap is reached. Some additional but small amount of mass or stiffness-proportional damping could be useful for numerical purposes.

During the response, the coordinates of the frame joints are updated, and in this way P-delta effects due to gravity loads carried by all the included frames are accounted for. If there are other frames in the building that carry gravity loads but are not included in the analysis, their contributions to P-delta can be incorporated through story shear forces that are applied to the included frames. These shear forces are computed using the horizontal floor displacements along with the gravity loads carried by the columns in the stories of the non-included frames.

Coordinate updating is also applied to the connectivity of the beams, columns and panel zones and to the interior nodes of the beams and columns. The latter means that moment amplification and member buckling (but not local flange buckling) effects are accounted for. For brace members, this procedure gives a good representation of buckling and post-buckling behavior under cyclic loads.

A building consisting of several parallel frames can be analyzed for loads in the plane of these frames by including the various frames in the model. Each frame is defined

independently and then they are hooked together by constraint matrices. An individual constraint matrix connects the horizontal joint degrees of freedom on one floor of one frame to those on the same floor of another frame, and the condition imposed is that the average displacement of the first set of degrees of freedom equals the average for the second set of degrees of freedom. The idea of using the average displacement is to allow for the length changes in the beams that occur under cyclic loading and especially after weld fracture. If some of the parallel frames are identical, they can be lumped into a single frame by specifying a width factor that is applied to all beams, slabs, columns, panel zones, walls and foundations. A frame along a center plane of symmetry in a half-building model would have a width factor of one half.

The solution technique is robust and very efficient. Failure to achieve convergence in a time step rarely occurs except under very large lateral displacements of the frames involving severe member deformations. Static push-over analyses can be run by using a ramp time history for horizontal ground motion that increases at a slow enough rate to make the inertial and damping forces negligible.

A.8 References

1A. Challa, V. Murty and J.F. Hall, "Earthquake Collapse Analysis of Steel Frames," *Earthquake Engineering and Structural Dynamics*, Vol. 23, No. 11, November 1994, pp. 1199-1218.

2A. J.F. Hall and M. Challa, "Beam-Column Modeling," *Journal of Engineering Mechanics*, ASCE, Vol. 121, No. 12, December 1995.